Fatigue Life Prediction for Aluminium 6261-T6 I-beams Welded with Cover Plates

Hendrik Oliver Lambrecht

A dissertation submitted to the faculty of Engineering, University of the Witwatersrand, Johannesburg, in fulfilment of the requirements for the degree of Master of Science in Engineering.

Johannesburg 1991

Declaration

I declare that this dissertation is my own unaided work, except where due reference is made to others. It is being submitted for the degree of Master of Science in Engineering at the University of the Witwatersrand, Johannesburg. It has not been submitted before for any degree or examination in any other University.

Hendrik Oliver Lambrecht

13 day of May 1991

Abstract

I-beams are a commonly used section in engineering, due to the high section modulus for a given cross sectional area of a beam. Their resistance to static loads is often increased through the use of cover plates welded to areas where the applied bending moment is high. Welding, however, has a severe detrimental effect on the fatigue life of both steel and aluminium I-beams. The effect of various categories of welded joints on fatigue life can be broadly assessed using published codes like BS 5400 Part 10[1] for steel or CP 118[2] for aluminium. It has also been proposed that BS 5400 Part 10[1] can be extended to cover aluminium weldments by dividing the prediction curve by 3[10].

This project examines two aspects of the fatigue life of aluminium 6261-T6 I-beams with welded 6261-T6 cover plates. Firstly, the effect on fatigue life of cover plate end geometry and a geometrical scaling of I-beam and cover plate were examined. S-N curves were obtained for three sizes of I-beams and cover plates, i.e. 101 x 150 mm, 75 x 100 mm and 27 x 48 mm. S-N curves for the various end weld geometries of the cover plates were only obtained for the middle size I-beams. The S-N curves were then compared with the predictions of design codes for the relevant class of weld in order to determine which code gave the best life predictions. The prediction curves of the design codes for CP 118[2] did not compare well with the S-N curves obtained in this project. The division of the prediction curve of the design code for steel, i.e. BS 5400 Part 10[1], by 2 corresponded better to the lower limit of the S-N data than the proposed division by 3[10].

Secondly, growth rate data was acquired from single-edge notched (SEN) bend specimens at stress ratios ranging from R = 0.1 to R = 0.7 for the parent plate material. Growth rate data obtained from K_{max} constant testing was also obtained for the parent plate, weld metal and HAZ specimens. Fatigue life predictions were then made for an I-beam welded with cover plates. A simple 2-dimensional finite element analysis was used to model the stresses and hence to obtain approximate stress intensity (K) values. These stress intensity values were combined with the experimentally derived growth rate curves in an integration of the Paris growth rate law to obtain the fatigue life between two defined crack size limits. Results of this analysis were compared with the empirical S-N curves. The prediction curves in all cases examined compared reasonably well with the empirical S-N curves, while prediction curves obtained using the HAZ material compared most favourably with the empirical S-N curves.

Acknowledgements

I would like to acknowledge and extend my gratitude to my supervisor, Dr. M.N. James, for his experience and guidance in this project.

I would like to extend my gratitude to Dr. A.E. Paterson for his support in this project, the Aluminium Federation of South Africa for sponsoring this project and supplying the aluminium, and Industrial Research and Development (Pty) Ltd. for welding the cover plates onto the I-beams.

The assistance in finite element analysis of Mr. C. Constancon is greatly appreciated.

Specimen machining and modifications to the test rig by J. Morffit and his workshop staff is greatly appreciated.

Finally, I would like to thank my fellow students, M. Mason and A. Jarvis, for their support and help in problems that arose during the project.

Table of Contents

1. Introduction

Aluminium has become an increasingly more important material in construction. The improved mechanical properties and light weight of the 2XXX, 5XXX, 6XXX and 7XXX series aluminium alloys have become almost indispensable in engineering applications. Efficient utilisation of aluminium alloys in construction requires that these alloys are joined by welding them together.

There is, however, a lack of information regarding the fatigue performance of welded joints in aluminium alloys. Although some codes exist, e.g. modified BS 5400 Part 10[1] and CP 118[2], which describe the fatigue performance of aluminium alloys, the accuracy and conservatism of these codes have been questioned.

I-beams are sections which are commonly used in engineering structures, due to their high section modulus for a given cross sectional area. Their resistance to loads can be increased by welding cover plates to regions where the applied bending moment is high.

If I-beams with welded cover plates are subjected to cyclic loading, as would be the case in, for example, a bridge, the fatigue performance of these beams is, however, reduced. Thus a fatigue life of about 10^7 cycles, corresponding to an applied stress range of 100 MPa for a plain steel I-beam, would be reduced to about 3×10^5 cycles if a cover plate was welded onto its tension flange. There is reason to believe that the end weld geometry of the cover plate affects the fatigue performance of the I-beams. Fisher[3] stipulated that the differences in fatigue lives between various end weld geometries in steel I-beams could be attributed to the differences in the width of the end welds, since a wider end weld would lead to multiple crack initiation sites. No published work is readily available on the fatigue life of such welded aluminium I-beams.

This project has therefore undertaken to study the fatigue performance of 6261-T6 aluminium alloy I-beams with welded cover plates such as might be used in engineering structures.

Two major aspects relating to the fatigue life behaviour of aluminium 6261-T6 I-beams with welded 6261-T6 cover plates will be investigated in this project. Firstly, the effect of cover plate and S-N curves for the various cover plate geometries and beam sizes generated. From this comparisons were made of the fatigue lives between the various cover plate and weld geometrics and beam sizes. In addition, the empirical S-N curves were compared with fatigue life design curves obtained from published codes of practice.

It is also important to examine the mode of fracture and to determine initial defect sizes in order to ascertain whether or not initiation plays an important role in the fatigue lives of the I-beams. Sizes of initial defects which initiated the fatigue cracks, were characterised and a fractographic library of fatigue crack growth mechanisms in this alloy was developed.

The second major aspect in this project was to obtain fracture mechanics based fatigue life predictions for an I-beam with welded cover plates and to compare these with the empirical S-N curves. In order for this to be possible fatigue crack growth rate curves, initial defect sizes and stress intensity correction factors had to be obtained.

Fatigue crack growth rate curves for the aluminium 6261-T6 alloy were produced at various stress ratios, R, to take the effect of residual stresses in the vicinity of the weld into account since residual stresses essentially raise the mean stress level, and hence the R ratio by an unknown amount. Tests were run at a constant K_{max} and decreasing ΔK in order to produce a crack closure free fatigue crack growth rate curve, for comparison with high R data. Fatigue crack growth rate curves for the weld metal and the heat affected zone (HAZ) were also determined so that the fatigue behaviour of the different microstructures could be compared, and because crack growth in the welded I-beams occurred in the HAZ.

Initial defects for the various end weld geometries and I-beam sizes were determined and classified with the aid of a scanning electron microscope. This data was used to define the initial crack size limit needed in the integration of the Paris growth rate law.

The presence of a welded cover plate on the I-beam introduces a stress concentration. This stress concentration affects the stress intensity factor felt by the crack. The stress intensity factor changes, however, with an increase in crack size. It is thus important to determine the change of stress concentration with crack size. This was achieved by creating a finite element model of the welded region in order to obtain a stress distribution in this region.

In summary, the objectives of this project were:

1 - To determine the fatigue lives and to produce S-N curves for three sizes of aluminium 6261-T6 I-beams welded with various cover plate geometries.

2 - To compare these empirical S-N curves with fatigue life design curves obtained from standard codes of practice.

3 - To determine the sizes of the initial defects which initiate fatigue cracks and to develop a fractographic library for fatigue crack growth in this alloy.

4 - To characterise the fatigue crack growth rate properties of the parent plate, heat affected zone of the 6261 aluminium alloy and the aluminium 5356 weld metal.

5 - To approximate the stress distribution in the weld toe region of the cover plate and weld with the aid of finite element analysis.

6 - To obtain fracture mechanics based fatigue life predictions for an I-beam with welded cover plates and to compare them with the experimentally obtained S-N data.

2. Literature Review

2.1. Introduction

The fatigue life properties of components are mainly dependent on the material and the geometry of the component. Introducing a weld can cause changes in microstructure and, in most cases, give rise to a stress concentration and welding defects.

Fatigue life estimates are based on the fact that the fatigue crack growth rate characteristics of a given material can be measured in terms of a single parameter, i.e. the stress intensity range, ΔK. The determination of ΔK itself, is however dependent on parameters such as the applied stress range, crack size, crack shape, amount of crack closure and local stress concentration. Thus, before one can attempt to predict the fatigue lives of various components, information is required to describe the underlying mechanisms affecting the local crack tip stress intensity range. Once the stress intensity range is sufficiently defined, successful fracture mechanics based predictions of the fatigue life can be made.

The introduction of a weld in a member can give rise to welding defects and may drastically changes the properties and fracture modes of the material. Some background knowledge of appropriate metallurgy and fracture modes is thus required in analysing the fatigue performance. Since welds reduce the fatigue life of components it is important to understand how and why this is the case.

To facilitate and simplify the process of designing against fatigue of welded joints, standard codes of practice have been produced. These group various types of welded joint into different classes and specify each class by a different fatigue life (S-N) curve. Thus, instead of determining the fatigue life curve for a specific geometry, only the welded joint type, i.e. its class, and the applied stress range is required to determine how long the component will last.

This literature review will briefly cover these points in order to provide an adequate background for understanding the scope of the project.

2.2. Fatigue in Aluminium Alloys

When a ductile metal is subjected to a monotonically increasing load, it will yield and finally fracture. This is accompanied by some amount of deformation and elongation. If the same material is dynamically loaded, with much lower peak cyclic stresses, it will eventually crack, with no apparent yielding. If the stress cycle is kept constant, the crack growth rate will increase as the crack size increases until failure occurs. This process of crack growth under cyclic stress is termed fatigue.

It can be very difficult to determine whether a crack results from fatigue or some other mechanism, unless the fracture surface is examined. A fatigue fracture surface usually has two or three characteristic areas. Fatigue cracks originate, in most cases, at the surface of the material and grow concentrically away from the origin of the crack. The plane of fracture is perpendicular to the direction of the applied stress. It should be noted however, especially in welded material, that fatigue cracks may initiate within the material itself.

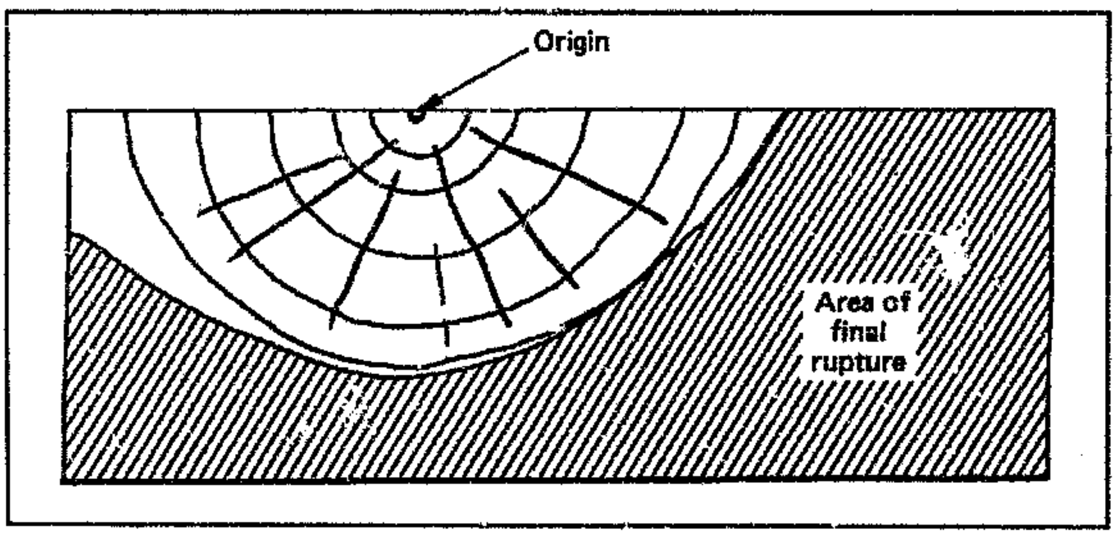

Fig. 2.1 - Diagrammatic representation of a typical fatigue fracture surface[4].

A typical fracture surface is shown in Fig. 2.1. The area in the immediate vicinity of the origin is usually very smooth. As the crack grows, the fracture surface becomes rougher and distinct lines, perpendicular to the direction of the growing crack, may become visible. These are called beach marks and are the most distinct evidence of fatigue cracking. Beach marks are the result of changes in loading conditions or environmental attack on the crack surface while the component was still in use and represent the crack front position at a particular point during the fracture process.

The final rupture regime on the fracture surface will either be smooth or rough depending on whether the material fails in a brittle or ductile fashion. If high stresses are applied, the fatigue surface is small and the regime of fast fracture large, and vice-versa for low applied stresses. The fatigue regime for low stressed fracture is usually smooth, while high stresses often lead to multiple initiation sites. This leads to radial ridges on the fracture surface where link-up of crack sections, which initiated on different planes, has occurred. Thus, the study of the fracture surface gives valuable information about the magnitude and type of applied stresses and the position at which a fatigue crack initiated. One can feed such information back into the design process to either prevent future failures or to increase the fatigue life of a particular member.

If the fracture surface is viewed at high magnification, e.g. 5000 x, fine lines, which lie perpendicular to the crack growth direction, can often be seen. These are called striations and represent instantaneous local crack front positions. Each striation is formed during one fatigue cycle, at least in the range of growth rates between 10^{-4} and 10^{-3} mm / cycle. Thus, if the spacing between striations is measured, one can determine the crack growth rate. It should be mentioned that finding these striations is not always possible since some materials do not develop striations and rubbing of the surface during cyclic loading can destroy them.

It has become widely accepted that flaws will inevitably exist in welded structures and the old idea of removing all detectable defects must be replaced by the 'fitness for purpose' design philosophy[illegible]. In order to apply such a design philosophy one has to be aware of the empirical laws which relate to fatigue life prediction.

The only way to quantify fatigue processes is by testing under controlled conditions. Knowledge of the impact or tensile properties of the material is not always of value, since the mechanisms governing these properties are different. The loading conditions used in fatigue testing should be similar to that experienced by the components in service. In fatigue, the following variables are most commonly used to describe the fatigue cycle[3,4,5]:

σ_{max} - maximum stress in the cycle.

σ_{min} - minimum stress in the cycle.

σ_r - stress range, which is the difference between σ_{max} and σ_{min}.

R - stress ratio $\sigma_{min} / \sigma_{max}$.

Tensile stresses are considered to be positive while compressive stresses are negative.

2.2.1. Stress Intensity Determination

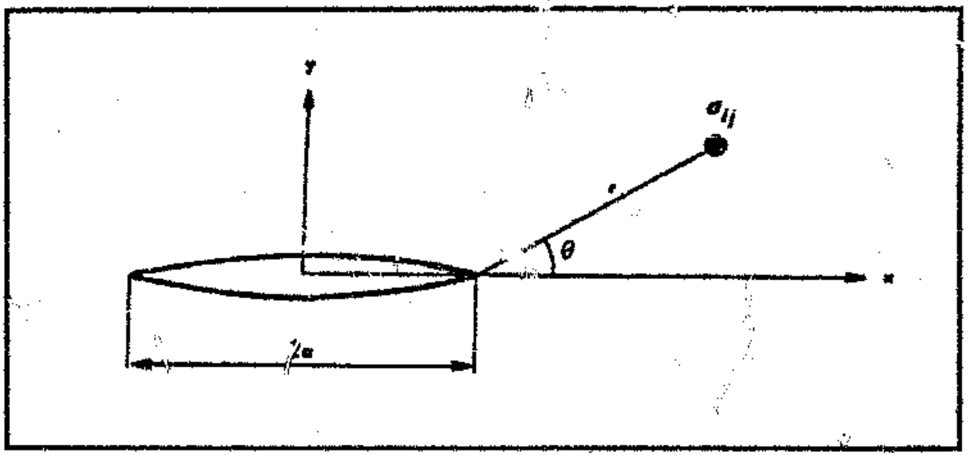

Fig. 2.2 - The stress at a point ahead of a crack tip[3].

Irwin[7] showed from linear elastic theory, that the stresses in the vicinity of a crack tip take the form of :

$$\sigma_{ij} = \frac{K\ f_{ij}(\theta)}{\sqrt{2\pi r}} + ... \qquad (2.1)$$

where r and θ are the cylindrical polar coordinates of a point with respect to the crack tip, as shown in Fig. 2.2. K is the stress intensity factor which gives the magnitude or 'intensity' of the elastic stress field near the crack tip. The general form for the stress intensity factor is given by :

$$K = Y\sigma\sqrt{\pi a} \qquad (2.2)$$

where σ is the applied stress at the crack tip and a is the size of the crack. Y is a dimensionless correction factor which is a function of the geometry of the crack and the cracked body under consideration[4, 5, 7-12]. It is defined as :

$$Y = \frac{M_k M_s M_t M_p}{\phi_0} \qquad (2.3)$$

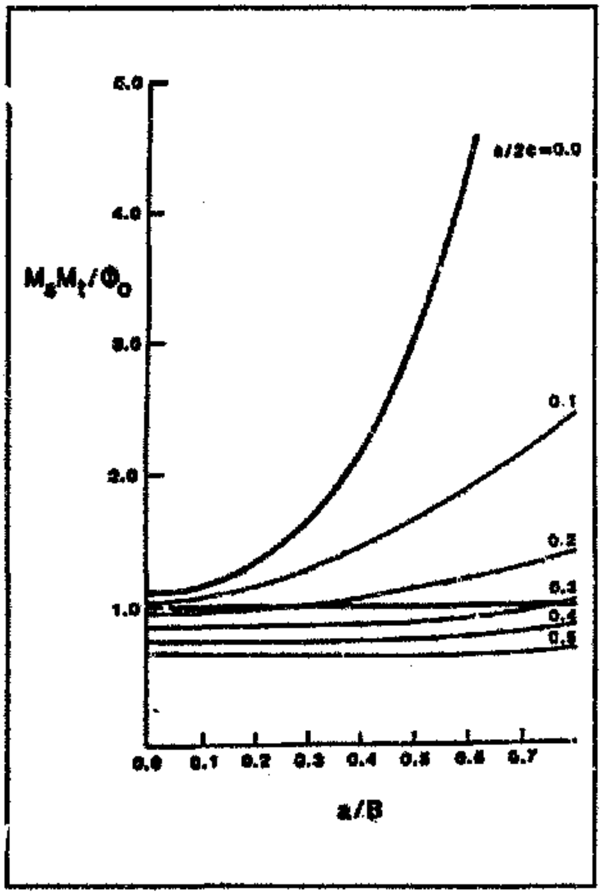

Fig. 2.3 - M_sM_t/ϕ_0 vs. a/B for different crack front shapes[12].

M_p accounts for the crack tip plasticity and is usually equal in magnitude to one, provided that the crack size is significantly less than the width of the plate. M_s is a correction factor to allow for the crack to be situated at a free surface. M_t is the correction factor for the plate thickness, which allows for the fact that there is a free surface ahead of the crack tip. ϕ_0 is the complete elliptical integral, for a range of values of a/B and a/2c, where a is the crack depth, B the plate thickness and 2c the surface crack length.

The term, M_sM_t/ϕ_0, is the correction factor for a single edge surface crack in a plate and its variation with a/B is shown in Fig. 2.3 for different a/2c[9, 13-16]. M_sM_t/ϕ_0, does not vary significantly with increasing crack length, as long as a/2c is greater than 0.3. With the introduction of transverse welds however, continuous defects may be present at the weld toe [9]. a/2c, for these cases can be estimated as tending towards zero. For this special case one can determine the correction factor from the 'Gross' equation[12, 13, 15]:

$$\frac{M_s M_t}{\Phi_0} = 1.122 - 0.231\left(\frac{a}{B}\right) + 10.55\left(\frac{a}{B}\right)^2 - 21.7\left(\frac{a}{B}\right)^3 + 33.19\left(\frac{a}{B}\right)^4 \qquad (2.4)$$

M_k is the correction factor which takes the presence of a stress concentration into account. The determination of M_k is described in sub-section 2.2.5.

2.2.2. Fatigue Crack Growth Rate Curves

When testing is performed under fatigue conditions with a stress range of $\Delta\sigma = \sigma_{max} - \sigma_{min}$, the stress intensity range, ΔK, is defined as :

$$\Delta K = K_{max} - K_{min} = Y\Delta\sigma\sqrt{\pi a} \qquad (2.5)$$

Paris[19] found that the stress intensity range was related to the fatigue growth rate. The crack growth rate is defined as $\Delta a / \Delta N$, where Δa is an increment in crack size, which occurs in ΔN cycles. In the limit this becomes da / dN. Paris showed experimentally [19] that a unique relationship between $\log da / dN$ and $\log \Delta K$ exists, which is a function of the stress ratio, R. A schematic representation of this relationship is shown in Fig. 2.4. The stress ratio is a measure of the mean stress in an applied stress cycle. The relationship can be expressed as :

$$\log\left(\frac{da}{dN}\right) = f\,(\log(\Delta K), R). \qquad (2.6)$$

Three main growth rate regimes can be identified in Fig. 2.4.

Regime I - is the near-threshold regime where the crack growth rate is small and ΔK is low. If ΔK increases slightly, then the crack growth increases sharply. There is a threshold stress intensity range, ΔK_{th}, below which no crack growth will take place[5,6,8,12,13].

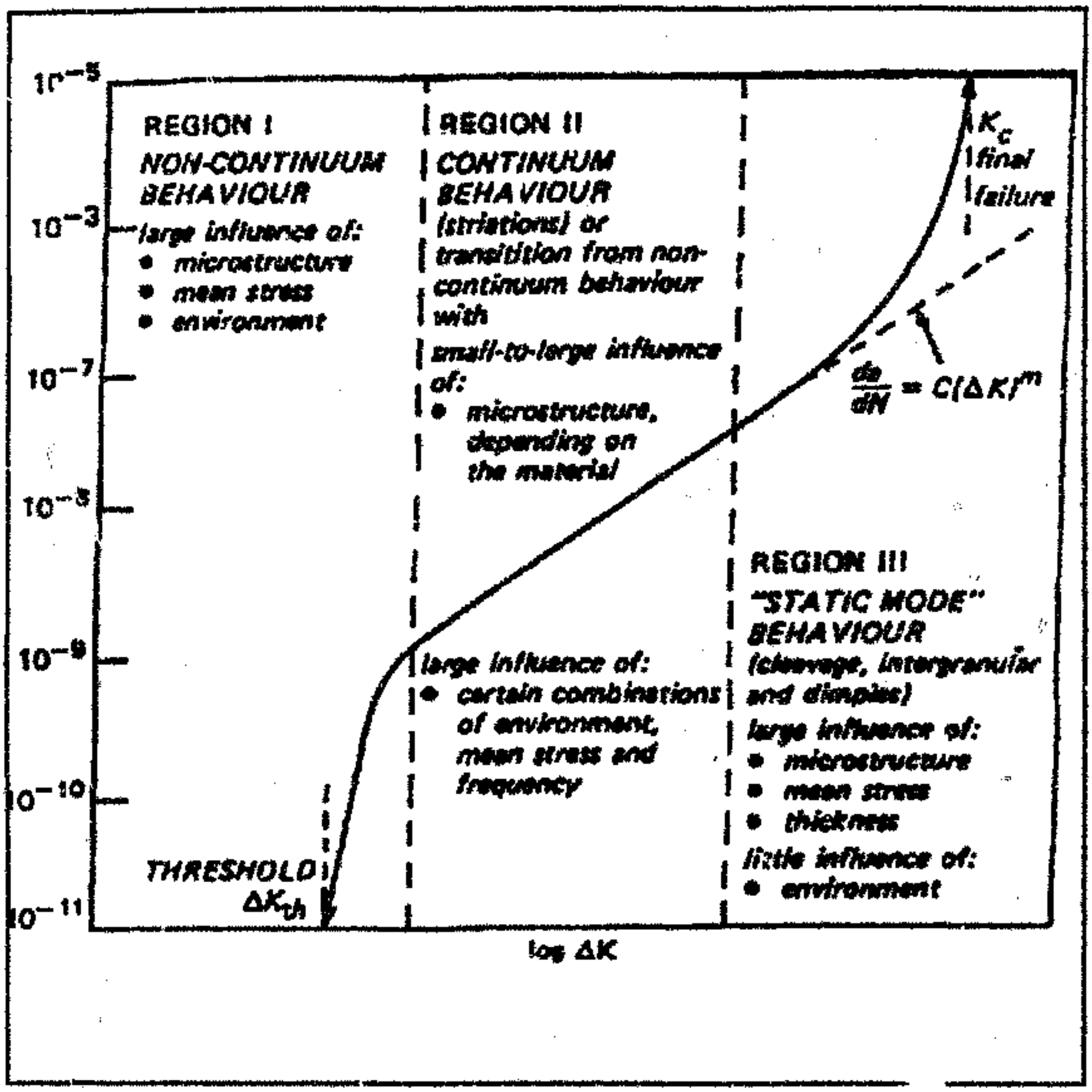

Fig. 2.4 - Idealised correlation between ΔK and da/dN[9].

Regime II - is the regime where a linear growth rate occurs, which can be effectively described by the Paris equation[19]

$$\frac{da}{dN} = C(\Delta K)^m, \tag{2.7}$$

where C and m are material constants for given loading conditions.

Regime III - is the region where the maximum stress intensity in the cycle, K_{max}, tends towards the fracture toughness of the material, where failure occurs by fast fracture. The growth rates are high because 'static' fracture modes such as cleavage and microvoid coalescence are added to the baseline fatigue crack growth rate[7].

Considerable research has been done on obtaining growth rate data of the format found in Fig. 2.4 for various materials. A high variability has been found particularly with growth rates in the near threshold region. This has been attributed to material and testing variables and to the effect of crack closure.

2.2.3. Crack Closure Effects

A crack is defined as being closed if parts of the two fracture surfaces are in contact and a force can be transmitted across them[20]. Plasticity at the crack tip, which leaves a plastically deformed wake containing residual stresses, the presence of oxides or the roughness of the fracture surface can cause premature wedging of the fracture surfaces[7, 20]. This 'wedging', or crack closure, decreases the stress intensity range at the crack tip from the applied value $\Delta K = K_{max} - K_{min}$ to some lower effective value $\Delta K_{eff} = K_{max} - K_{op}$. K_{op} is the stress intensity at which the fracture surfaces part on loading (see Fig. 2.5). ΔK_{eff} varies non-linearly with change in ΔK[7].

Differences in growth rate caused by variables such as change in mean stress, change in the stress ratio, periodic overloads, the presence of residual stresses and some environmental effects[12] can often be normalised with the introduction of the effective stress intensity factor as shown schematically for the case of mean stress in Fig. 2.6 [8,9,11,17]. Many attempts have been made to predict how the ratio :

$$U = \frac{\Delta K_{eff}}{\Delta K}\,, \tag{2.8}$$

varies with parameters such as crack length and stress ratio[11, 17], in order to simplify life predictions.

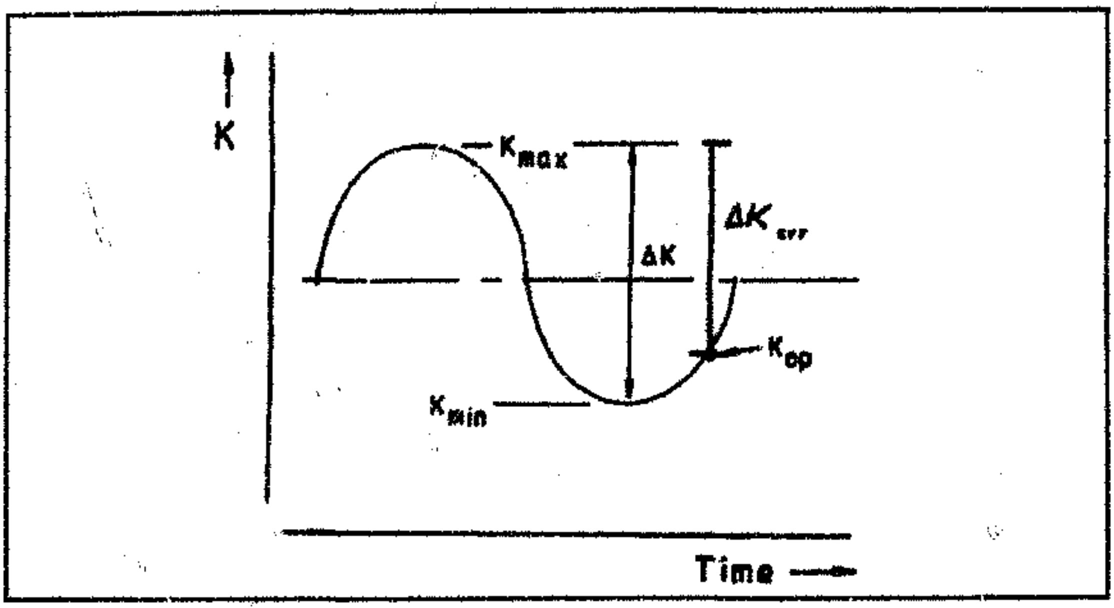

Fig. 2.5 - Characterisation of cyclic loading in LEFM terms. K_{op} is the point on the cycle where fracture surface contact is lost during loading[7].

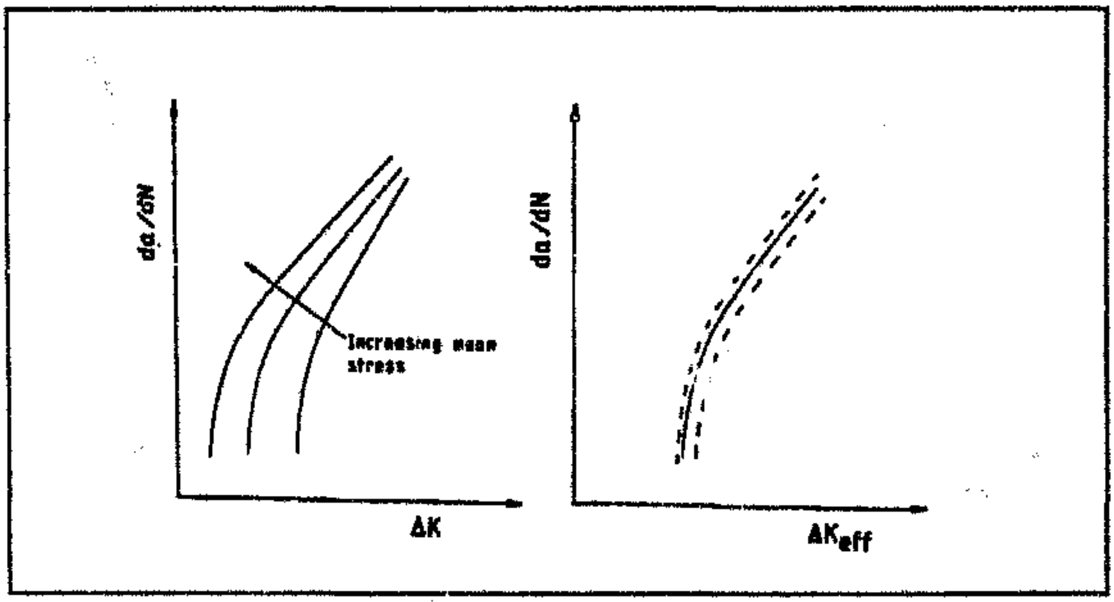

Fig. 2.6 - The observed mean stress can often be rationalised through the use of the effective stress intensity factor, ΔK_{eff}[7].

Success has been limited, however, since neither sufficiently theoretical analyses nor systematic experiments are available to enable general prediction of closure in members of arbitrary geometry and loading conditions. Crack closure loads are measured with a load-displacement recorder, where the displacement of the crack surface is measured with the respect to the load. Thus, as a load cycle is applied, a compliance curve for the cracked specimen is obtained.

This curve can be approximated by two straight lines with different slopes. The point where a change of slope is observed on unloading, corresponds to the closure load. This can be seen in Fig. 2.7. This point is not always easy to determine, since the change in slope can be indistinct. Also, since the load-displacement curves very often exhibit hysteresis, the closure load is not always the same as the opening load.

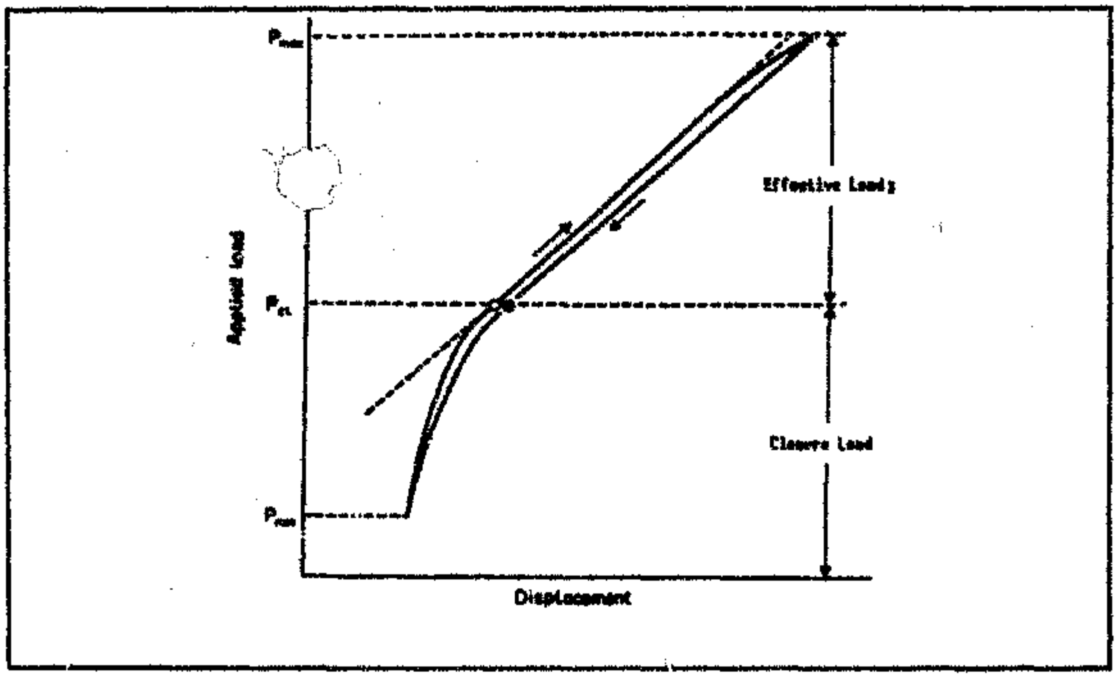

Fig. 2.7 - Typical load-displacement curve [20].

When crack closure is taken into account, ΔK_{eff} can be defined. It is thus now possible to successfully use prediction methods, based on fracture mechanics, in order to obtain the fatigue lives of components.

2.2.4. S-N Curves

Components and structures in the engineering environment are often subjected to alternating stresses which are sufficiently severe to make fatigue resistance an important design criterion. This means that one has to ensure that the component has an adequate fatigue life. This involves taking both the crack initiation and the crack propagation stages of the fatigue life into account[8]. An exact definition of the initiation and propagation stages is usually not possible. The most one can say for the two stages, as is shown in Fig. 2.8, is that in the low stress - high fatigue life regime the initiation stage contributes towards most the fatigue life.

The fatigue life of a component, N, is generally plotted against the applied stress range, $\Delta\sigma$, on a log-log or semi-log basis. When a number of specimens are tested at various stresses, a curve similar to Fig. 2.8 will emerge. Generally the data is linear, when plotted on a log-log basis, and runs out, in the case of ferrous materials, at the fatigue limit. The fatigue limit is the stress below which the component has an infinite fatigue life. For non-ferrous materials the curve does not become asymptotic at high lives and it is usual, for design purposes, to take an endurance stress limit corresponding to a given cyclic life.

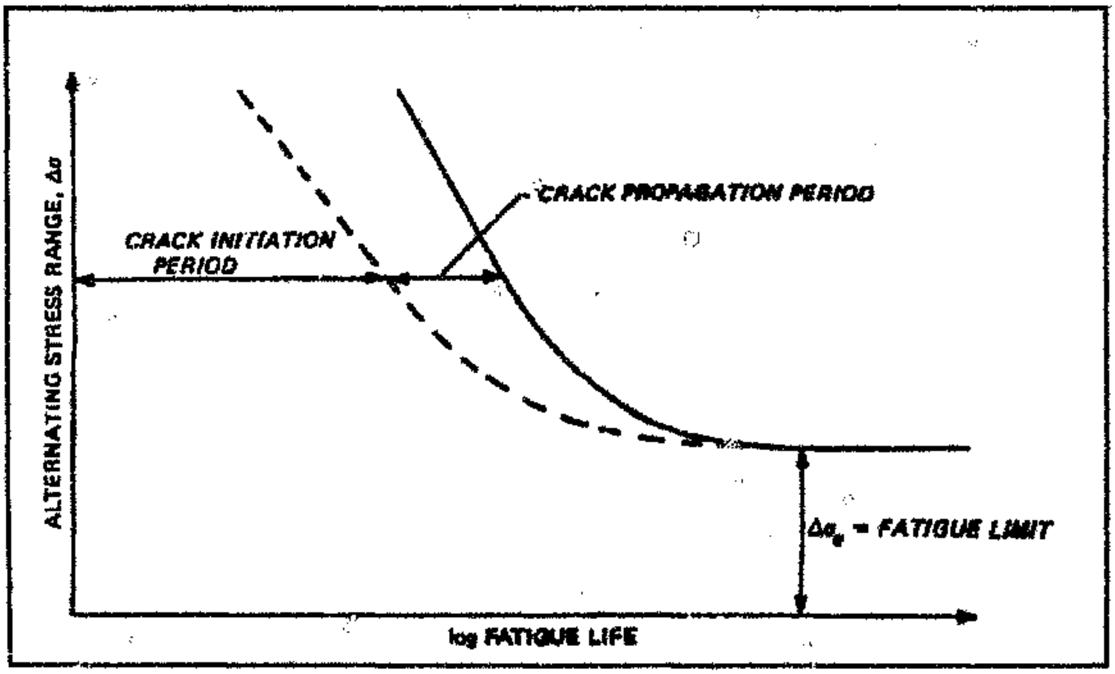

Fig. 2.8 - Schematic representation of the fatigue life and its dependence on stress levels. [8]

The stress versus fatigue life curves, or S-N curves are generally used for two types of application[8] :

1 - for predicting the fatigue life of components

2 - for presenting the fatigue life of tested components

and can include both the crack initiation and propagation periods, or relate solely to the crack propagation life for components which enter service containing cracks or crack like defects.

In the latter case, the main concern in fatigue crack growth is the number of cycles required to grow a fatigue crack from an initial crack of size a_i to a final crack of size a_f. If the loading conditions are known, i.e. the stresses at the crack tip can be found, then ΔK can be calculated. If ΔK lies in the linear regime of the fatigue crack growth rate curve of the specific material then crack growth follows the Paris Law[19], i.e. Equation 2.7. On integrating the Paris Law one obtains the following equation

$$N = C\,(Y\,\Delta\sigma\,\sqrt{\pi}\,)^{m}\left(a_f^{(\frac{m}{2}+1)} - a_i^{(\frac{m}{2}+1)}\right) \qquad (2.9)$$

where the fatigue life, N, is related to the initial crack size, a_i, the final crack size, a_f, and the applied stress range, $\Delta\sigma$. The material constants, C and m, are experimentally obtained from the fatigue crack growth rate curve for the specific material. Y is a geometry correction factor and depends on the geometry of the crack and the component[21-26]. Hence an S-N curve for an initially defected component can be constructed.

The Paris Law does not always give accurate life predictions for a component. This may be attributed to differences in parameters such as stress ratio, R, threshold stress intensity, ΔK_{th} and crack closure, which affect the fatigue crack growth[5, 12, 16]. Thus attempts have been made to find alternative equations to describe fatigue crack growth rate curves. These equations are usually semi- or completely empirical. The two most widely known alternative equation are :

$$\frac{da}{dN} = C\,(\Delta K - \Delta K_{Th})^n \quad \text{- Hartman equation} \tag{2.10}$$

$$\frac{da}{dN} = \frac{C\,(\Delta K)^m}{(1-R)\,K_c - \Delta K} \quad \text{- Forman equation} \tag{2.11}$$

The Paris equation only describes the linear regime, i.e. region II. The Hartman[29] equation also takes the threshold regime, i.e. region I, into account, while the Forman[5] equation also describes region III.

The fatigue life prediction methods described above are powerful tools which, when used correctly, can give fairly accurate results. There are, however, many factors such as residual stresses, stress concentrations, crack closure, accurate measurement of the initial defect, etc., which make the theoretical prediction of the fatigue life very difficult.

To use the classical approach to design against fatigue failure, S-N curves have to be obtained by testing specimens and components under similar conditions at various stress levels. This can become very tedious and expensive, since every curve is only valid for a specific geometry and material. In order to simplify the procedure of designing against fatigue, for the specific case of welded structures fatigue life design codes, such as BS 5400 Part 10[1] for steel and CP 118[2] for aluminium, have been developed (see section 2.5).

2.2.5. Stress Concentration Effects

Adding a weld to a component introduces a stress concentration, which in turn increases ΔK and thus the fatigue crack growth rate. To explain the effect of stress concentration we consider a uniform, smooth component with no notches whatsoever, *i.e.* a plate. When this component is loaded with an axial tensile load, P, the stress distribution across the cross section X-X of the component, in Fig. 2.9a, is uniform. The stress over the cross sectional area A, is P/A. The effect of introducing a notch by drilling a hole is to reduce the cross sectional area to A_1. Therefore, the average stress will be P/A_1. The stress distribution will no longer be uniform but will have a general form as shown in Fig. 2.9b. The peak stress at the edge of the hole will be much higher than the average stress. This type of peak stress will arise from any change in shape across the component and is known as a stress concentration[4].

The stress concentration factor, K_t, is defined as the ratio of the peak stress, S_p, to the average stress, S_{net}, *i.e.*

$$K_t = \frac{S_p}{S_{net}} , \tag{2.12}$$

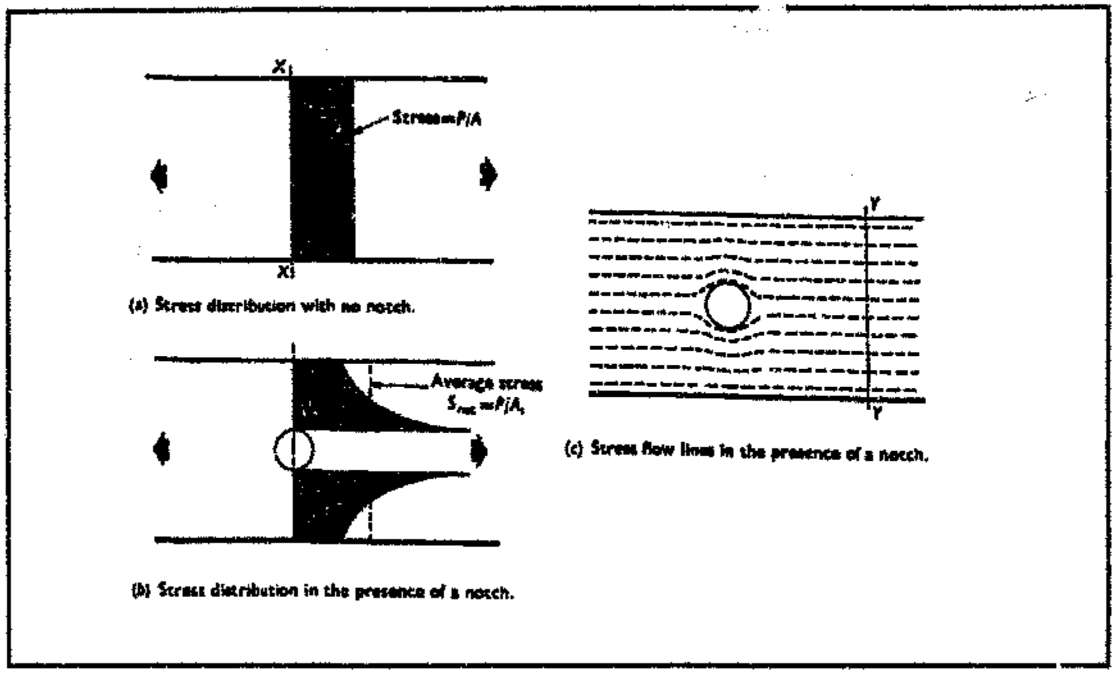

Fig. 2.9 - The effect of a notch on the stress distribution in a plate[4].

The reason for the non-uniform stress distribution across a notch can be seen qualitatively with the introduction of stress flow lines, in Fig. 2.9c. The flow lines are spaced evenly about the cross section Y-Y, which is well removed from the notch. The flow lines which would normally pass through the material are deflected from the drilled hole. Thus, the stress flow lines are more concentrated in the vicinity of the hole than they are at the edge of the plate. Hence there is a stress concentration. The stress concentration factor can be determined in several ways[4]:

1 - By placing strain gauges at strategic positions and measuring the amount of strain in the material and then extrapolating back to the point of stress concentration.

2 - By using the photo-elastic technique. This involves modelling of the component with a suitable plastic material which is then loaded and viewed under polarised light. By this method the stress patterns of the geometry can be seen and analyzed.

3 - By using a numerical finite element method. This is done with the aid of a computer software package. It requires input of the component geometry, material parameters, loading and restraining conditions. The computer will then work out an approximate stress distribution.

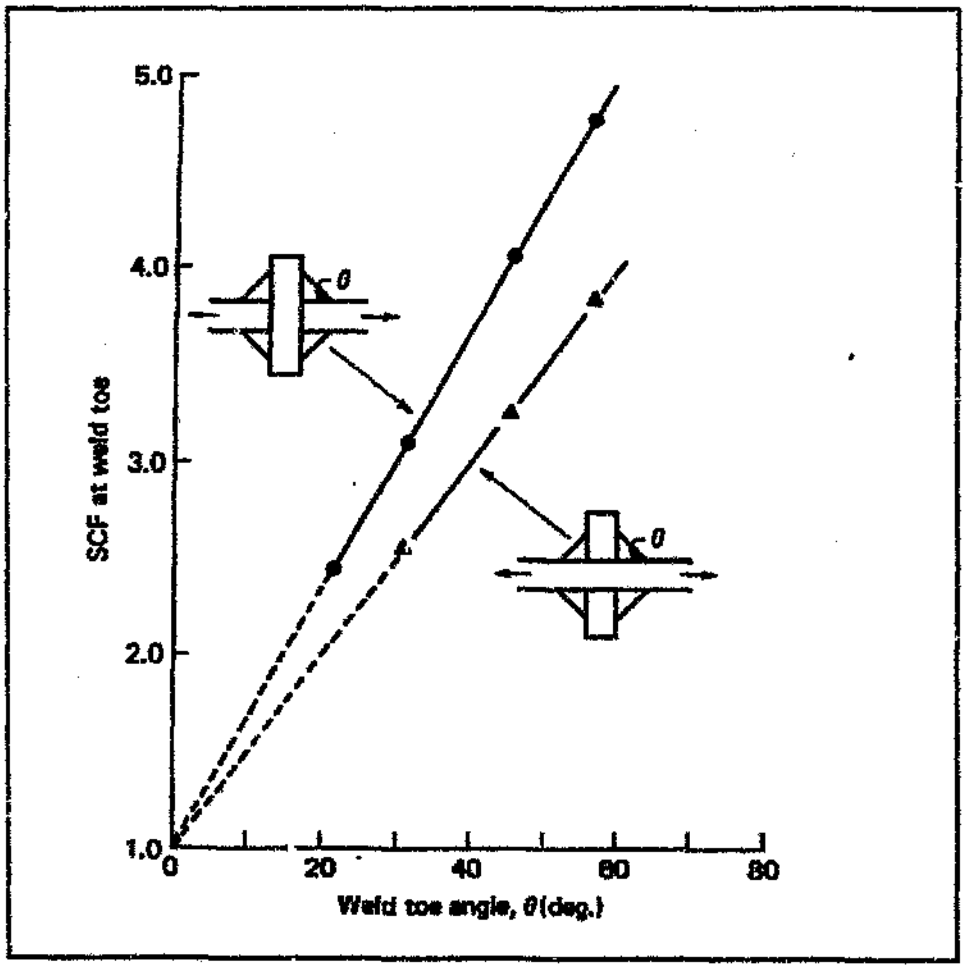

Fig. 2.10 - The effect of the weld toe angle on the stress concentration factor[21,30].

As has already been stated, stress concentrations take place at sudden changes in cross sectional area. It is therefore not surprising to find significant stress concentrations at fillet welded joints. The weld angle and size in relation to the overall joint geometry has an effect on the stress concentration factor[19-25, 31-35]. This can be seen in Fig. 2.10 and Fig. 2.11. Finite element analysis has been used by Gurney[19-21, 30] to study the influence of weld shape on load carrying and non-load carrying transverse fillet welds. As can be seen in Fig. 2.10, the angle of the weld toe seems to have a pronounced effect on the stress concentration factor, while Fig. 2.11 shows that the stress concentration tends towards a peak value as the ratio of weld leg length / plate thickness is increased.

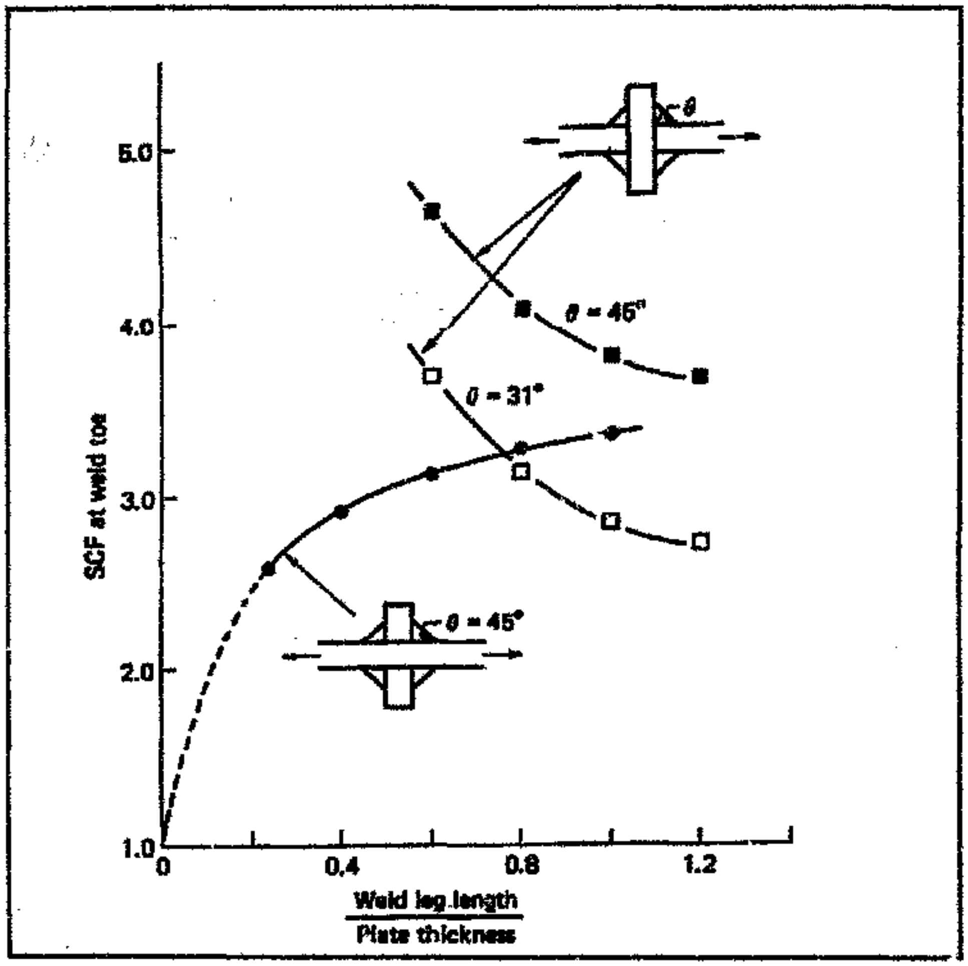

Fig. 2.11 - The effect of the weld size on the stress concentration factor[21, 30].

Niu and Glinka [35] analysed the effect of stress concentration on the weld profile and confirmed the above mentioned effect of the weld angle on the stress concentration. They also analyzed the effect of the weld toe radius on the stress concentration. They showed, in Fig. 2.12, that as the weld toe radius is decreased, the stress concentration factor is increased.

It should be noted that defects due to welding are often sharp or crack like, and hence are often the cause of high local stress concentrations even if the general geometry is smooth and has a low K_t. It is thus important to take into account the presence of such defects when modelling with finite elements.

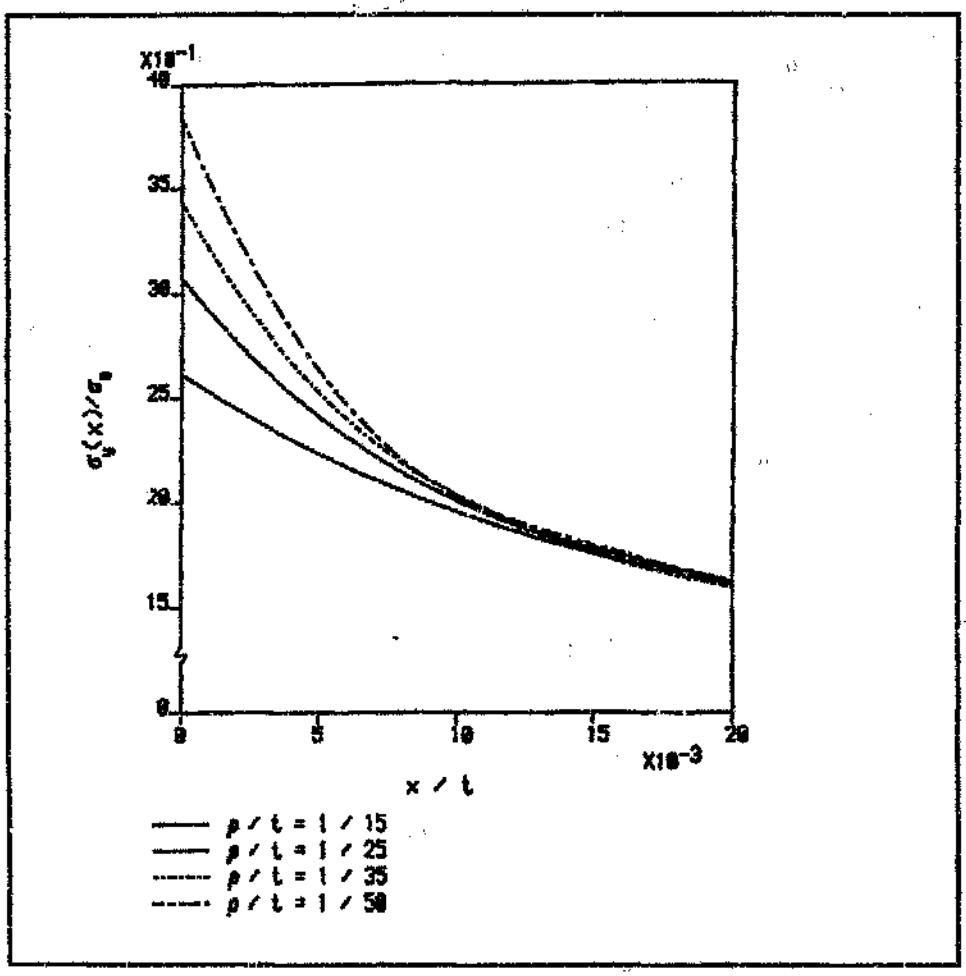

Fig. 2.12 - The effect of the toe radius, ρ, on the stress concentration factor, where t is the plate thickness and x, the distance into the plate[35].

When a crack is in the vicinity of a stress concentration the stresses local to the crack tip are increased by a certain factor, M_k, and thus the stress intensity will also be affected by the same factor. M_k is thus the geometry correction factor which allows for an increase in the stress intensity factor due to the presence of a stress concentration. For an infinitely small crack depth M_k is equal to the stress concentration factor, K_t. As the crack grows, the crack tip moves away from the stress concentration feature so that M_k decreases with increasing crack depth. The value of M_k can be determined with the aid of finite element stress analysis.

Maddox(10) and Glinka(25) obtained a relation for M_k with respect to crack depth, a/B, for transverse non-load carrying fillet welds. This is shown in Fig. 2.13, where for a small crack, M_k is high. As the crack grew, M_k decreased rapidly. As a/B reached about 0.1, M_k hardly decreased any more with an increase in crack size. They also showed that M_k increased with the weld toe angle.

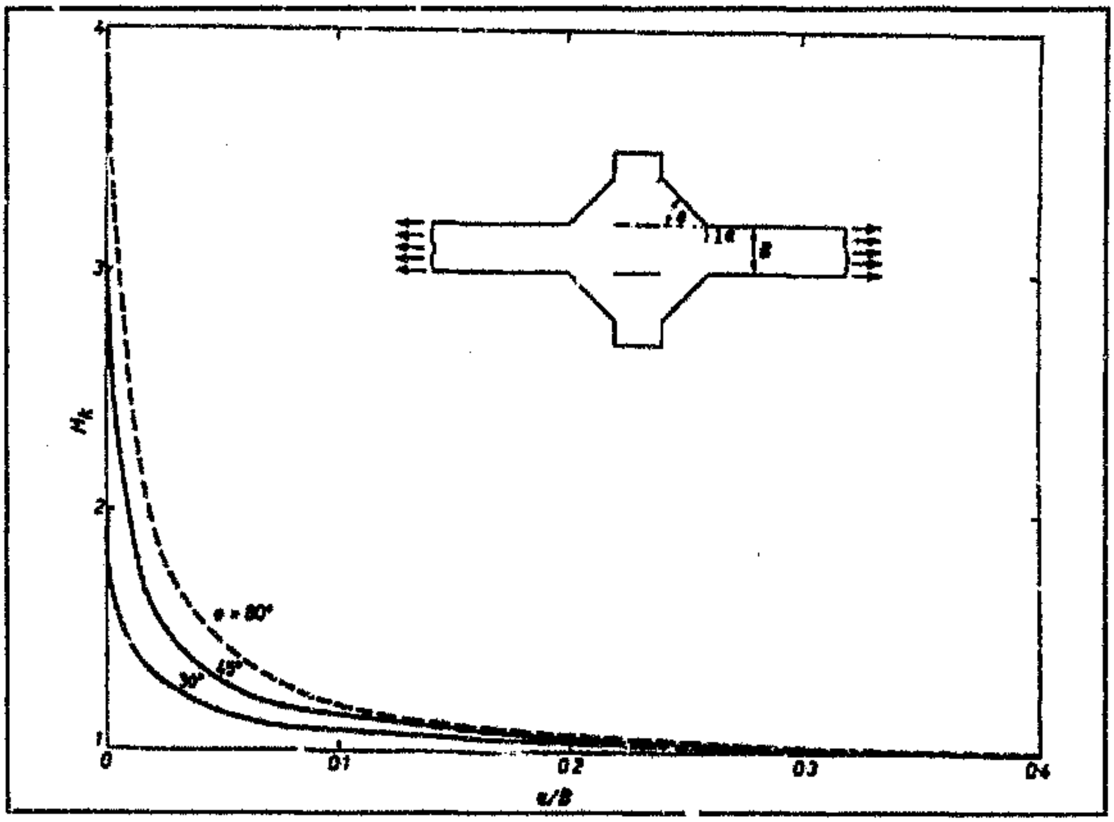

Fig. 2.13 - Variation of stress concentration factor, M_k, with crack depth for various weld toe angles (10).

Gurney *et al*[21] carried out a 2-D finite element stress analysis for fillet welded joints (a/2c=0, plane strain) using a range of weld sizes and plate thicknesses. They derived the following formula for the correction factor at the weld toe

$$M_k = 0.7297\left(\frac{l}{B}\right)^{0.068}\left(\frac{a}{B}\right)^{-0.2796} \qquad for\frac{a}{B} \leq 0.05 \tag{2.13}$$

$$M_k = 1.0 \qquad for\frac{a}{B} \geq 0.325$$

where l is the weld leg length.

2.2.6. Metallurgy and Mode of Fracture of 6XXX Aluminium Alloys

If one wants to study the fatigue behaviour of a certain material one needs to understand why the material behaves in the way it does and what makes it different to other materials. In order to do this some background knowledge of the production and metallurgy of the material is required. This will assist in the determination of micro-mechanisms of crack growth which may take place during fatigue.

The primary alloying elements of the 6XXX series aluminium alloy are magnesium and silicon which form the Mg_2Si binary phase[36]. The single binary phase in the magnesium-silicon system forms a quasi-binary system with aluminium and with the binary intermetallic phases of the aluminium-magnesium system. No ternary intermetallic phases are formed.

The ternary phase diagrams of the aluminium, magnesium and silicon system, showing the liquidus surface and the solvus surface, are shown in Fig. 2.14 and Fig. 2.15 respectively. Fig. 2.16 shows the quasi-binary phase diagram of aluminium and magnesium silicide. The limits of solubility of the aluminium-magnesium system is shown in Fig. 2.17.

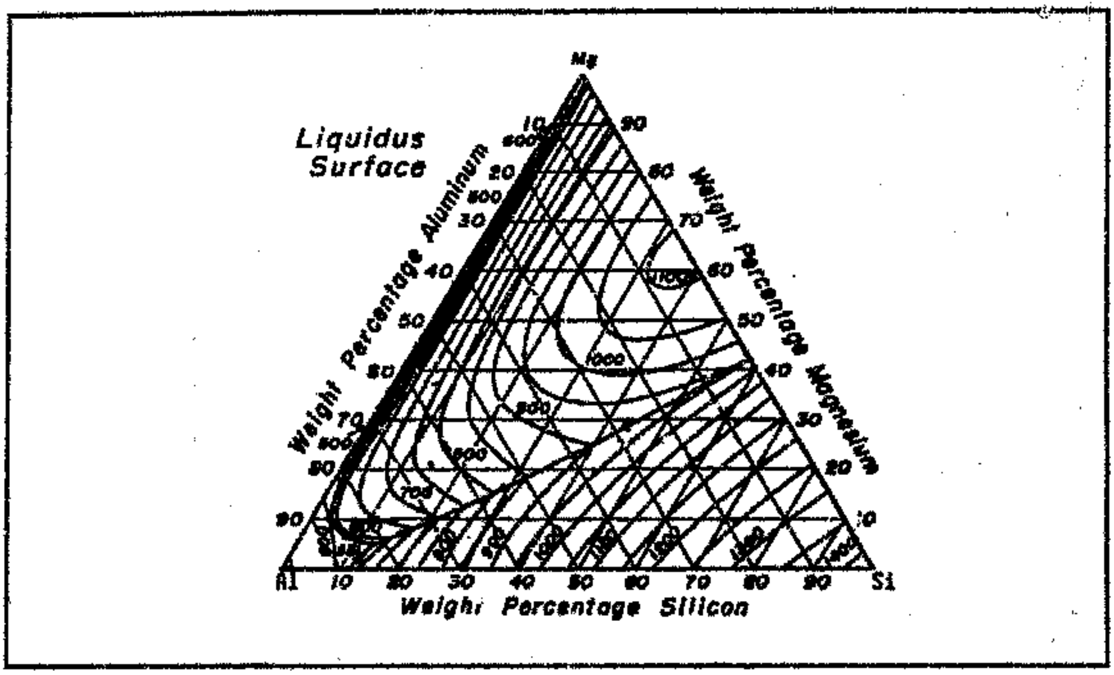

Fig. 2.14 - Ternary phase diagrams of the Al-Mg-Si system showing the liquidus surface.[36]

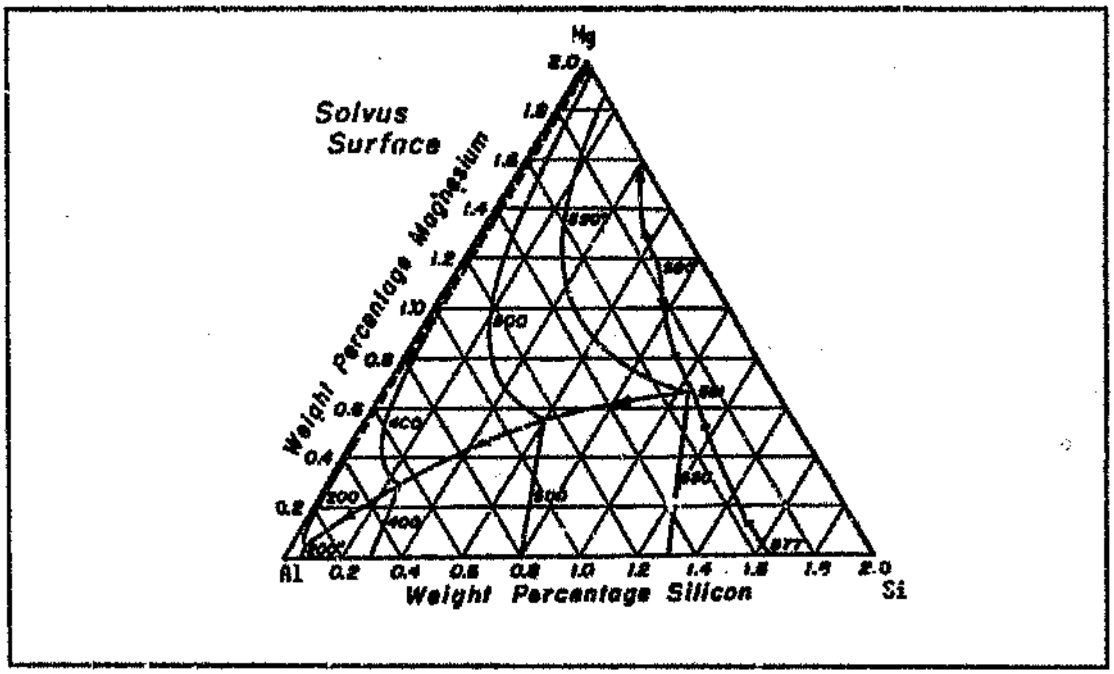

Fig. 2.15 - Ternary phase diagrams of the Al-Mg-Si system showing the solvus surface.[36]

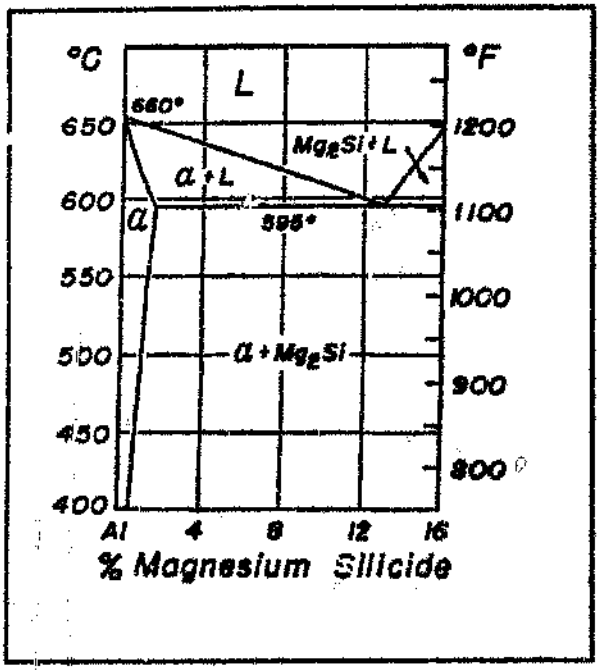

Fig. 2.16 - The quasi-binary phase diagram of the Al-Mg_2Si system.[36]

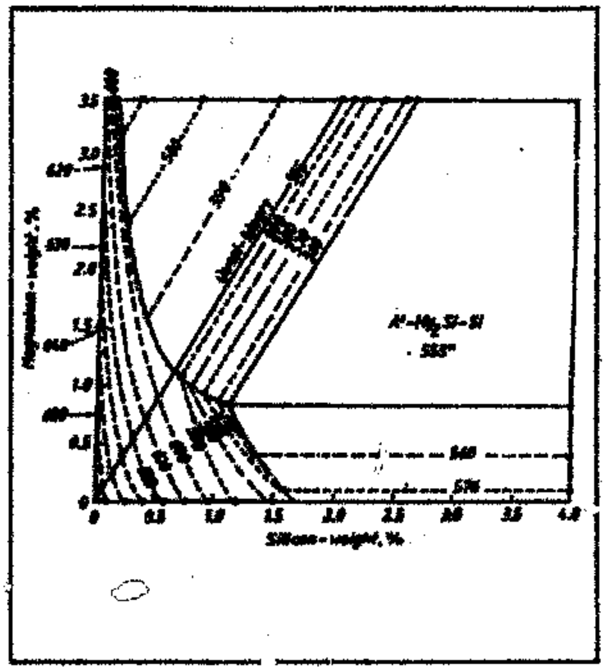

Fig. 2.17 - Limits of solubility of the Al-Mg-Si system.[36]

A knowledge of the limits of solubility in this alloy system is of great importance because of the wide range of solubility along the quasi-binary line. A marked decrease in solid solubility with temperature renders these alloys susceptible to heat treatment for improved mechanical properties. It is thus important to know how the relationships are affected by an excess of magnesium or silicon over that required to form Mg_2Si.

The reaction between magnesium and silicon is a balanced one, requiring an excess of either magnesium or silicon for its completion[36]. It is therefore possible for free silicon or magnesium to appear as a micro-constituent in these alloys.

Under equilibrium conditions, Mg_2Si does not appear as a constituent of the eutectic until a magnesium content of about 0.8 per cent has been reached. The aluminium-rich phase is incapable of reaching saturation during casting. This results in the appearance of Mg_2Si at as little as 0.2 per cent magnesium.

The quenching of a Al-Mg-Si commercial alloy from high temperatures produces a supersaturated solution of magnesium and silicon in α-aluminium. Clusters of Mg_2Si survive however, since the attraction between magnesium and silicon is very high. On tempering at about 175°C the solute atoms migrate out of the α phase to form Mg_2Si dispersoids. The hardness obtained after quenching and tempering is due to the dispersion of Mg_2Si in the α phase, while α itself is hardened by the excess of magnesium or silicon compared with the stoichiometric Mg_2Si ratio.

Commercial 6XXX series, heat treatable aluminium alloys generally contain a high density of fine coherent or semi-coherent particles of the precipitating phase, i.e. Mg_2Si, which are its source of strengthening. In addition, two types of incoherent particles are present[37,38]. These are the coarse (>1 μm) particles which originate during casting and are linked to the iron impurity content in the alloy, as well as the fine, intermetallic particles approximately 0.1 μm in size and consisting of the transition elements Cr, Mn, Zr, or V. These elements are usually added to inhibit recrystallisation and to control grain growth during heat treatment. The dispersoid particles are formed during homogenisation and hot working of the alloy[38]. These dispersoids have been shown to promote homogenisation of slip and thereby increase the tensile ductility and fracture toughness of the alloy.

The effect of dispersoids on fatigue crack propagation is not very clear cut. It has been shown that rod-like Cr bearing dispersoids which are commonly present in ASTM 7075 alloys accelerate the rate of propagation of fatigue cracks[37]. This is apparently due to the fact that the particles fracture ahead of the crack tip, thus accelerating crack growth.

In work concerned with equiaxed, Mn bearing dispersoids, it could be shown that the particles did not break, even in regions of high plastic strain. Edwards and Martin[37] used three different peak aged Al-Mg-Si alloys with different volume percentages of equiaxed dispersoids to establish the effects of these particles on the fatigue properties. They showed that for any one alloy, the degree of intergranular failure increased with ΔK and hence with the fatigue crack growth rate. For any given applied ΔK however, the degree of intergranular failure decreased as the volume fraction of dispersoids increased. Additionally, the fatigue crack growth rate decreased as volume fraction of dispersoids increased. The increase in fatigue crack growth rate is therefore generally accompanied by increased amounts of intergranular failure.

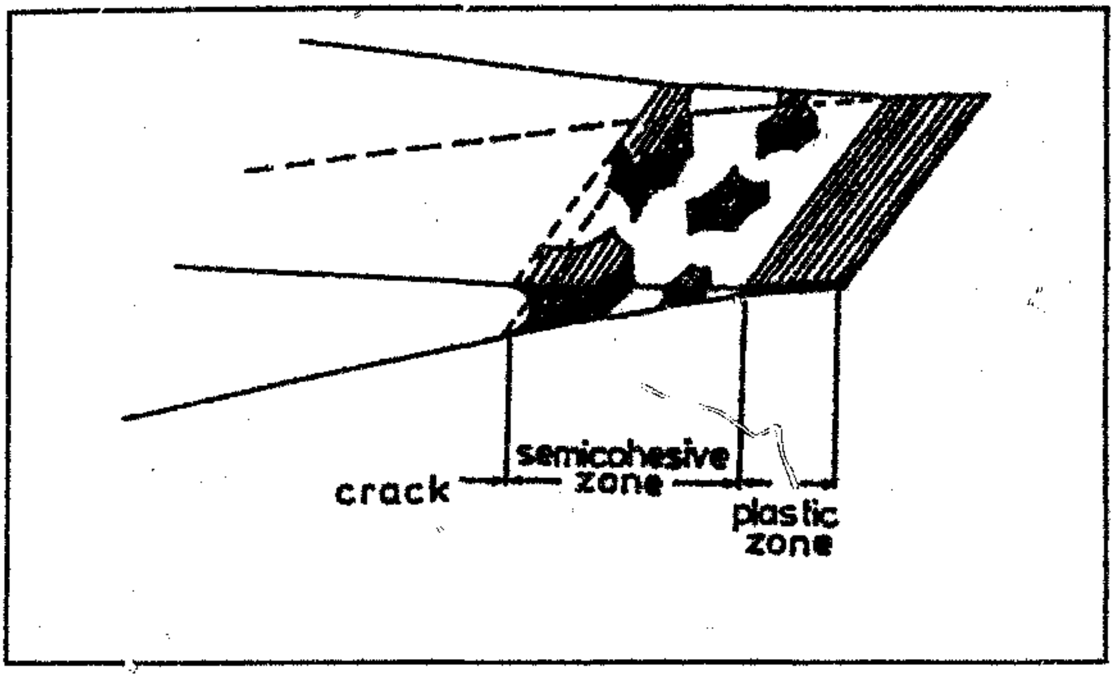

Fig. 2.18 - Schematic illustration of the semi-cohesive zone at the crack tip[37].

The decrease in intergranular failure with increase in volume fraction of dispersoids is due to the homogenisation of slip by the dispersoids. Raymond and Martin[38] have studied the effect of dispersoids in the crack tip zone. They suggest that if a critical local strain is required to cause failure at the grain boundary, the homogenisation of slip by the dispersoids will lead to larger overall strains being required in order to reach the critical local grain boundary fracture strain. A crack subjected to the same stress intensity, will therefore experience less intergranular fracture if the homogenisation of slip is increased.

In the work done by Edwards and Martin[37] it is clearly shown that only a percentage of the various fracture surfaces are intergranular. The rest of the surface has a transgranular appearance consisting primarily of striations. On closer examination of the intergranular fracture regions, the fracture surface was seen to be covered in fine dimples. This indicated that the failure mechanism was by microvoid coalescence along the grain boundary precipitate free zone (PFZ). The spacing of the dimples (0.1 μm) was similar in size to that of the grain boundary precipitates.

Thus it was suggested by Edwards and Martin[37] that the micro-mechanisms of fatigue crack growth, in peak aged Al-Mg-Si alloys, can be explained in terms of a main crack, a semi-cohesive zone and a plastic zone, as shown in Fig. 2.18. Grain boundaries orientated favourably ahead of the crack tip will fracture by microvoid coalescence along the PFZ. The resulting fracture surface will be kept apart by the remaining ligaments. These will undergo reversed plastic deformation. The fine microvoids, which were formed on the intergranular fracture surface will thus be preserved. The restraining ligaments will fail by a reversed plastic fatigue process, which at levels of ΔK in the Paris regime, will probably lead to fatigue striations.

Welding can affect the microstructure of aluminium alloys. In the case of the 6XXX aluminium alloy, welding would age the parent material which in turn would increase the Mg_2Si dispersoids volume fraction and decrease the fatigue crack growth rate[37].

The extent of the heat affected zone (HAZ) in aluminium used to be estimated by the "1-inch" rule (25mm). This states that the parent plate will be softened up to 25mm away from the weld bead. Beyond 25mm, the parent plate resumes its original hardness. By using classical heat flow theory, Robertson and Dwight[39] have proposed a better approximation than the "1-inch" rule.

They classified the HAZ into two variables:

1 - The extent, *i.e.* the size of the HAZ.

2 - The severity, *i.e.* the amount of softening.

On testing the HAZ for hardness, Robertson and Dwight showed that the extent of the HAZ can be subdivided into three zones. Zone A is immediately next to the weld bead and has a low, but constant hardness. Bordering on zone A is zone B, which gradually increases in hardness until zone C is reached, where the properties of the parent plate are resumed[39, 40]. A schematic representation of the various zones is shown in Fig. 2.19.

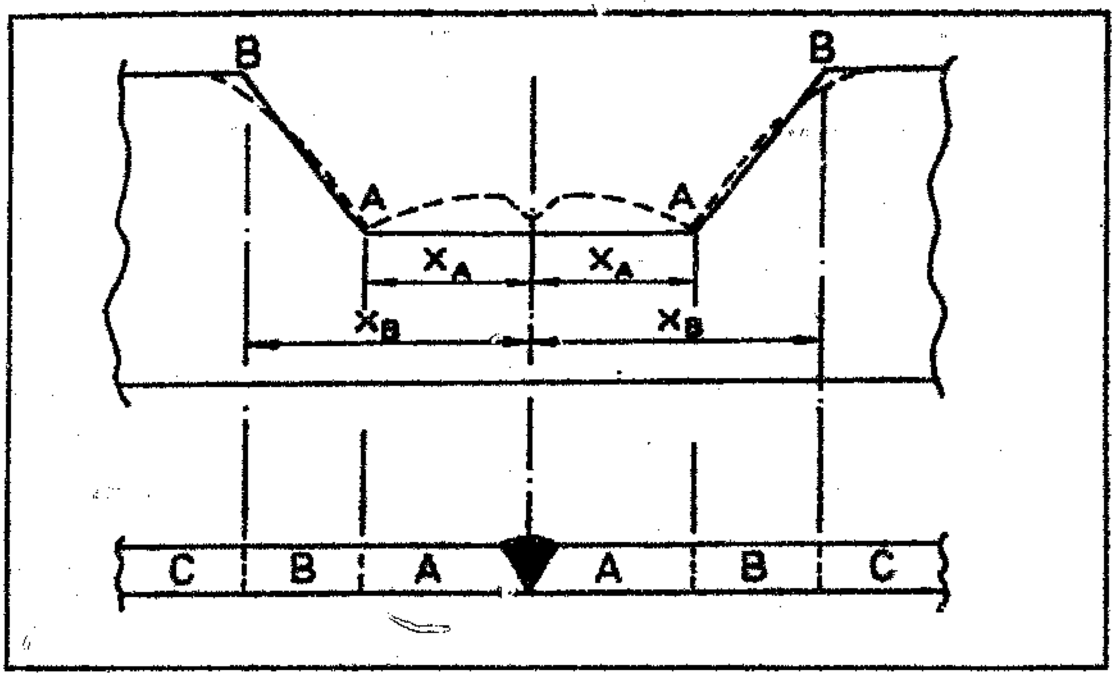

Fig. 2.19 - The simplified pattern of the HAZ hardness compared to the actual hardness[26].

The size of zone A, X_A, and the size of zone B, X_B, are dependent on the heat flow, parent plate thickness and material.

The severity of the HAZ is quantified by the ratio,

$$s = \frac{H_A}{H_P} \tag{2.14}$$

where H_A is the approximate minimum hardness of zone A and H_P is the hardness of the parent plate.

2.3. Effects of Welding on Fatigue

2.3.1. Classification and Crack Initiation Sites

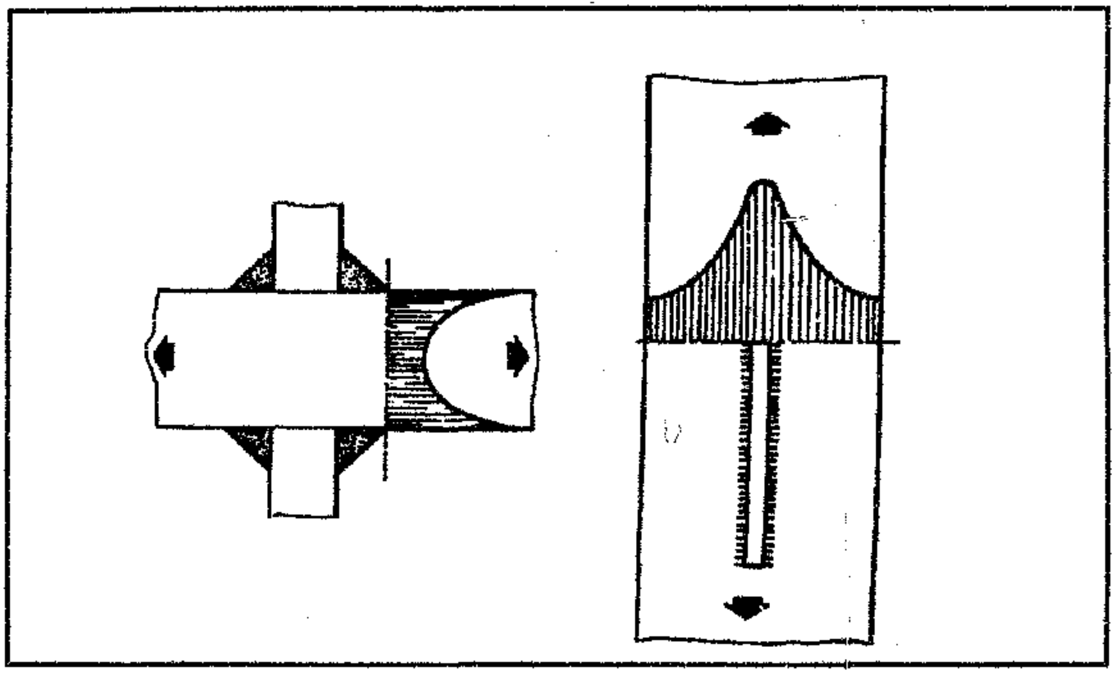

Fig. 2.20 - Stress distribution in (a) transverse and (b) longitudinal non-load carrying fillet welded joints.[4]

Fillet welds can be classified into four categories : load carrying welds, non-load carrying welds, welds transverse to and welds parallel to the direction of stress. A load carrying weld is defined as any weld through which all the load of the section is transmitted. A non-load carrying weld is not entirely load free, since it will be strained by the load carrying member on which it is welded.

Fig. 2.20 shows a qualitative stress distribution for non-load carrying welds. It should be noted that although the stress distribution along the length of transverse welds may be uniform, the stress distribution across the width of the welds varies since there is a high stress concentration at the weld toe. It is therefore logical to predict that fatigue cracks will initiate at the weld toe.

Alternatively, in longitudinal welds, it is the weld ends which give rise to stress concentrations and the stress distribution along the width and through its thickness is non-uniform. Thus, the weld end would be the favoured initiation site for cracks[4].

Transverse, load carrying welds experience a stress concentration at the weld root, while the longitudinal load carrying welds tend to transmit the majority of the load by shear towards the ends and less towards the centre.

2.3.2. Welding Defects

Welding defects such as lack of penetration, shrinkage cracks and porosity may be. introduced into a component during welding and are in many cases the reason why the life of the component is dominated only by the fatigue crack growth stage and not by the fatigue crack initiation stage.

Lack of penetration refers to the incomplete fusion of the weld metal with the parent plate and can exist almost at any level of severity from local to general. It may occur as an internal or surface defect[4,41].

Shrinkage cracks are the result of excessive shrinkage in the weld and may either lie parallel or transverse to the direction of the weld. The extent of cracking is directly related to the solidification rate of the weld metal and the problem can be overcome by controlling the heat input during welding and the use of preheat. In aluminium alloys, the shrinkage cracks usually lie parallel to the direction of the applied stress and are situated in the weld metal. Cracking at, or adjacent to, the weld boundary can occur if unsuitable filler materials are used[4,41].

Porosity in the weld metal is caused by the entrapment of gas during solidification. The pores are usually spherical in shape and may exist locally or throughout the weld. The pores may be as large as 5 mm in diameter. The weld porosity is generally caused by insufficient gas shielding surrounding the arc. This is often due to draughts or large distance between the electrode tip and the weld pool. Nitrogen is thereby introduced into the arc area and can penetrate the liquid weld metal[4,41,42].

Residual stresses exist in a structure when a geometrically incompatible structure is forced to be compatible. This is often done by bending, clamping or welding. Welding itself produces local residual stresses.[4, 8, 41] As is shown in Fig. 2.21a, it is assumed that immediately after welding, the weld is hot and the component is cold and that each of the elements are of the same length. If the elements were separate, the situation after the weld has cooled down would be that of Fig. 2.21b, with the weld having contracted in relation to the component. The elements, however, are not separate. This state can only exist as a result of the stresses as shown in Fig. 2.21c. The resulting stress distribution is shown in Fig. 2.21d and Fig. 2.21e. Thus, parallel to the direction of the weld, there will be tension in the weld and compression in the component. The distribution of residual stresses due to welding is the result of a number of parameters. Of these, the effect of geometry, *i.e.* length, width, thickness and the number of welding passes has the greatest effect on the residual stress distribution[4, 8].

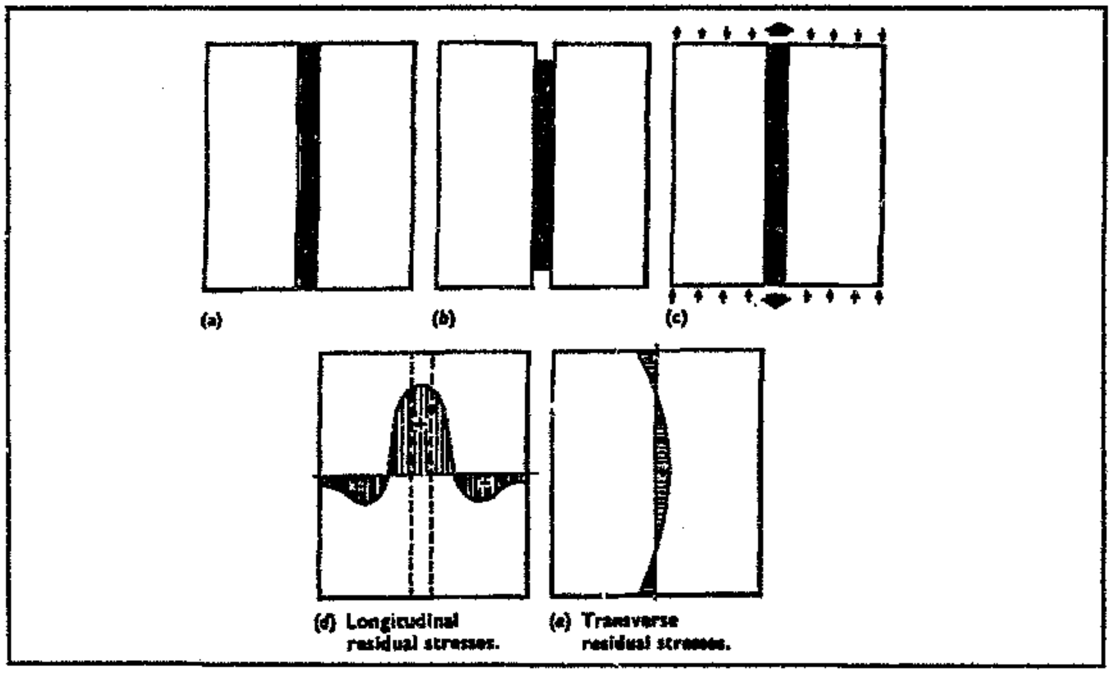

Fig. 2.21 - The formation of residual stresses around a welded joint[4].

When a structure containing residual stresses is loaded the internal stresses will be the sum of the applied and the residual stresses. The aim of designing against fatigue, is to have as few high tensile stress regions as possible, since a crack will initiate and grow much faster at high tensile stresses than at low ones. Thus, decreasing residual stresses or even making them compressive, will in most cases increase the fatigue life[3,7,43].

2.3.3. Life Improvement Techniques

The introduction of a weld into a joint can drastically reduce the fatigue strength of a component[33]. It is usually found that the design stresses of structures are limited by the fatigue strength of the welded components. There are several guidelines regarding the design of welded structures, e.g. BS 5400 Part 10[1]. The fatigue performance of many metal structures, such as bridges and offshore rigs, is limited by the welds made in critical stress areas. It is therefore often desirable to increase the fatigue lives of critical weld joints. There are three fundamental methods of improving the fatigue life of these joints [4, 41]:

1 - Reduction of local stresses by improving the structural design. By designing for lower local stresses and less structural vibration, many fatigue problems can be reduced or even eliminated.

2 - Using joint detail with higher fatigue strengths, e.g. by welding in a workshop under controlled conditions instead of welding at the site, the joint class is increased from Class E to Class D in BS 5400 Part 10[1].

3 - Local treatment of joint detail such as weld toe grinding, TIG dressing, etc. [41,43].

Use of the first two improvement methods is often not technically possible or economically viable. Thus, local joint treatment will often be the only available method to improve the fatigue life of the structure. The application of local treatment on welded joints can be divided into two broad groups:

1 - Modification of the weld profile.

2 - Modification of the residual stress distribution.

When the weld profile is modified, material is either added or removed, or the shape of the profile is changed. In welds, the potential crack initiation site depends on the geometry of the weld joint. In the case of non-load carrying fillet welds, fatigue cracks may initiate at the weld toe and propagate through the parent plate until failure occurs. By increasing the throat size of the weld, using additional weld overlays, the stress concentration at the weld toe is reduced and the fatigue strength of the weld joint is increased. As the weld size is increased, the fatigue strength of the joint will increase until the crack initiation site is transferred from the toe to the root. Any further increase in the weld size will not increase the fatigue strength. The purpose of modifying the weld profile is thus to increase the fatigue performance by changing the existing high stress concentration caused by the weld profile, non-metallic inclusions and undercut[41-46]. Such improvements will result in a smooth transition between the weld metal and the parent plate. The processes that are used to modify the weld profile are local machining of the weld toe and TIG dressing.

If the applied stresses are fully tensile the whole of the stress range contributes towards the fatigue process. If, however, the applied stresses are partly compressive, the fatigue crack may be subjected to crack closure. As a result only part of the stress range will contribute to the fatigue process. Thus, if compressive residual stresses are placed in the region of the crack tip, the fatigue crack growth rate will be reduced[41,43].

Introducing compressive residual stresses to the material is often done to increase the fatigue life of the member. This is generally applied in areas where fatigue cracks are most likely to occur. Processes which introduce local compression to a potential fatigue initiation site at a weld are overloading, peening, shot blasting, local compression and spot heating.

Work performed at the Welding Institute, Abington, has assessed the various fatigue life improvement techniques on transverse and longitudinal fillet welds[4, 41]. The results for the transverse non-load carrying fillet welded steel specimens are shown in Fig. 2.22. Overloading is the least beneficial process followed by weld toe grinding and peening. TIG dressing seems to be the most beneficial process. Fig. 2.23 shows that for the longitudinal, non-load carrying, fillet welded specimens, overloading gave the least desirable results. Peening, pressing and spot heating gave very similar, but better results.

Most of the fatigue data seem to converge at high fatigue strengths and approach that of the as-welded condition. As the fatigue strength is lowered, the differences between the various techniques becomes more obvious. It also seems that the fatigue limits of the improved specimens are higher than that of the as-welded condition. This leads to the conclusion that improving the welded joints is only justified if the stresses applied are relatively low.

The fatigue improvement of the weld is expensive and dependent on the process used. Cost should therefore be taken into account when deciding which improvement process should be used.

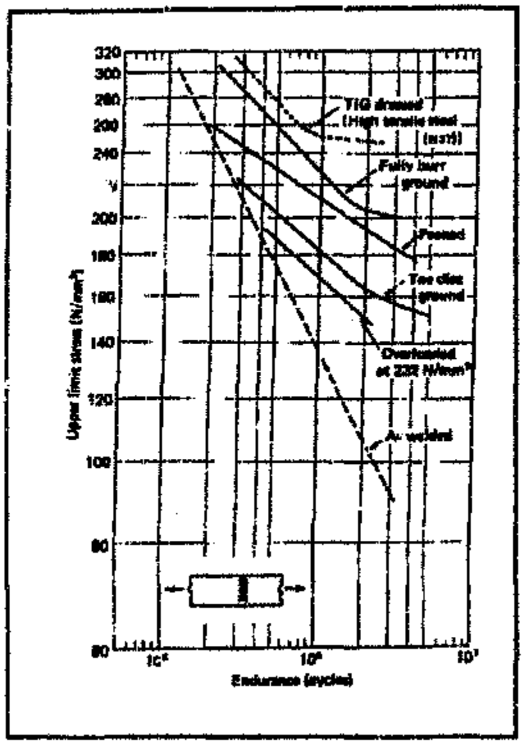

Fig. 2.22 - The comparison of improvement methods for mild steel specimens with transverse, non-load carrying, fillet welds[4].

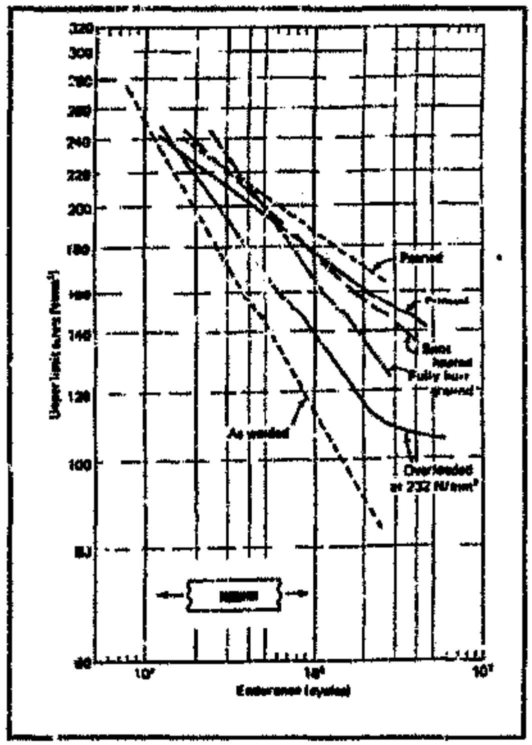

Fig. 2.23 - The comparison of improvement methods for mild steel specimens with longitudinal, non-load carrying fillet welds[4].

2.4. I-beams with Cover Plates

As was previously discussed, it is clear that the most critical factor in determining the fatigue strength is the degree of stress concentration in the specimen. There will be, for all practical purposes, no stress concentration in a rolled or extruded I-beam. It is thus not surprising that the fatigue strength of the plain I-beam is almost identical to that of a plate subjected to the same stresses[4].

In research done by Fisher *et al*[3], cracks in rolled steel I-beams originated only at the tension flange. Some cracks initiated at the fillet between the web and the tension flange, where a transition in the fillet caused a stress concentration. Others initiated at the tension flange tip. No distinct notch was visible and the cracks seemed to originate from random flaws on the rolled surface of the flange.

Cover plates are widely used on I-beams to improve the section modulus of the beam. Therefore, by welding a cover plate over only the high stressed region of the beam , the I-beam can carry higher static loads in bending. It also saves on material costs, since only the highly stressed regions receive extra material. If however, the beam is subjected to dynamic loading, the fatigue strength is reduced by a considerable amount[1, 3, 4], due to the introduction of a high stress concentration at the weld ends or weld toes perpendicular to the axis of the beam.

2.4.1. Effect of Stress Variables on Fatigue Life

It is a well established fact that tensile residual stresses of yield strength magnitude are present in as-welded structures[3, 4, 41]. As a result of this, it has been shown that the fatigue life of steel I-beams with welded cover plates is independent of the mean applied stress and depends only on the stress range[3]. Fisher *et al*[3] tested steel I-beams, with cover plates, to determine the effect of mean stress on the fatigue life. They varied either only the maximum stress, S_{max}, or only the minimum stress, S_{min},in their testsThe results, which are shown in Fig. 2.24, show that the stress ratio, R, had no clear effect on the S-N data, when R varied between -1.4 and 0.7.

In aluminium there are indications that the tensile residual stresses do not reach the yield point[49] of the parent plate. This is due to the softening effect of welding on the microstructure. They are, however, generally high enough to counteract any compressive applied stresses, so that the local stress at the crack tip is always tensile. Thus the fatigue life of aluminium beams, with cover plates, should also be independent of the mean applied stress. This was confirmed by Niemi *et al*[50] and Aabo[51] *et al* who stated that there was no evident effect on the R ratio on fillet welded aluminium 6061-T6 joints.

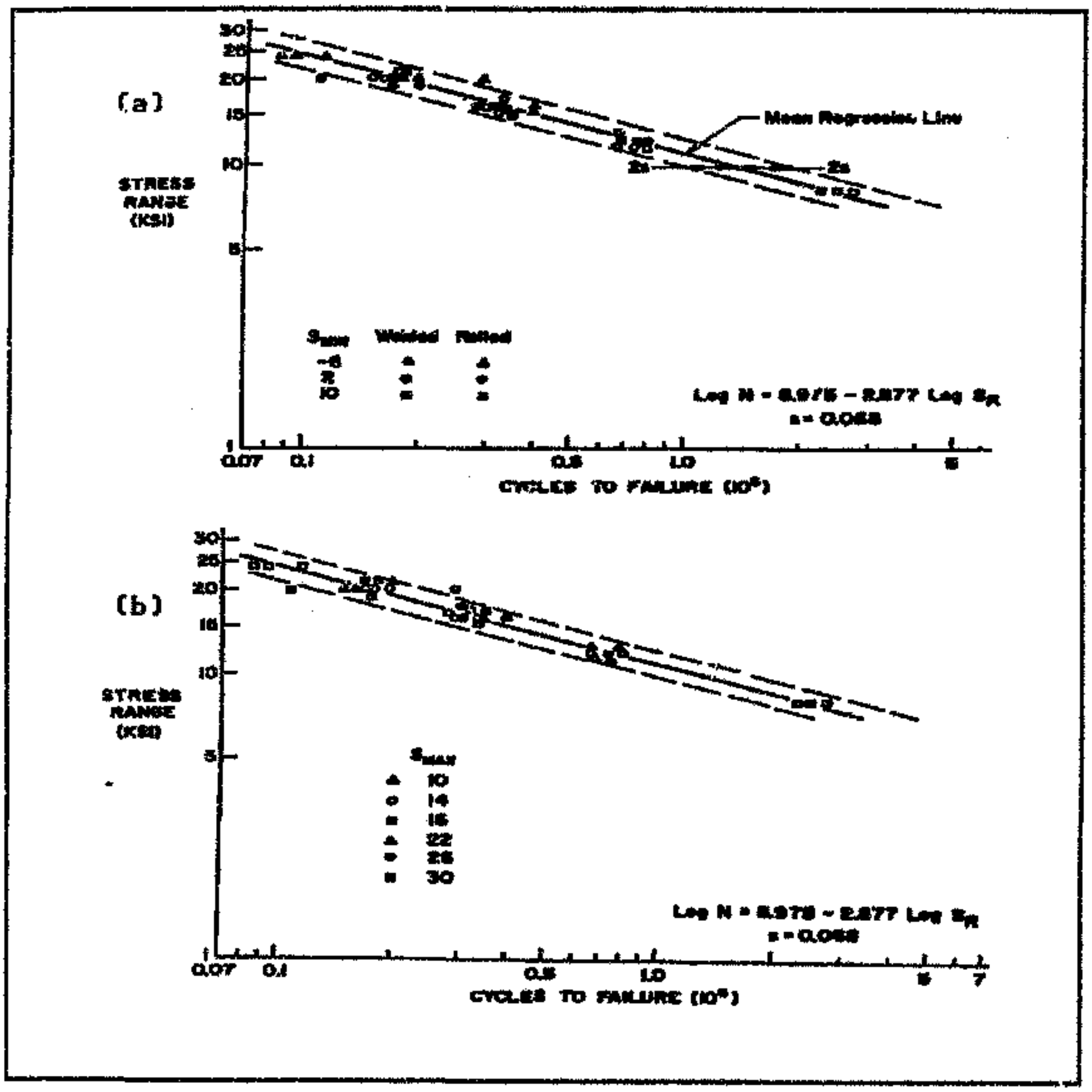

Fig. 2.24 - The effect of stress range and minimum stress (a) or maximum stress (b) on the fatigue life of cover plate welded steel beams[3].

2.4.2. Effect of Cover Plate Geometry on Fatigue Life

Fischer *et al*[3] tested steel I-beams with various cover plate geometries. Theses consisted of cover plates which were rolled to the same thickness as the flange but were less wide than the flange, cover plates which were thicker than the flange and cover plates which were wider than the flange. I-beams with multiple cover plates were also tested. The cover plates were attached either with end welds, i.e. welded ends, or with out end welds, i.e. unwelded ends. The results of the tests that Fischer carried out are shown in Fig. 2.25 and Fig. 2.26.

Superposition of the welded end and unwelded end data, as seen in Fig. 2.27, indicates that the fatigue behaviour of all these cover plate geometries was essentially the same. The linear regression line for each of the end weld details is shown in Fig. 2.27. From this it can be clearly seen that the geometries without end welds had longer lives than those with end welds. The only exception to this rule was for the cover plate geometry which was wider than the flange.

Here the trend was reversed. The significantly shorter lives of the cover plates which were wider than the flange and had no end weld could be attributed the elimination of 'Stage 1' crack growth (see Section 5.1.1.). The weld was situated at the flange tip causing 'Stage 3' crack growth to occur immediately. The crack growth pattern of the cover plate geometry which was wider than the flange and which had a welded end was similar to that of the other geometries. The fatigue life of this geometry is thus comparable to that of the other geometries.

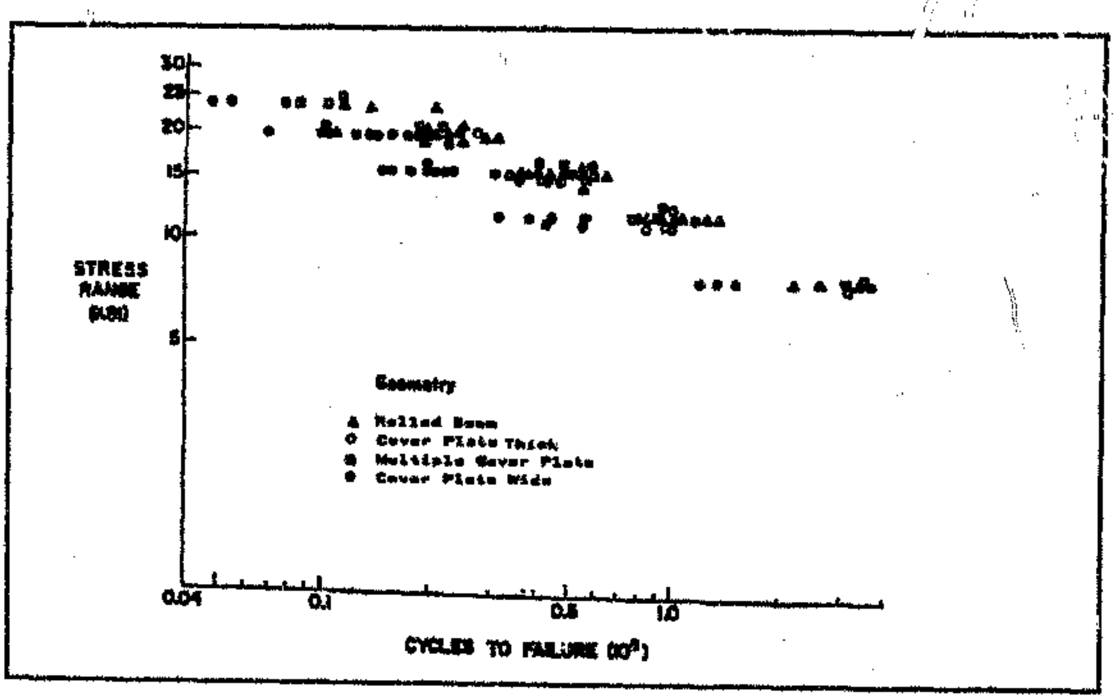

Fig. 2.25 - Effect of cover plate geometry on the fatigue strength of cover plated beams without end welds[3].

In all the geometries where the cover plate was narrower than the flange, it was observed that most of the fatigue life was consumed in initiating and propagating the crack through the thickness of the flange. The number of cycles corresponding to the 'Stage 1' of crack growth was observed to be almost the same for both end details. The difference in life between the two end details must therefore be due to the differences in the later stages of crack growth.

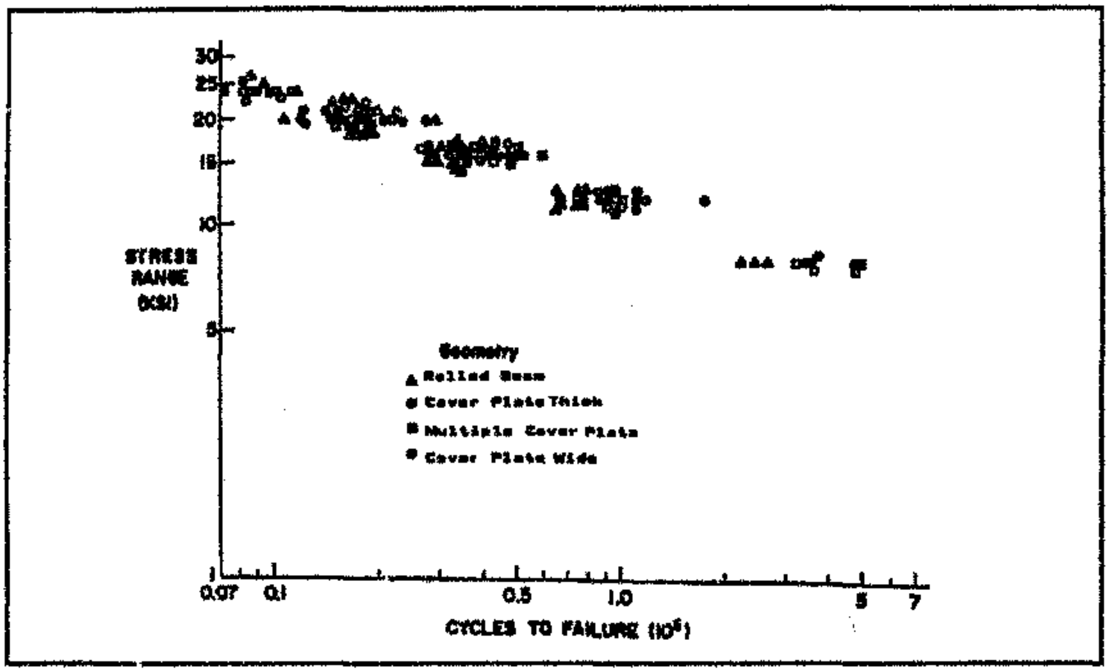

Fig. 2.26 - Effect of cover plate geometry on the fatigue strength of cover plated beams with end welds[3].

The cross-sectional flange area that the fatigue crack occupied immediately after 'Stage 1' of crack growth was compared by Fisher[3] for both end details. In the end welded cover plate geometries the 'Stage 1' crack occupied a much larger cross sectional area of the flange than those without an end weld. This is because multiple crack initiation occurred along the end weld. These multiple cracks eventually joined up to form one wide crack with a high aspect ratio, 2c/a. It was thus logical to assume that the remaining life of the end welded geometries would be less than the geometries without an end weld. The crack at the end weld not only had to grow through less flange area to cause failure, it still had to grow in the area adjacent to the weld, i.e. an area of high stress concentration and residual stresses. The crack, where no end weld was present, grew away from the stress concentration and also had a longer distance to travel before failure occurred.

This type of phenomenon was confirmed by Yongji[30] *et al* who tested I-beams with square end welded cover plates and pointed end welded cover plates. Their results are shown in Fig. 2.28. The square end detail yielded lower fatigue lives than the pointed end detail. This again was due to the difference in the width of the weld at the end of the cover plate.

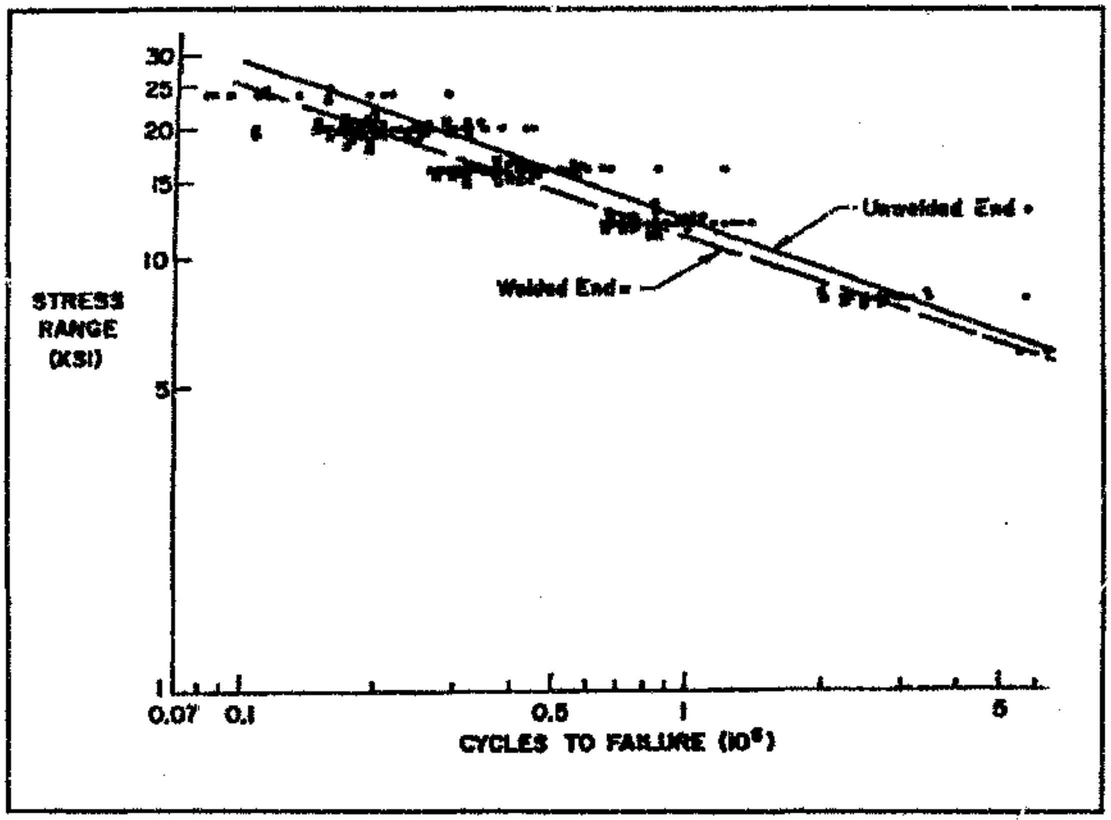

Fig. 2.27 - Comparative fatigue strength of cover plated beams with and without end welds[3].

Gurney[4] compiled data, from different sources, on the fatigue life of different cover plate geometries on steel I-beams. The S-N curves for the various geometries are shown in Fig. 2.29. Some scatter may be expected between the various test results because they were obtained from different sources. There is also bound to be a difference in material and thus a difference in the fatigue life. It is interesting to note however, that those geometries which had the widest end weld yielded the lowest fatigue strengths at low fatigue lives. At high fatigue lives, four out of six geometries yielded almost identical fatigue lives. This is because the dominant portion of fatigue life is consumed in crack initiation and the other stages of fatigue crack growth become insignificant.

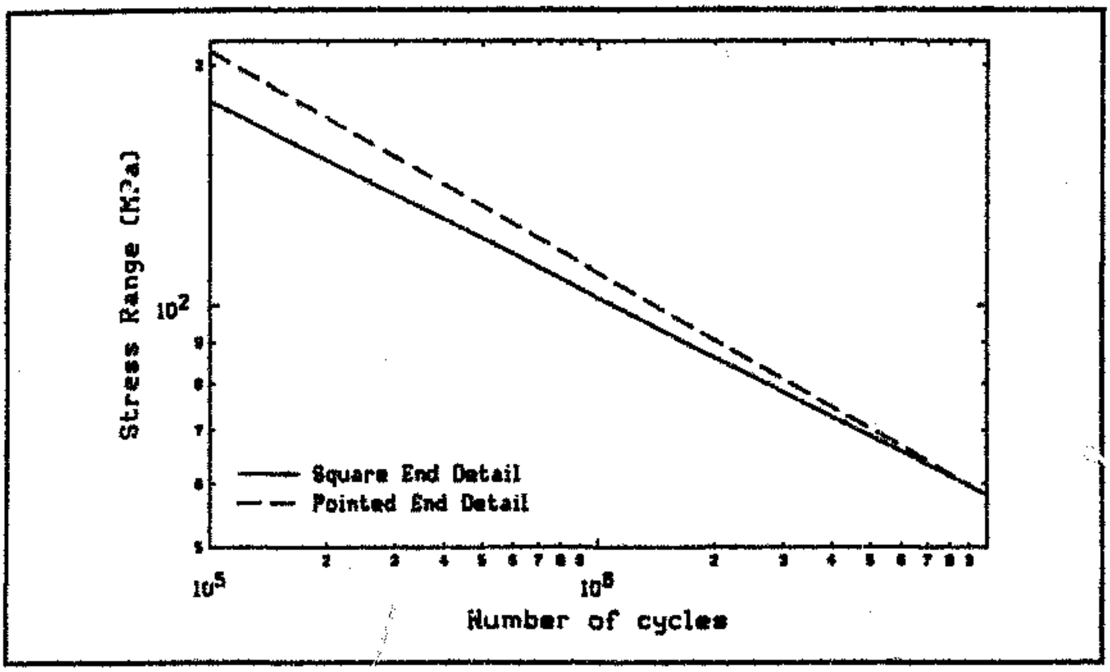

Fig. 2.28 - Comparison between the square and the pointed cover plate geometry[illegible].

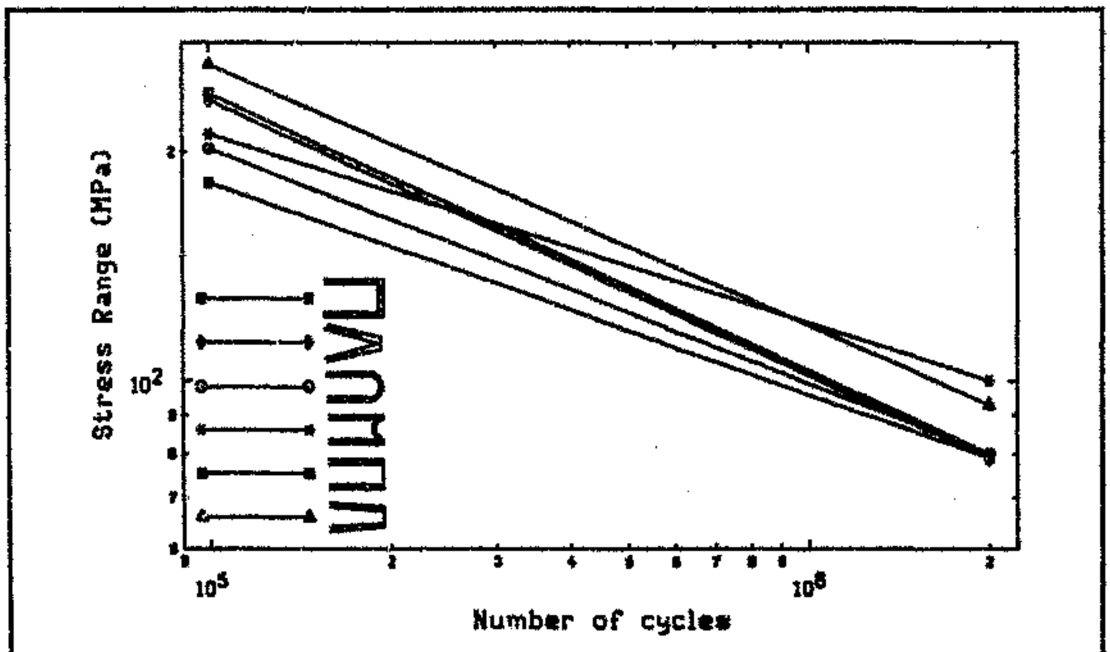

Fig. 2.29 - Comparison of fatigue lives of steel I-beams with various cover plate geometries[4].

Yamada[11] *et al* concluded that the end shape of the cover plates on steel I-beams does not significantly affect the fatigue strength for design purposes. Basler[53] made a similar deduction and added that the cost of making fancy shaped cover plates was not justified in terms of fatigue improvements. He added that square cover plates without an end weld should be used, since they are the cheapest to cut and weld.

The main contributing factor to the decrease in fatigue life is the increase in stress concentration at the end weld of the cover plate geometry. Weld improvement techniques can decrease this stress concentration. Equally, decreasing the slope of the transverse fillet weld or increasing the weld leg size can reduce the stress concentration in I-beams welded with cover plates.

Yamada *et al*[11] stated that grinding the weld to a taper of 1:3, improved the fatigue strength from category E to Category C according to the American Association of State Highway and Transportation Officials (AASHTO)[54]. In this work the cracks initiated either at the weld toes or at the weld roots. Initiation at the weld root represents the upper bound of the fatigue strengths of the cover plated beams. The improvement obtained by grinding the transverse weld to a taper of 1:3 was confirmed by Simon *et al*[55]. According to Albrecht *et al*[56] the fatigue life improvement factor due to grinding was about 6.5. TIG dressing and shot peening of the weld increased the fatigue life by a factor of 2.1 and 4.4 respectively.

2.5. Design Codes

Welded joints in some structures can be very complex. Furthermore, various materials may be used within a structure, and information about the fatigue strength and material properties is not always available. Thus designing against fatigue often becomes a very difficult task if the stress intensity factor and Paris law integration approach are to be applied to each welded detail. However, at least for the case of steel structures a simple design code, based on this approach is now available, i.e. BS 5400 Part 10[1].

Since most joints, especially welded joints, have a high stress concentration, residual tensile stresses and large initial defects (approximately 0.5 mm), the British Standards Institution[1] proposed that the fatigue life of welded joints is dominated by fatigue crack growth. The parameters governing the fatigue life are less material dependent than geometry dependent. This is due to the fact that the mean stress has hardly any effect on the fatigue life[3]. Furthermore, the linear regime of fatigue crack growth is little influenced by material properties.

Thus the British Standards Institution brought out a code of practice for fatigue, BS 5400 Part 10[1], 'Steel, Concrete and Composite Bridges', which grouped various types of steels joints into eight different fatigue life classes. These classes are shown in Fig. 2.30. The code of practice is applicable to almost any type of structural member except tubular joints. Welded, bolted and riveted joints are considered. An extruded plate or I-beam will for example be grouped into class B, whereas an I-beam with a welded cover plate would be grouped into class G. Only the joint detail and the applied stress range need to be known to be able to find the appropriate fatigue life. Thus, a joint detail belonging to say Class G has a life of about 10^6 cycles at a stress range of 60 MPa. These predictions assume that initial defects, such as welding defects, are present. Thus the S-N curve is based on fatigue crack growth and does not include initiation. The use of this design code has made design against fatigue in welded structures very simple.

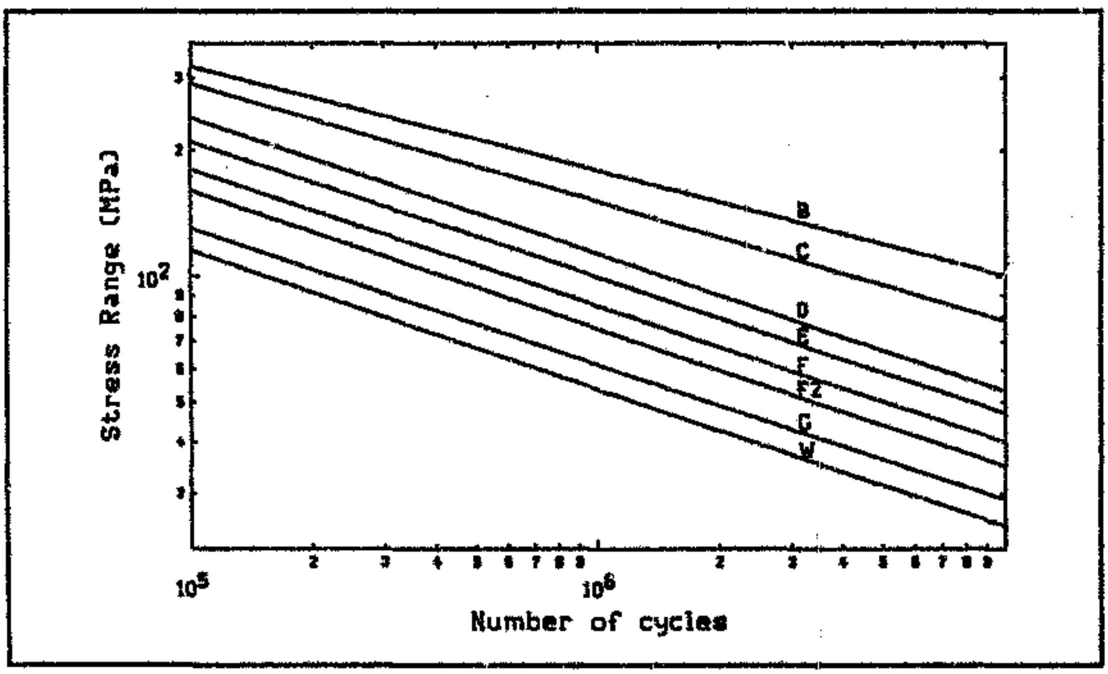

Fig. 2.30 - Fatigue design curves from BS 5400 Part 10 for welded steel joints[1] (mean minus two standard deviations).

Another code of practice was developed earlier by the British Standards Institution, i.e. CP 118[2], 'The Structural Use of Aluminium', one section of which covers fatigue design. Again, various types of joints are grouped together and given different fatigue life classes. This code, however, takes the stress ratio and stress range into consideration. Its presentation of the fatigue life data is different to that of BS 5400. For every class of joint, five curves, which represent five fatigue cyclic lives are plotted with respect to the maximum stress and the stress ratio (maximum stress / minimum stress)in the applied stress cycle. Thus if the maximum stress and the stress ratio is known, the fatigue life can be estimated. A sample plot for class 5, which would represent I-beams welded with cover plates, is shown in Fig. 2.31. These design curves are based on the total fatigue lives of the members and do not distinguish between initiation and crack growth.

With the increased availability of fatigue data and greater understanding of fatigue behaviour of weldments revisions are being made to the design codes for steel and aluminium[58-61]. With this influx of data, there seems to be increasing evidence that the fatigue lives of many aluminium joints are also dominated by fatigue crack growth[49]. Thus, in many respects, the factors which influence the fatigue behaviour of welded aluminium and steel joints appear to be the same. There seems to be, therefore, a strong possibility that the new design curves, which apply to steel, could be applied equally to aluminium by simply adjusting the design stresses in accordance with the observed difference in fatigue crack growth rates between steel and aluminium. Maddox[49] points out that fatigue crack growth rate data for the two materials correlate well on the basis of $\Delta K/E$, where E is the elastic modulus. This would simply mean that the design stresses for steel joints, obtained from BS 5400 Part 10, would be divided by 3 in order to obtain the design stresses for aluminium joints.

In order to substantiate his assumption, Maddox compared fatigue data for aluminium weldments taken from the published literature in terms of the joint classifications in BS 5400 Part 10, dividing its S-N curves by a factor of 3. Empirical data for some of the joint geometries in the proposed classes E, F, G and W, fitted the predictions quite well. An example of this is shown in Fig. 2.32. Here the proposed mean minus two standard deviations line of Class F forms the lower limit of the empirical data. Other data for joint geometries in classes D, E and F did not fit the predicted aluminium S-N curve very well. An example of this is shown in Fig. 2.33 where the proposed mean minus two standard deviations line of class F does not form the lower limit of the empirical data.

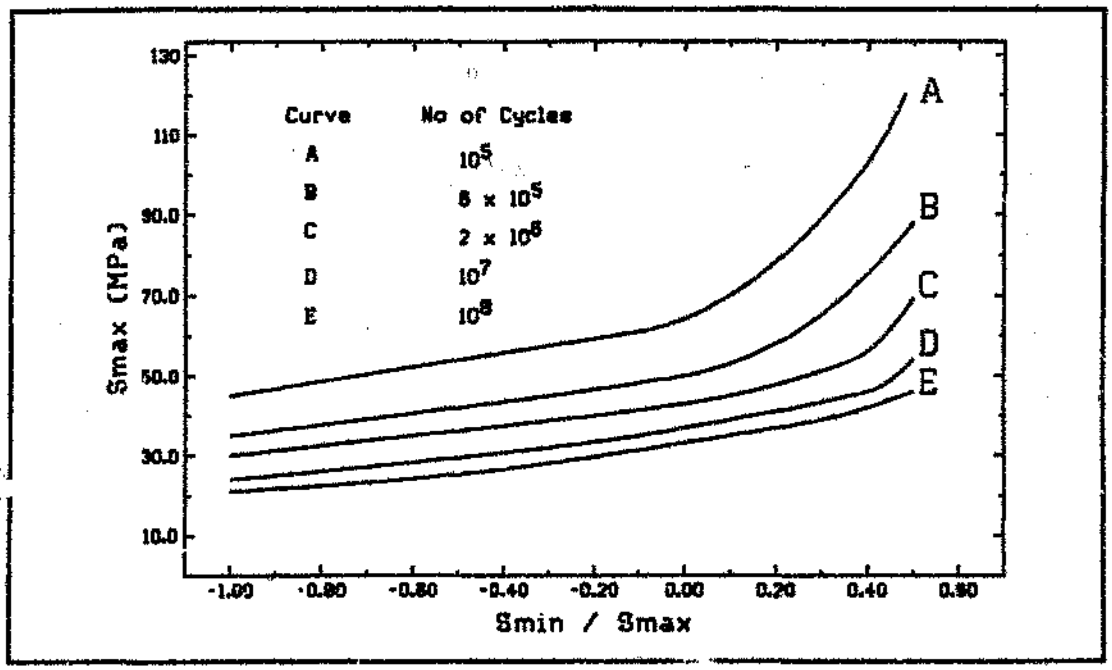

Fig. 2.31 - CP 118[2] curves relating maximum stress, stress ratio and number of cycles of class 5 members.

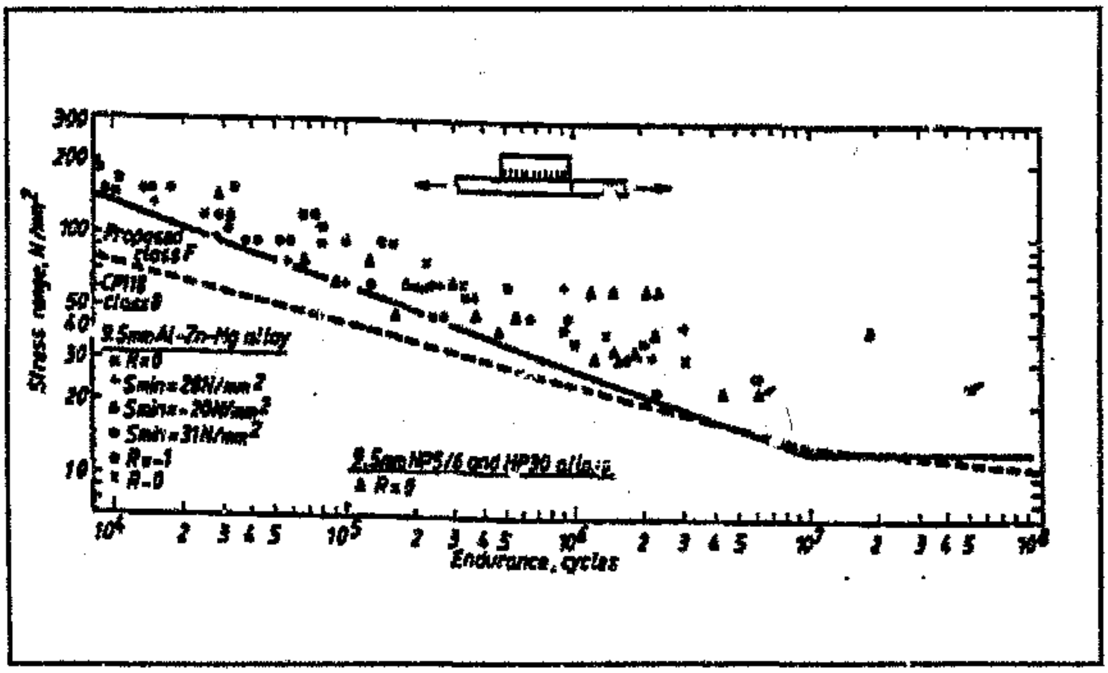

Fig. 2.32 - Fatigue design curves and test results for longitudinal non-load carrying fillet welded surface attachments[49].

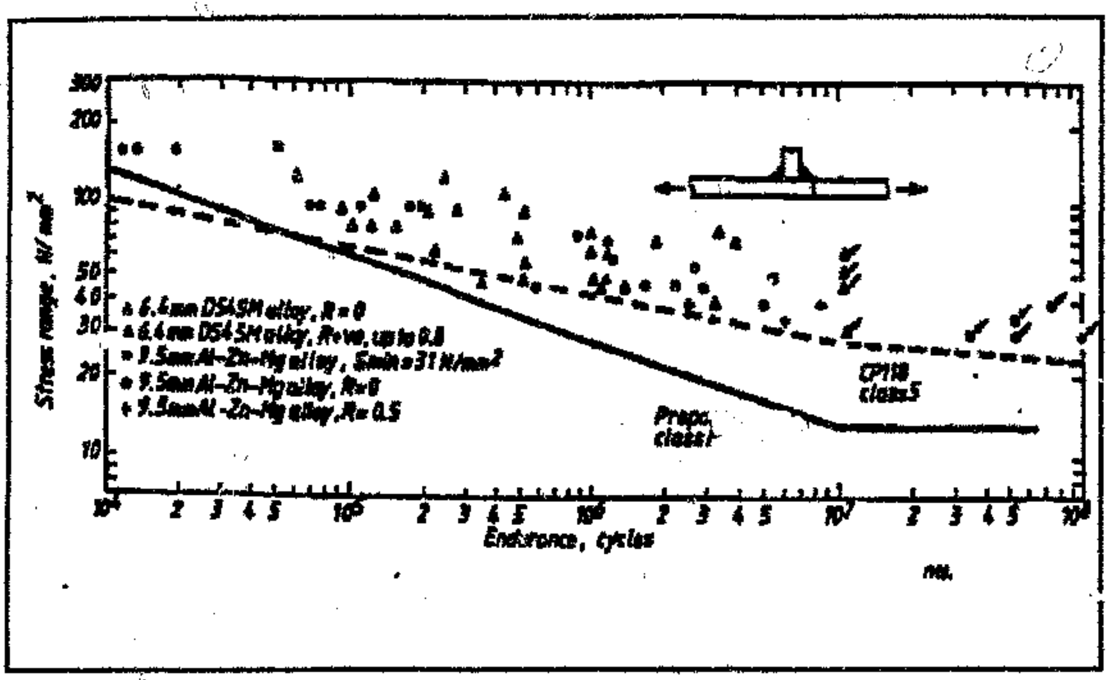

Fig. 2.33 - Fatigue design curves and test results for transverse non load-carrying fillet welded surface attachments[49].

Armstrong[58] confirmed this observation by pointing out that the division of the fatigue design stresses of BS 5400 Part 10[1] by a factor of 3 was satisfactory for only a few geometries such as the longitudinal, non-load carrying fillet welds. For other joint classes however, such a strategy was not representative of the experimental data. The use of CP 118[3], with a high R ratio of 0.5, gave a better prediction of the data that Maddox[49] compiled in Fig. 2.33 than the proposed line based on BS 5400 Part 10[1].

Clearly, further experimental work is required to elucidate those joint geometries for which this approach will provide adequate life estimates. Equally, it is not clear whether the ratio of Young's modulus in steel and aluminium is the best factor to use in dividing the design stresses obtained from BS 5400 Part 10.

3. Finite Element Analysis

Finite element analysis is a procedure by which the internal stresses in a loaded component can be determined. It involves the modelling of the component with mesh type elements, or struts, which are joined at nodes. The strut type elements do not bend and can only transmit a force in the direction of the strut. The element segments are, however, allowed to rotate at the nodes. Thus any bending will only take place at the nodes. Each node, depending on the complexity of the element, can posses up 6 degrees of freedom, i.e. three directions and three rotations. Forces and restraints have to be placed onto some of the nodes in the model so that the model is placed in the correct state of stress. The stresses at every nodal point are then calculated by solving a large number of simultaneous equations. The number of simultaneous equations is related to the number of nodes in the model. The solutions are only accurate at the nodes. If nodes with the same stress values are linked up, a stress contour plot of the model is produced. Intermediate stresses between two nodes could be approximated by using the mean value for the two nodes. This is however only an approximation and the model will lose its accuracy for stresses between nodes. Thus, in order to obtain a more accurate solution the model can be refined by introducing more nodes and elements into the model. An increase in the number of elements and nodes will increase the number simultaneous equations and thus increase the number of calculations required to solve these equations.

Finite element analysis generally involves vast amounts of calculation and is normally done with the aid of a computer software package. Since computer time is costly, the aim in creating a finite element model is to use as few elements and nodes as possible while still maintaining the required accuracy. This was taken into consideration in the following manner, when modelling the I-beams which were welded with cover plates.

1 - A two-dimensional model was used instead of a three-dimensional model. The cracks all initiated at the weld toe of the I-beam during the experimental testing programme. This was therefore the area of interest. The end welds of the cover plates were in some cases up to 40 mm wide. Thus the stress concentration in this region would remain approximately the same throughout the span of the end weld. There was therefore no need to create a three-dimensional model.

2 - Most of the fatigue life of the I-beams was consumed during 'Stage 1'[3] of fatigue crack growth. This means that the fatigue life was dominated by crack growth through the flange thickness. It was thus unnecessary to model the web of the I-beam.

3 - Only the region around the weld needed to be modelled. This is because there is a stress concentration only at the weld. Remote from the weld, the stress distribution will equilibrate itself and remain constant throughout the rest of the I-beam.

4 - The dimensions of the I-beam are large in comparison to the welded region and the beams were tested in four point bending. The positions where the loads are applied are thus far removed from the welded region. The stresses that the I-beam will experience in the weld region are mainly tensile, lying parallel to the direction of the flange surface. As the flange thickness is small compared to the depth of the beam, a uniform tensile stress was modelled, rather than the actual bending case. The difference in stress at the bottom of the flange is small being of the order of about 9%. This

6 - The weld toe angle of the I-beam specimens varied considerably from I-beam to I-beam, even for the same joint geometry. When the S-N data was evaluated, reasonable linear trends were observed with little scatter. Although the scatter might be attributed to the various weld toe angles the I-beam specimens, this was too difficult to determine since the weld toe angle even varied from position to position on a single specimen. If various weld toe angles had to be modelled it would have taken up extensive computer time. It was thus decided to use a weld toe angle which was typical for the joint geometry modelled.

A basic outline of the model showing the cover plate, the weld and the flange is shown in Fig. 3.1. The region where the highest variation in stress is expected is at the weld toe. In order to ensure that the stresses are represented accurately, the mesh elements had to be refined in this region. The model, with the mesh elements, the applied loads (blue arrows) and the restraints (light blue arrows), is shown in Fig. 3.2. The refinement of the mesh at the weld toe is shown in Fig. 3.3. The stress distribution of the model is shown in Fig. 3.4. The stress distribution of the weld toe region is shown in Fig. 3.5.

2 - Most of the fatigue life of the I-beams was consumed during 'Stage 1'[3] of fatigue crack growth. This means that the fatigue life was dominated by crack growth through the flange thickness. It was thus unnecessary to model the web of the I-beam.

3 - Only the region around the weld needed to be modelled. This is because there is a stress concentration only at the weld. Remote from the weld, the stress distribution will equilibrate itself and remain constant throughout the rest of the I-beam.

4 - The dimensions of the I-beam are large in comparison to the welded region and the beams were tested in four point bending. The positions where the loads are applied are thus far removed from the welded region. The stresses that the I-beam will experience in the weld region are mainly tensile, lying parallel to the direction of the flange surface. As the flange thickness is small compared to the depth of the beam, a uniform tensile stress was modelled, rather than the actual bending case. The difference in stress at the bottom of the flange is small, being of the order of about 9%. This difference was, however, taken into consideration when the fatigue life predictions were performed (see section 4.5).

5 - If the component has any axis of symmetry, the stress distribution will be mirrored along this axis. It was thus only necessary to model one half of the I-beam. Restraints of deflection and moments were placed on this axis in order to maintain the integrity of the system.

A basic outline of the model showing the cover plate, the weld and the flange is shown in Fig. 3.1. The region where the highest variation in stress is expected is at the weld toe. In order to ensure that the stresses are represented accurately, the mesh elements had to be refined in this region. The model, with the mesh elements, the applied loads (blue arrows) and the restraints (light blue arrows), is shown in Fig. 3.2. The refinement of the mesh at the weld toe is shown in Fig. 3.3. The stress distribution of the model is shown in Fig. 3.4. The stress distribution of the weld toe region is shown in Fig. 3.5.

6 - The weld toe angle of the I-beam specimens varied considerably from I-beam to I-beam, even for the same joint geometry. When the S-N data was evaluated, reasonable linear trends were observed with little scatter. Although the scatter might be attributed to the various weld toe angles the I-beam specimens, this was too difficult to determine since the weld toe angle even varied from position to position on a single specimen. If various weld toe angles had to be modelled it would have taken up extensive computer time. It was thus decided to use a weld toe angle which was typical for the joint geometry modelled.

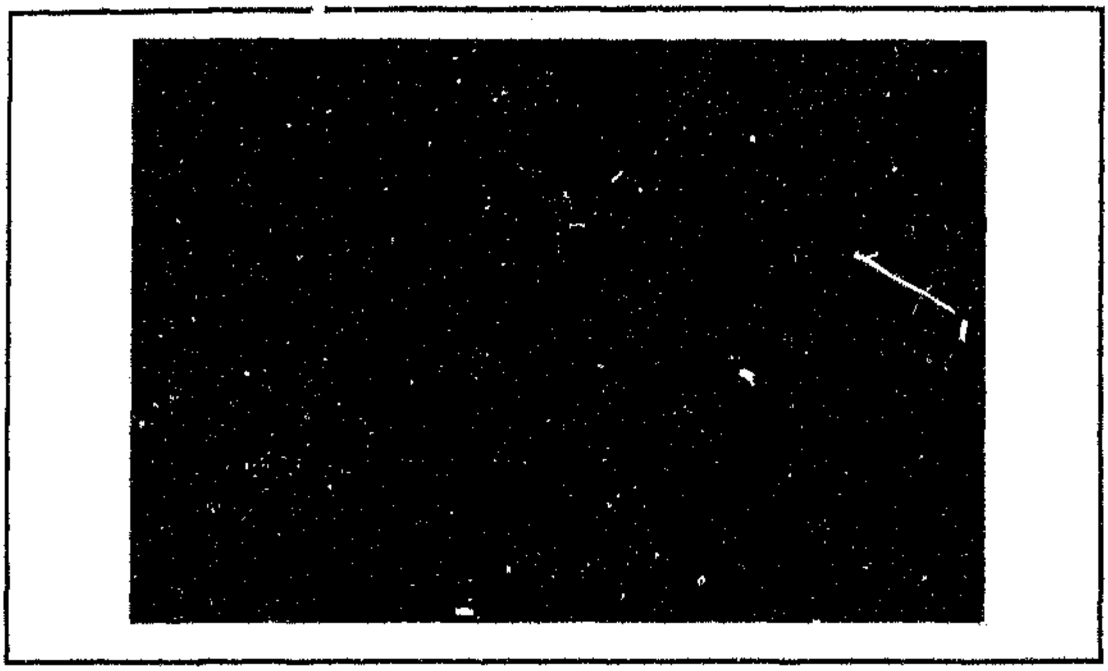

Fig. 3.1 - Outline of the geometry modelled.

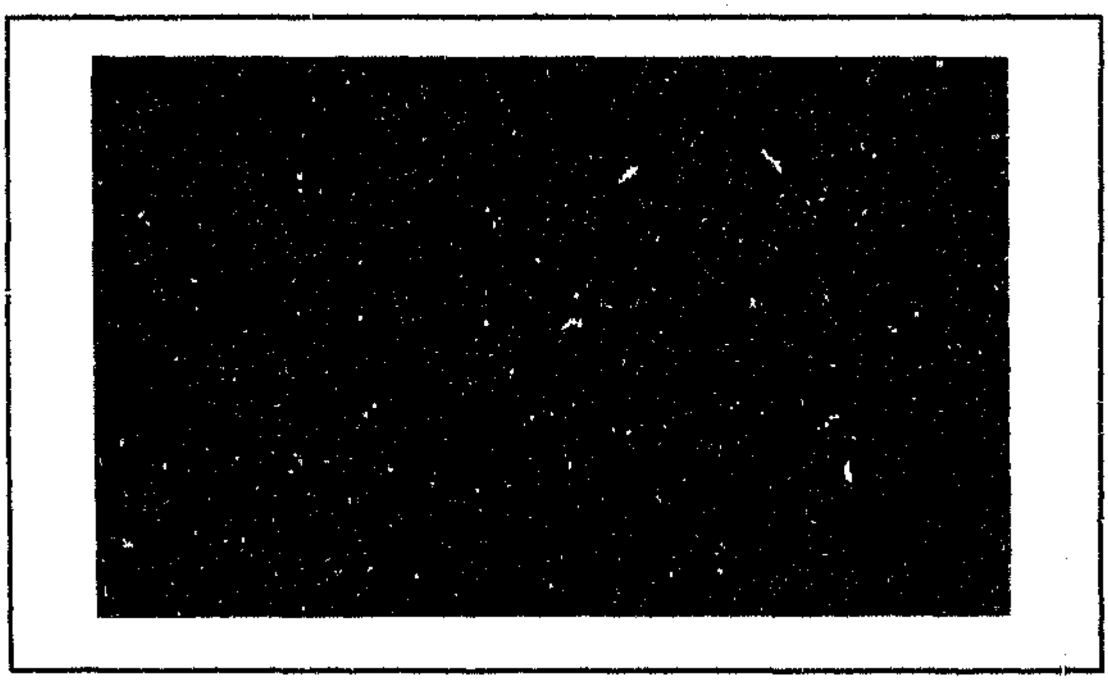

Fig. 3.2 - Finite element mesh of the model showing the loads (blue arrows) and restraints (light blue arrows).

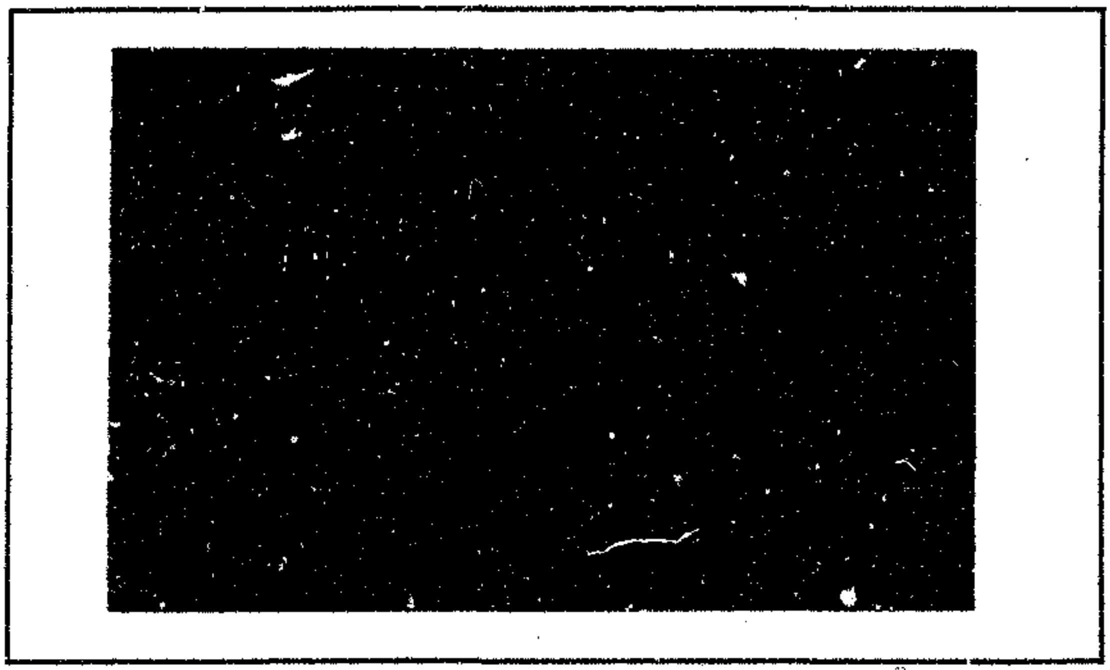

Fig. 3.3 - Finite element mesh of the model, showing the refined weld toe region.

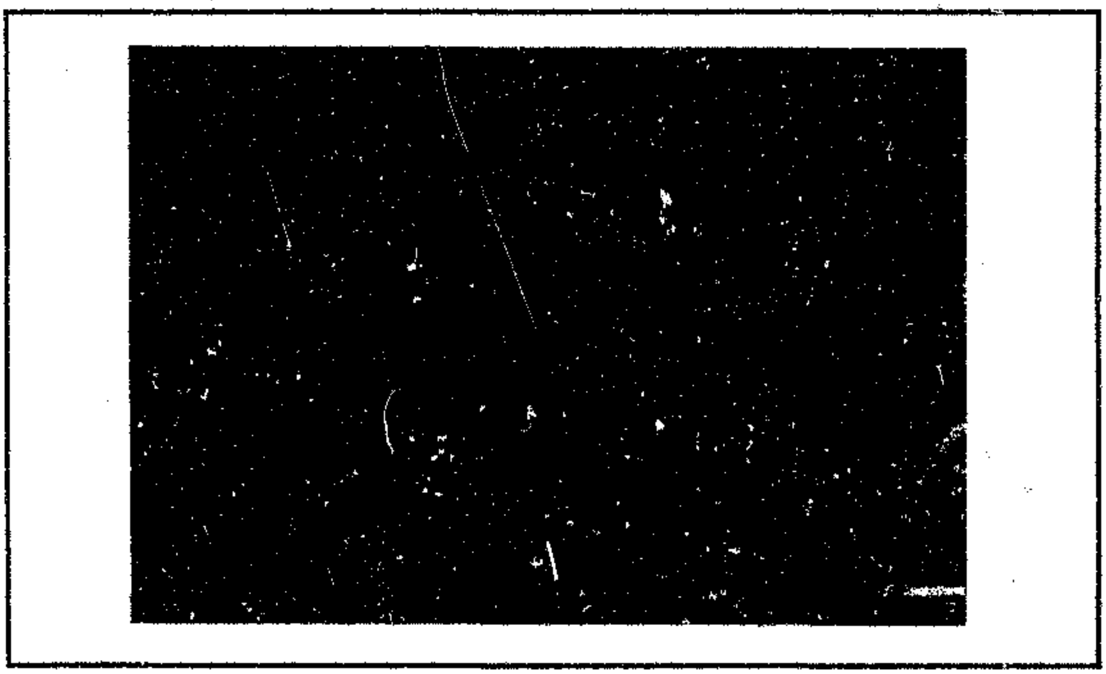

Fig. 3.4 - Stress distribution of the finite element model.

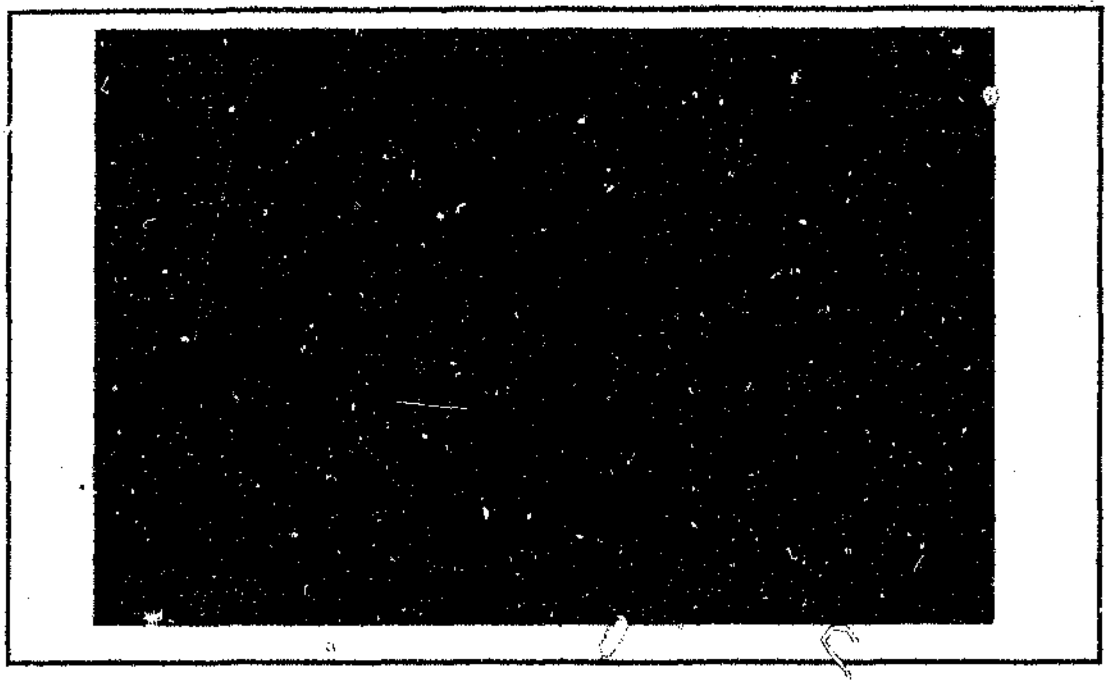

Fig. 3.5 - Stress distribution of the weld toe region.

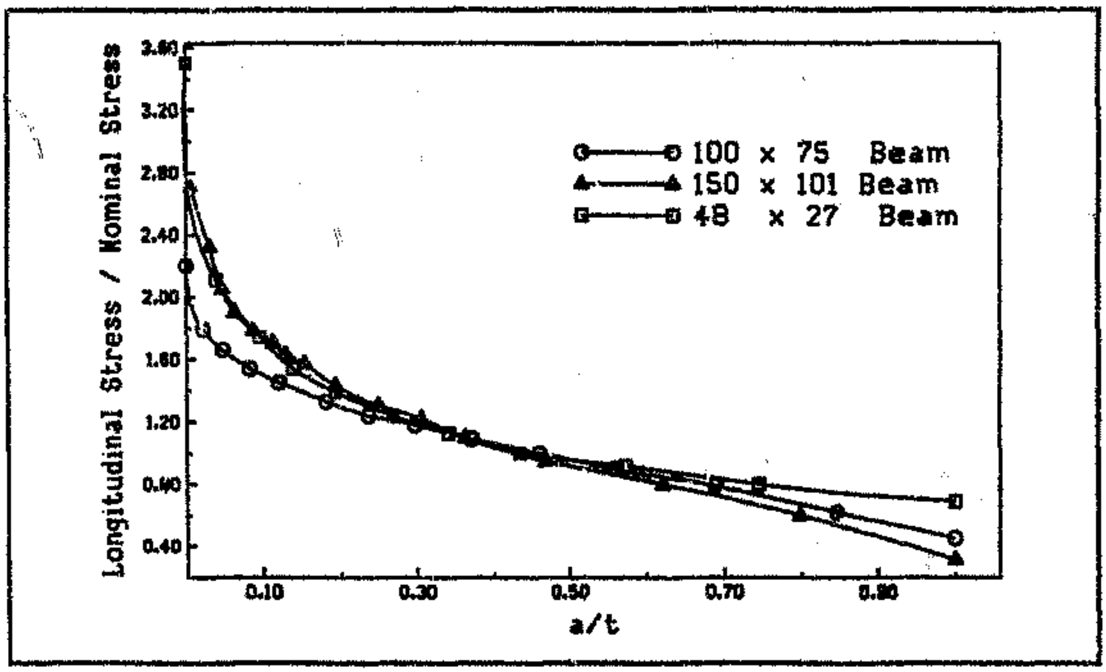

Fig. 3.6 - Stress concentration correction factor, M_k, with depth into the flange from the weld toe.

A finite element model was created for each of the three sizes of I-beam used in the experimental programme. A plot of M_k, i.e. nominal stress / applied stress, with distance from the weld toe through the flange was produced for every finite element model, as shown in Fig. 3.6. From Fig. 3.6 one can see that the stress concentrations at the surface of the of the different I-beams vary considerably. The surface stress concentration factors for each I-beam model is given in Table 3.1. Once a crack depth of a/t = 0.3 is reached, the stress concentration solutions of all the different models are almost the same. At larger crack lengths, i.e. a/t = 1, the solutions vary again.

An attempt was made to fit the solutions of M_k to equations so that they could be used in the integration procedure of the Paris Law. Quadratic regression curves, on a semi-log basis, were used to fit these stress concentration curves. The equations of the these curves are shown in Table 3.1.

Beam	M_k with crack depth (a)	K_t
150x101	$M_k = 1.530 - 0.5$[illegible]$a) - 0.048 (\ln (a))^2$	2.7
100x75	$M_k = 1.125 - 0.2$[illegible]$(a) - 0.0371 (\ln(a))^2$	2.3
48x27	$M_k = 0.826 - 0.468 \ln(a) - 0.0090 (\ln(a))^2$	3.5

4. Experimental Procedure

The experimental work that was carried out in this project can be divided into five section

1 - determination of fatigue crack growth rate curves for the 6261-T6 aluminium alloy, heat affected zone and the weld metal. This was done in order to make Paris L predictions of the fatigue life.

2 - determination of S-N curves for 6261-T6 aluminium I-beams, which had cover pla of various geometries welded onto the tension flange.

3 - metallography and fractography, to determine fracture mechanisms and crack initiat sites.

4 - finite element analysis, to determine the stress concentration associated with the fil weld and the M_k values for use in calculating stress intensity factors. This has alrea been discussed in the previous section.

5 - integration of the Paris Law obtained from the fatigue crack growth rate curves order to model the S-N curves, which were obtained experimentally.

4.1. Material Characterisation

All the material that was used in the testing was supplied by the Aluminium Federation South Africa (AFSA). In developing the S-N curves three sizes of extruded 6261-T6 alumini I-beams were used. The sizes of the I-beams were 150 x 101 mm, 100 x 75 mm and 48 x mm. These were cut into 450 mm lengths. Extruded 6261-T6 aluminium plates, of th different sizes, were used for the cover plates. The widths of these plates that were used for different sizes of I-beams were 53 mm, 40 mm and 13 mm respectively. For the 150 x 101 beams and the 48 x 27 I-beams, only square cover plates were used. For the intermediate si I-beams, square, diamond shaped and rounded cover plates were used.

Fig. 4.1 - Sizes of the various I-beams used in developing S-N curves.

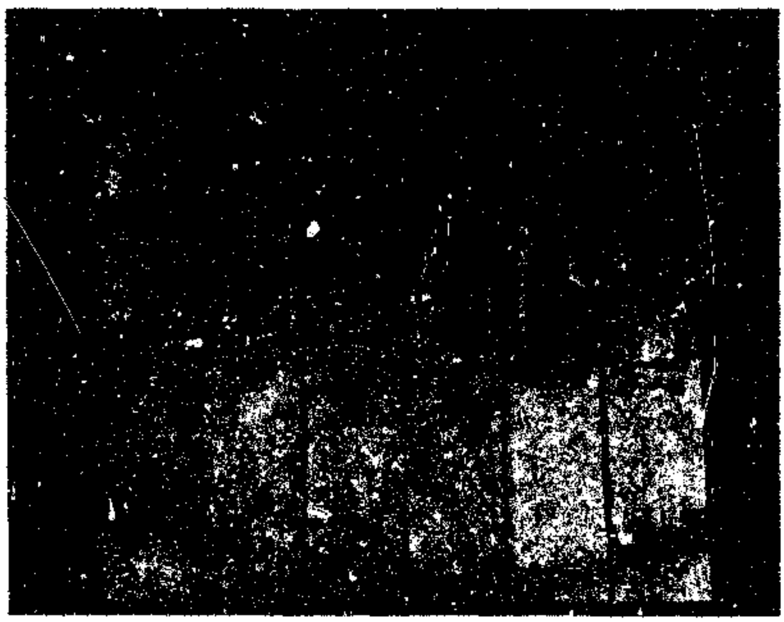

Fig. 4.2 - Cover plate geometries used in generating S-N curves from the 100 x 75 mm sized I-beam.

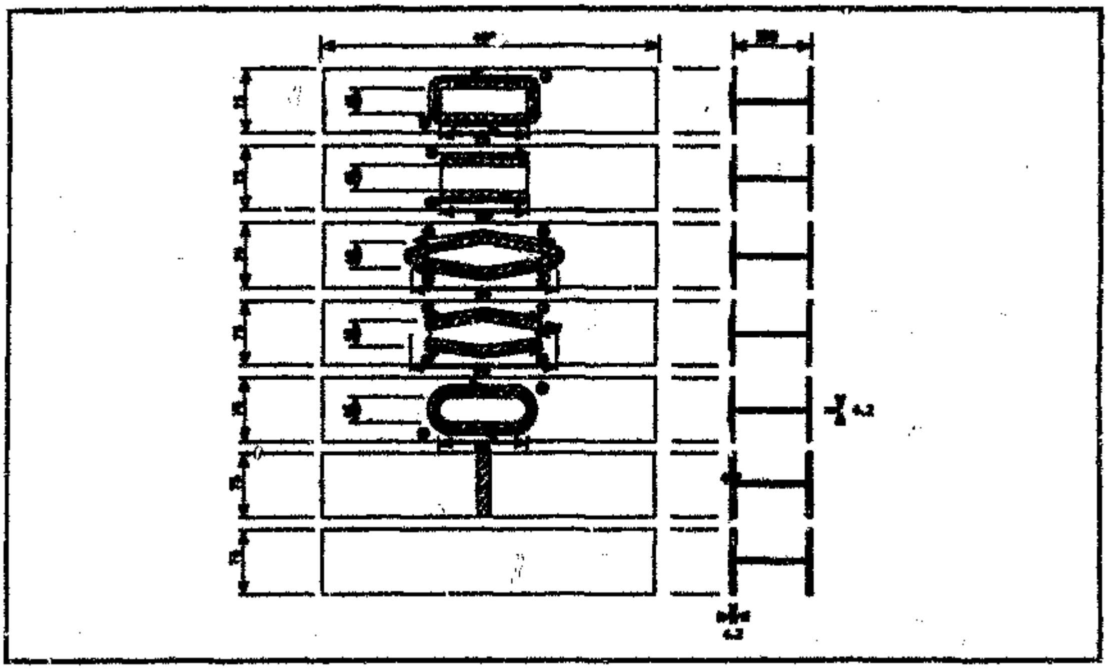

Fig. 4.3 - Cover plate details for the 100 x 75 mm I-beams. Welding directions are shown by the arrows.

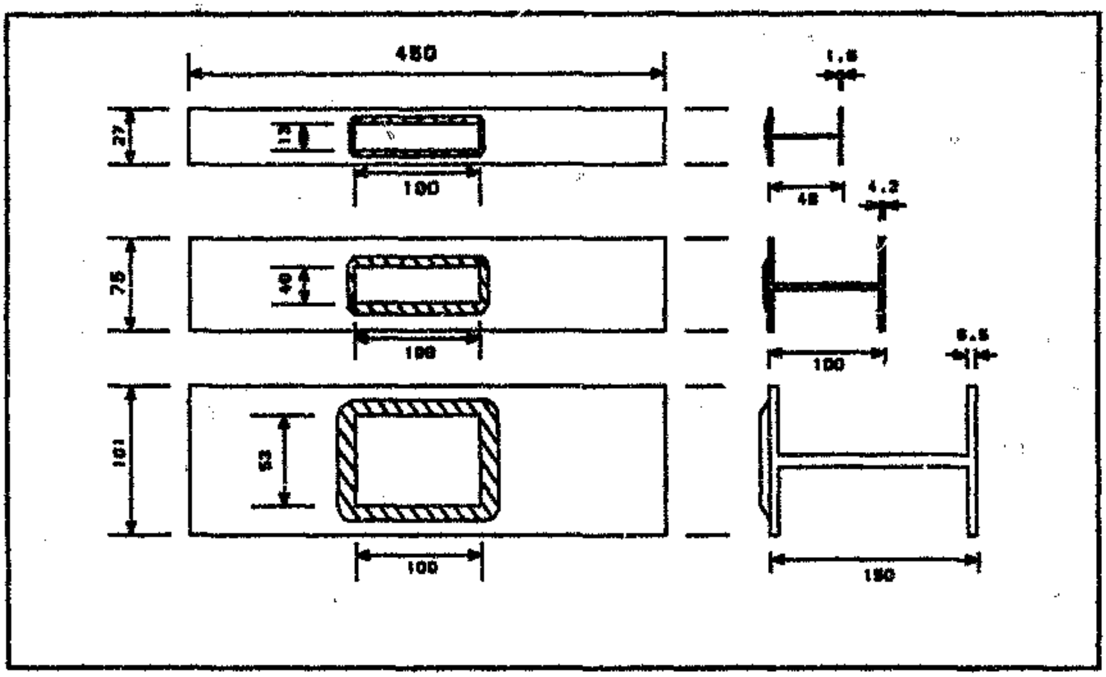

Fig. 4.4 - Three sizes of I-beams used and their rectangular cover plates.

The cover plates were then welded centrally onto the I-beams by Industrial Research and Development (IRD). The welding parameters which were used are listed in Appendix A. In order to see how the I-beams would perform in the presence of a weld with no stress concentration present, some I-beams were given a weld run across the centre of the beam. This was then ground flat with the flange surface so that no stress concentration was present. The different types of cover plates and I-beams that were used in S-N testing are shown in Fig. 4.1 and Fig. 4.2. The dimensions of the welded I-beams and the welding directions are shown in Fig. 4.3 and Fig. 4.4. The mechanical properties of the cover plates are given in Table 4.1, while the compositions of the I-beams and the cover plates are given in Table 4.2.

Fig. 4.5 - Microstructure of the section longitudinal to the direction of extrusion of aluminium 6261-T6 I-beams. (x 100)

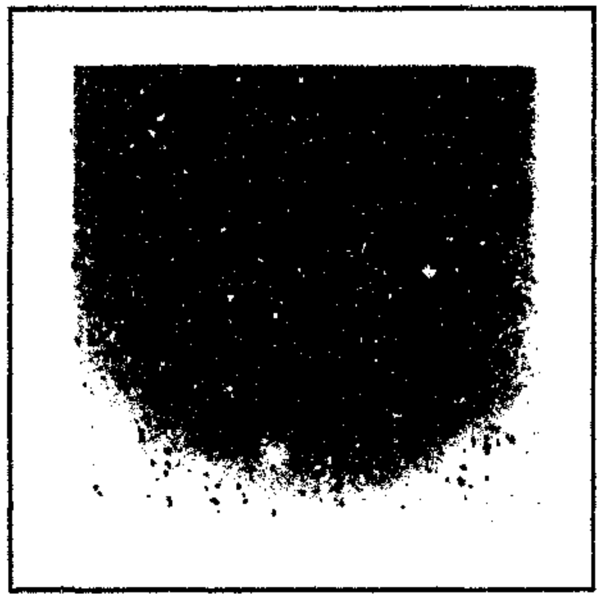

Fig. 4.6 - Microstructure of the section transverse to the direction of extrusion of aluminium 6261-T6 I-beams. (x 100)

Sections of the parent material, longitudinal and transverse to the direction of extrusion, were cut out in order to characterise the microstructure of the I-beams. They were ground smooth and polished to a finish of 1 μm and subsequently etched for 10 seconds in 0.5% HF solution. The microstructures of these sections are shown in Fig. 4.5 and Fig. 4.6 respectively. Fig. 4.6 shows Mg_2Si dispersoids distributed evenly throughout the transverse section of the parent material. From Fig. 4.5 the extrusion direction of the of the parent material is clearly seen by the lining up of the Mg_2Si dispersoids in single direction.

A longitudinal section through the welded region was cut out of an I-beam in order to determine the severity and extent of the heat affected zone (HAZ). This was ground smooth and polished to a finish of 1 μm. The section was then etched in a 10% NaOH solutio. . r 20 seconds at 70°C to produce a macro-etch. A typical macrostructure of this section is shown in Fig. 4.7. Vickers micro-hardness measurements were taken transverse to the I-beam's axis across the flange and the cover plate. The results are shown in Fig. 4.8. From Fig. 4.8 the severity and extent of the HAZ was determined according to Robertson and Dwight[45] (see sub-section 2.2.6). The sizes of zone A and zone B were measured to be 16 mm and 13 mm respectively. The severity of the HAZ was

$$s = \frac{H_A}{H_p} = \frac{65}{125} = 0.52$$

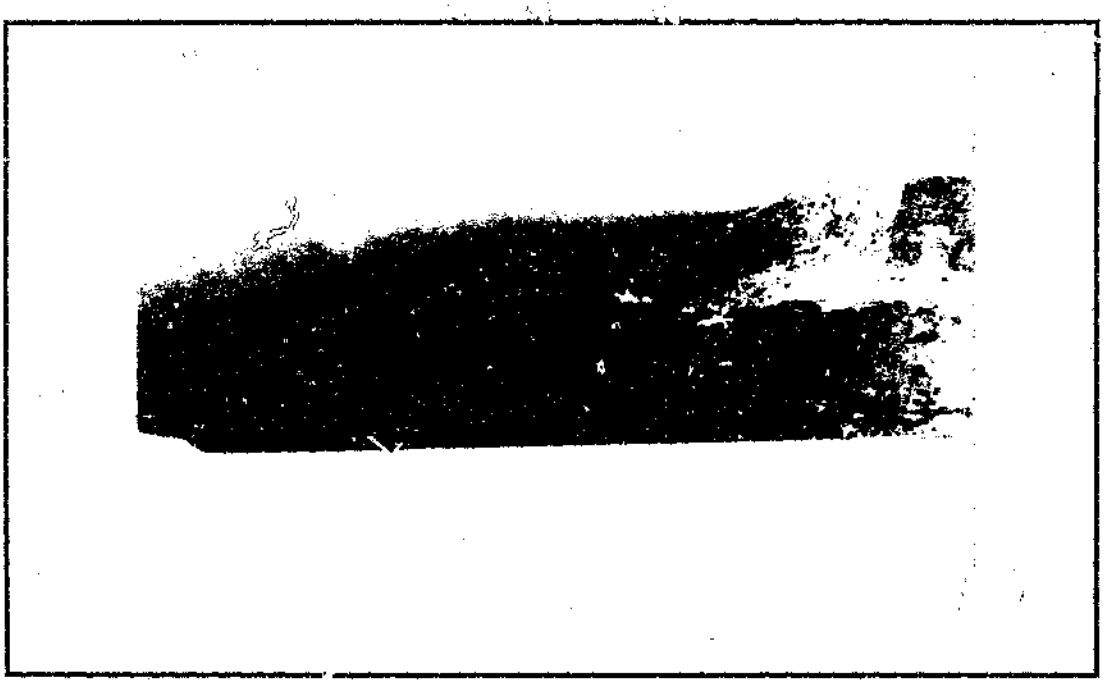

Fig. 4.7 - Cross section of the welded region of the I-beams. (x 5)

	0.2% Proof Stress (MPa)	UTS (MPa)	Elongation (%)
SENB Specimens	354	375	16
Cover Plates	282	301	10

Table 4.1 - Mechanical properties of the material used in testing.

(%)	Si	Fe	Cu	Mn	Mg	Cr	Zn	Pb	Ti
SENB Specimen	.67	.27	.34	.30	.74	.019	.106	.003	.016
Beams	.63	.19	.26	.27	.74	NA	.025	NA	.020
Cover Plates	.63	.28	.33	.25	.74	.002	.12	.003	.040

Table 4.2 - Chemical composition of material used in testing, with a balance of aluminium.

In order to simulate the bend loading condition of the I-beams, a single-edge-notch bend (SENB) specimen geometry was used for the determination of the fatigue crack growth rate curves of the aluminium 6261-T6 alloy. Specimens were machined from an extruded 6261-T6 aluminium alloy bar with a 10 x 30 mm^2 cross section. This bar was cut into 120 mm lengths. A 45°, 5 mm deep notch was machined into each specimen at the centre of one on the faces, to initiate a crack centrally in the specimens. The dimensions and loading positions for the SENB specimens is shown in Fig. 4.9. To facilitate crack growth measurements, using a travelling microscope, the two side faces of each specimen were given a 5 μm polish.

Strain gauges were mounted onto the back face of each specimen, i.e. on the face opposite to the notch, so that crack closure could be measured from compliance traces. The compositions and mechanical properties of the bar used for the SENB specimens are listed in Table 4.1 and Table 4.2 respectively.

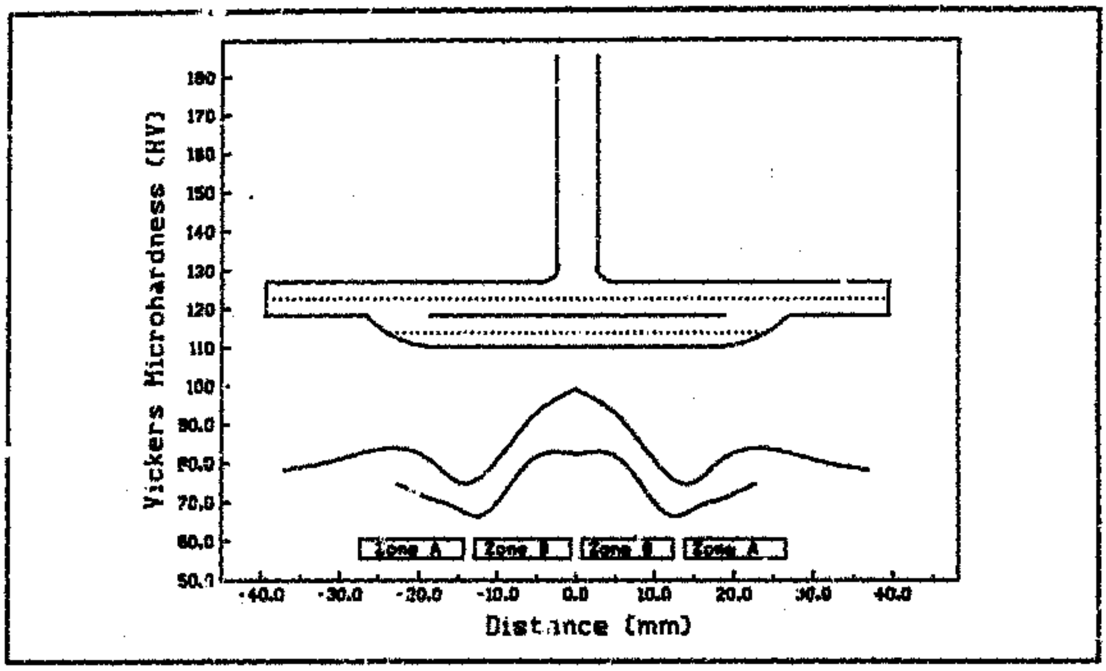

Fig. 4.8 - Hardness plot across the flange and cover plate of a welded cover plate.

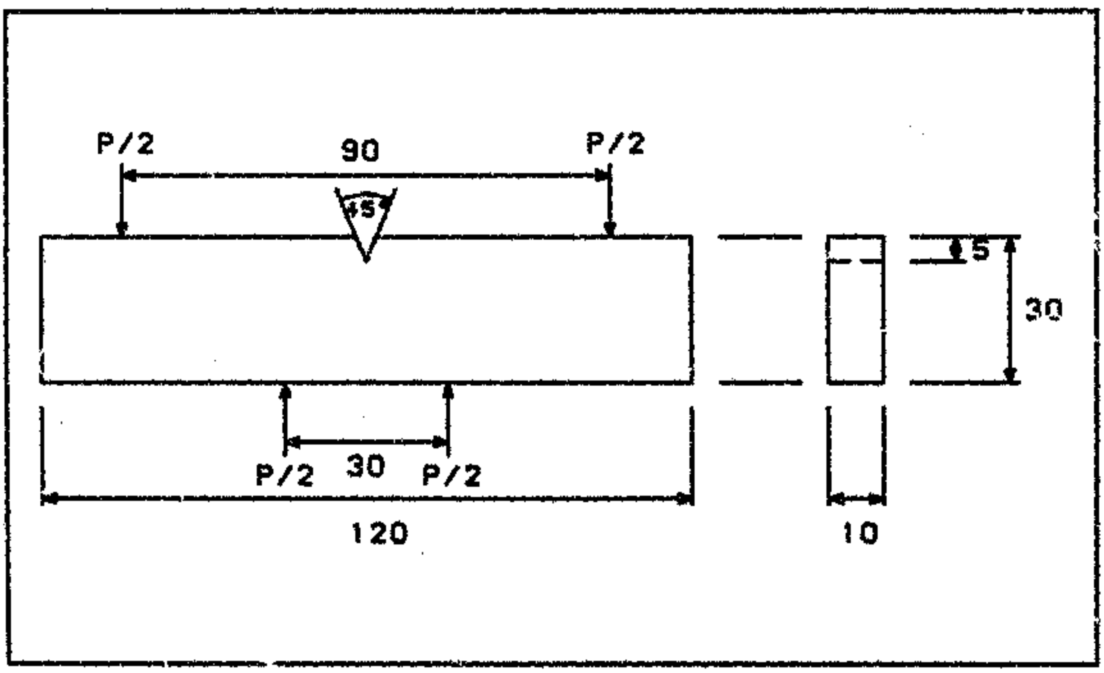

Fig. 4.9 - SENB specimen dimensions and loading positions.

In order to obtain fatigue crack growth rate curves representative of the welded region, 70 mm sections of the extruded bar were butt welded together by IRD. A 45°, 5 mm deep notch was machined into either the HAZ or the weld metal of each specimen. The side faces were again given a 5 μm finish and strain gauges were mounted on the face opposite to the notch.

4.2. S-N Testing

The I-beam specimens were tested using a 10 ton Amsler Vibrophore, which is an electro-magnetic testing machine which operates at the resonant frequency of the machine-specimen system. Each specimen was subjected to cyclic loading with a constant load range and a load ratio of R = 0.1. The test frequency was 110 Hz. A typical test setup is shown in Fig. 4.10 and Fig. 4.11.

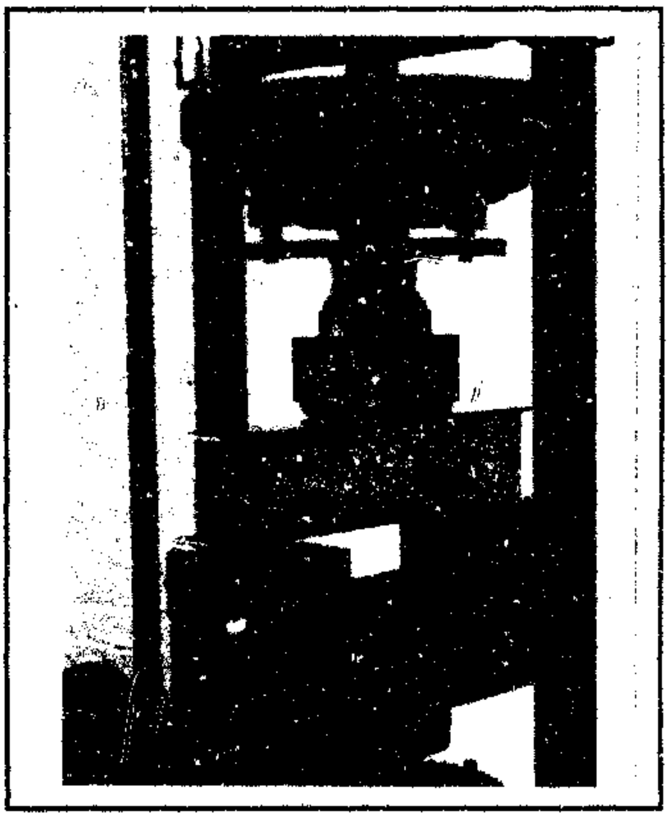

Fig. 4.10 - Loading setup for the I-beam specimens.

Under most loading conditions, cracks initiated at the weld toe of the end weld of the cover plates. These cracks then grew under continued cyclic loading. Failure was taken as occurring when the total width of the flange had cracked. The number of cycles that were required for this to occur was then recorded.

However, not all the specimens cracked. Some of the applied stress ranges were too low to induce fatigue cracking. Tests were stopped at about 2 x 10^7 cycles if no fatigue crack was observed.

These tests thus gave an endurance limit stress range corresponding to a life of 2×10^7 cycles. The upper stress range limit of fatigue testing was reached when the web of the I-beams started to buckle under the high applied loads.

Fig. 4.11 - 10 ton Amsler Vibrophore used for S-N testing.

A number of tests were run at stresses between these limits for each I-beam geometry. The stress range and the number of cycles required to failure were then plotted on a log-log basis, in order to obtain a S-N curve.

4.3. Fatigue Crack Growth Rate Testing

The SENB specimens, which were used to produce the fatigue crack growth rate curves, were tested in an ESH servo-hydraulic testing machine with a maximum load capacity of 50 kN. A typical test setup is shown in Fig. 4.12 and Fig. 4.13. The stress intensity range, ΔK, for this geometry was calculated using the empirical formula[84]:

$$\Delta K = \frac{Y\,\Delta P}{B W^{0.5}} \tag{4.1}$$

where

$$Y = \frac{\left(\frac{S}{W}\right)\sqrt{2\tan\frac{\pi a}{2W}}}{\cos\frac{\pi a}{2W}}\left[0.923 + 0.199\left(1 - \sin\frac{\pi a}{2W}\right)^4\right] \tag{4.2}$$

which has an accuracy of 2% for $0.2 < a/W < 0.7$. ΔP is the applied load range, S the length of the loading span (S = 90 mm, see Fig. 4.9), W the width, B the thickness and a the crack length of the specimen. The maximum and minimum applied loads are dependent on the stress ratio, R, and the stress intensity range, ΔK.

Fatigue crack growth rate data was obtained in accordance with the ASTM Standard E 647-86a [62] for threshold determination. This involved manual load shedding with load reductions of less than 10% and a crack growth increment greater than 3 times the monotonic plane stress plastic zone size between load reductions.

Before useful crack growth rate data could be acquired, the specimens had to be pre-fatigued in order to induce a fatigue crack beyond the notch plastic zone. This involved applying a cyclic load to the specimens until a crack grew from the notch. Care was taken to keep the initiation stress intensity range as low as possible and hence the notch plastic zone as small as possible.

The crack length was measured optically with a travelling microscope on both sides of the specimen. The resolution of the travelling microscopes, was about 0.01 mm. The crack increments used to calculate fatigue crack growth rates were never less than 0.15 mm. This was done in order to minimise scatter observed in growth rates.

When tests were halted for any reasonable period of time during the load shedding procedure, the loads were increased to 10 - 20% above that used when the test was halted, before the load shedding procedure was continued.

Fatigue crack growth rate curves, using the load shedding procedure, were produced at stress ratios of 0.1, 0.2, 0.5 and 0.7. This was done so that the effect of crack closure with respect to the fatigue growth rate could be examined. Crack closure free curves were obtained by performing tests, using the load shedding routine, where K_{max} was kept constant and ΔK was decreased.

Crack closure measurements were made using the load-offset displacement technique, where voltage readings from the output of the back face strain gauge and corresponding to the load were used to produce compliance traces. Crack closure readings were made using as few cycles as possible.

Fig. 4.12 - Load setup for SENB specimen.

Fig. 4.13 - SENB specimen in ESH servo-hydraulic machine.

4.4. Fractography

The purpose of the fractographic examination was to determine the initiation site and hence the initial defect, and the mode of fracture. The initial defect size was required for the integration of the Paris Law used in fatigue life predictions. In order to examine the fracture surfaces, failed I-beam specimens were broken apart. One half of the fracture surface was then cut from the beam and cleaned ultrasonically in acetone. Some of the fracture surface specimens were sputter coated with gold-palladium. This was done to improve the surface conductivity of the specimens and thus improve the viewing resolution under the scanning electron microscope (SEM). The specimens were mounted onto the stage of an SEM, ensuring that good electrical conductivity was maintained.

4.5. Prediction Procedure

Since shrinkage cracks around the size of 0.7 mm existed at the weld toes, the fatigue lives of the I-beam specimens were not dominated by initiation, but by fatigue crack growth. It was thus reasonable to assume that the Paris Law would hold true for most, if not all of the fatigue life. As is already known, the Paris Law is defined as :

$$\frac{da}{dN} = C\,\Delta K^{m} \tag{4.3}$$

where C and m are material constants. For the aluminium 6261-T6 alloy, C and m were obtained using linear regression techniques on the Paris regime data in the fatigue crack growth curves which were experimentally obtained for the 6261-T6 aluminium alloy. Equation 4.3 can be written as

$$\frac{da}{dN} = C\,(Y\,\Delta\sigma\,\sqrt{\pi a})^{m} \tag{4.4}$$

where Y is the geometry correction factor at a crack length, a, and a nominal applied stress range, $\Delta\sigma$. The geometry correction factor is defined as $M_k M_s M_t/\phi_0$. M_k is the correction factor which takes the presence of a stress concentration into account and varies with crack length. The relation between M_k and crack length was found with the aid of finite element stress analysis, and is shown in Fig. 3.6. $M_s M_t/\phi_0$ is the correction factor which takes the presence of a free surface ahead of a crack tip and the crack shape into account. Since the surface defects at the end welds have a very low aspect ratio, a/2c, the Gross[18] equation, Equation 2.4, was used to define the correction factor $M_s M_t/\phi_0$. Thus after every cycle, i.e. dN = 1, the crack grows by da.

As was discussed in Chapter 3, the finite element model did not take bending into consideration. When a part width crack grows under a bending load, the non-uniform stress distribution means that the stresses at the crack tip steadily decrease. This reduction is linear with crack depth and is defined as:

$$\sigma_{Res} = \sigma \left(1 - \frac{2a}{H}\right) \tag{4.5}$$

where σ_{Res} is the resultant stress, σ is the stress at the upper surface of the flange, a is the crack depth and H is the height of the beam.

For a specific stress range and initial crack size, Equation 4.3 can be integrated, cycle by cycle, until the final crack size is reached. The final crack size is defined here as the thickness of the flange, since most of the fatigue life is spent in growing the crack through the flange. Thus, if the appropriate geometry correction factors are used, and the initial crack size is determined using fractography, Equation 4.3 can be used in the prediction of the fatigue life of the I-beam at a stress range, $\Delta\sigma$.

If this procedure is repeated at various stress ranges, a predicted S-N curve for the fatigue lives of the aluminium I-beams, welded with cover plates is obtained.

A computer programme was written to integrate the Paris Law, cycle by cycle, and to produce such S-N curves. A listing of this programme can be found in Appendix B.

5. Results and Discussion

5.1. Fractography

The purpose of fractogaphic examination is to determine and define the initiation site and the size of initial defect, crack shape development and the fracture mode. By doing this, in-depth knowledge regarding the fatigue mechanisms in the welded aluminium I-beams can be obtained.

5.1.1. Initiation Sites and Crack Shape Development

On work performed at The Welding Institute by Booth and Maddox[34] on non-load carrying fillet weld attachments, the crack initiation did not always occur at the end of the weld. For the geometries where the longitudinal welds extended past the attachment, the fatigue cracks would initiate at the attachment. The attachment itself, however, produced a far more significant stress concentration than the end of the weld did causing the fatigue crack to initiate at the end of the attachment. For geometries where the longitudinal welds were as long as the attachment or stopped short of the end of the attachment, the fatigue cracks would initiate at the weld toe at the end of the longitudinal weld.

centre line of the beams at the weld toe. There were often multiple initiation sites along the transverse welds, which linked up to form one large crack.

The crack growth pattern in I-beams welded with cover plates can be classified into three stages, as illustrated in Fig. 5.1[3].

Stage 1 - During the first stage, the crack grows through the thickness of the flange in an elliptical shape. The crack size, a, is defined as the depth of the crack and the crack width, 2c, is the length of the crack visible on the flange surface. The crack width is usually related to the width of the end weld detail.

5. Results and Discussion

5.1. Fractography

The purpose of fractographic examination is to determine and define the initiation site and the size of initial defect, crack shape development and the fracture mode. By doing this, indepth knowledge regarding the fatigue mechanisms in the welded aluminium I-beams can be obtained.

5.1.1. Initiation Sites and Crack Shape Development

In previous work on steel I-beams with welded cover plates[2], the critical initial defects which were the cause of failure all seemed to initiate at the toe of the fillet weld which connected the cover plate end to the flange. For those cover plate geometries where no end welds were present, the cracks initiated at the end of the longitudinal welds. This was found to be true regardless of whether the longitudinal welds were stopped short or extended past the cover plate. The location of the end of the welds appeared to have no effect on crack initiation (see Fig. 2.26).

Fischer *et al*[3] found that fatigue cracks in transverse fillet welds initiated predominantly at the centre line of the beams at the weld toe. There were often multiple initiation sites along the transverse welds, which linked up to form one large crack.

The crack growth pattern in I-beams welded with cover plates can be classified into three stages, as illustrated in Fig. 5.1[3].

Stage 1 - During the first stage, the crack grows through the thickness of the flange in an elliptical shape. The crack size, a, is defined as the depth of the crack and the crack width, 2c, is the length of the crack visible on the flange surface. The crack width is usually related to the width of the end weld detail.

On work performed at The Welding Institute by Booth and Maddox[84] on non-load carrying fillet weld attachments, the crack initiation did not always occur at the end of the weld. For the geometries where the longitudinal welds extended past the attachment, the fatigue cracks would initiate at the attachment. The attachment itself, however, produced a far more significant stress concentration than the end of the weld did causing the fatigue crack to initiate at the end of the attachment. For geometries where the longitudinal welds were as long as the attachment or stopped short of the end of the attachment, the fatigue cracks would initiate at the weld toe at the end of the longitudinal weld.

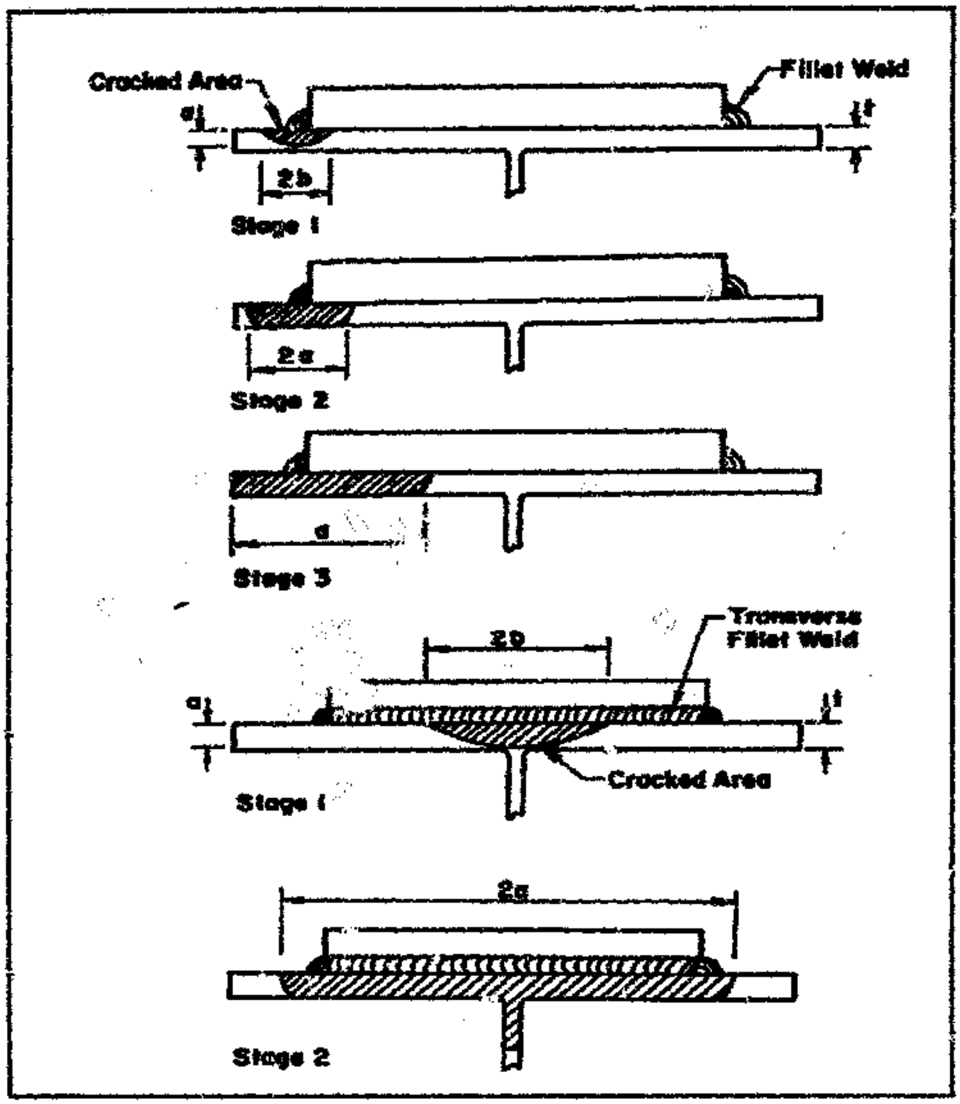

Fig. 5.1 - The typical stages in the growth of cracks at longitudinal and transverse fillet welds in I-beams welded with cover plates[1].

Stage 2 - The second stage is initiated as soon as the crack has penetrated the thickness of the beam. The crack size is then redefined from a in 'Stage 1' to 2a in 'Stage 2'. This arises because of the size definitions of surface and through-thickness cracks in expressions for K.

Stage 3 - The third stage is initiated when one side of the crack has reached a tip of the flange of the I-beam. The crack length is again redefined from 2a in 'Stage 2' to a in 'Stage 3'.

Almost all of the fatigue life is consumed in 'Stage 1'. This is because the initial defect, caused by welding, is small (approximately 0.5 mm). This results in a low stress intensity range and, initially, low crack growth rates. When 'Stage 2' is reached, the crack is considerably larger. Since the crack growth rates increase exponentially with crack size, the portion of life consumed in 'Stage 2' and 'Stage 3' growth is relatively small.

Fig. 5.2. - Typical fracture surfaces of the 100 x 75 mm I-beams with rounded, diamond and square cover plate end geometries and an end weld. Crack initiation sites are indicated by arrows.

The crack growth behaviour found for these steel I-beams is very similar to that of the aluminium I-beams that were tested in this project. All the aluminium I-beams which were welded with cover plates failed at the toe of the end weld of the cover plates. The cracks seemed to develop in a similar fashion to that described by Fisher *et al*[3]. Typical fracture surfaces of every cover plate geometry were selected and grouped into those with an end weld, Fig. 5.2, those without an end weld, Fig. 5.3 and the different sizes of I-beams with square end welded cover plates, Fig. 5.4. The cover plate geometries with end welds were all wide with respect to the flange width. Thus multiple cracks, initiated along the weld toe of the end weld. This is substantiated by the presence of ridges seen on the fracture surfaces of 'Stage 1' crack growth, in Fig. 5.2 and Fig. 5.4. As the cracks grew, these multiple cracks joined up to form a single large crack with a high aspect ratio, 2c / a. The cracks of the end welded cover plate geometries

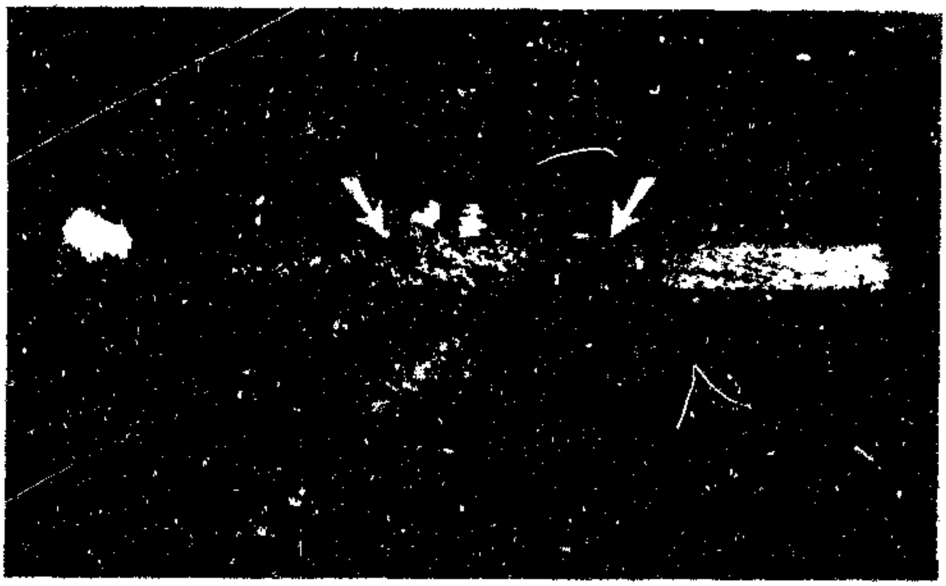

Fig. 5.3a - A typical fracture surface of a 100 x 75 mm I-beam with a diamond cover plate geometry without an end weld. The arrows indicate the crack initiation sites.

Fig. 5.3b - A typical fracture surface of a 100 x 75 mm I-beam with a square cover plate geometry without an end weld. The arrows indicate the crack initiation sites.

Fig. 5.3. - Typical fracture surfaces of the 100 x 75 mm I-beams with diamond and square cover plate end geometries without an end weld. Crack initiation sites are indicated by arrows.

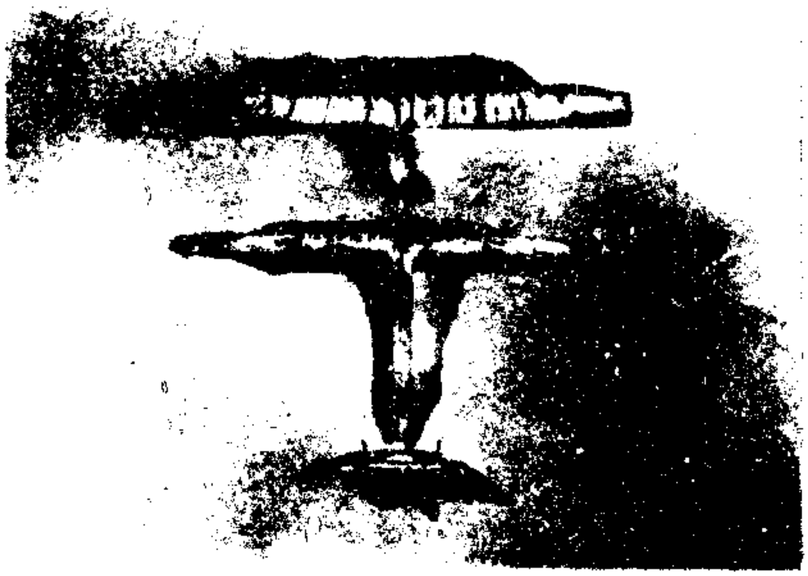

Fig. 5.4. - Typical fracture surfaces of the 150 x 101 mm, the 100 x 75 mm and the 48 x 27 mm I-beams with a square cover plate end geometries and an end weld. Crack initiation sites are indicated by arrows.

thus had a large surface length once 'Stage 1' of crack growth was complete. Thus 'Stage 2' and 'Stage 3' of crack growth did not contribute very much towards the total fatigue life.

In cover plate geometries with no end weld, i.e. which had only longitudinal welds, the crack initiated at the weld toe at the end of the longitudinal welds. For the square cover plate geometry, which had no end weld, a crack would initiate at only one of the longitudinal welds. No significant crack initiation was found at the other longitudinal weld. Thus 'Stage 3' of crack growth of this geometry contributes more to the total fatigue life than the end welded geometries do. For the diamond cover plate geometry, which had no end weld, fatigue cracks would initiate at both of the longitudinal welds. The two cracks would eventually join up, in 'Stage 2' of fatigue crack growth, to form a single crack. Thus 'Stage 2' of fatigue crack growth was more significant to the total fatigue life in this test geometry than the square, no end weld cover plate geometry.

5.1.2. Initial Defect Size

The determination of initial defect size plays an important role in fatigue life predictions for I-beams. This is because the 'Paris Law' is integrated from the initial crack size to the final crack size. For plain I-beam specimens, with no cover plates and where no stress concentration is present, this initial crack size is very important. This is because the majority of the fatigue life occurs while the crack is small. The fatigue crack growth rate increases exponentially with crack size. Thus, the final stage of the fatigue cracking is less significant in the overall fatigue life than the initial stage is.

Fatigue cracks in the plain I-beams initiated at the centre of the beam, in the tension flange, where the stress was the highest. The position of the initiation site depended on where the largest defect was present. Thus, some of the plain I-beams had their initiation sites at the flange tips, while others had them at the centre of the flanges. The initial defects were generally surface scratches or extrusion irregularities such as surface roughness or extrusion defects. The extrusion defects were generally buried below the flange surface. An initiation site of a plain I-beam can be seen in Fig. 5.5, where a small surface defect caused the fatigue crack to initiate. The size of this defect was measured to be about 0.04 mm. The initial defect sizes in all the plain I-beams were measured and were found to range from 0.02 mm to 0.12 mm. Thus, for the purpose of integrating the 'Paris Law', the initial defect size of the fatigue cracks of the plain I-beams was taken as 0.1 mm.

Certain I-beam specimens were given a weld run, which was then ground flush with the surface. In theses cases the fatigue cracks all initiated in the weld metal. The initial defects were grinding marks and welding defects, such as porosity and shrinkage cracks. An initiation site in I-beams with a ground weld run can be seen in Fig. 5.6 and Fig. 5.7. The size of the initial defect was measured to be about 0.1 mm. The defect size of all the I-beams with weld runs ranged from 0.07 to 0.15 mm. Thus, for the purpose of integrating the 'Paris Law', the average defect size was taken as 0.12 mm.

All the fatigue cracks of the welded I-beams initiated at the weld toe of the end welds or the ends of the longitudinal welds. This is in agreement with the results of the finite element analysis which was done of the welded region. This analysis showed that there was a stress concentration at the weld toe. According to Fig. 3.4, the stress concentration at the weld toe of the 100 x 75mm was 2.2. Thus the effective stress at the weld toe is 2.2 times the applied stress. As the crack grows, the stress concentration decreases rapidly. This offsets the increase in K due to increase in crack length and slows down the increase in the crack growth rate. It is therefore likely that a significant portion of the fatigue life takes place even when the crack is large. Thus, although the initial defect size is important in determining the fatigue life, the dominant portion of the fatigue life is not necessarily confined to the initial stages of fatigue crack growth.

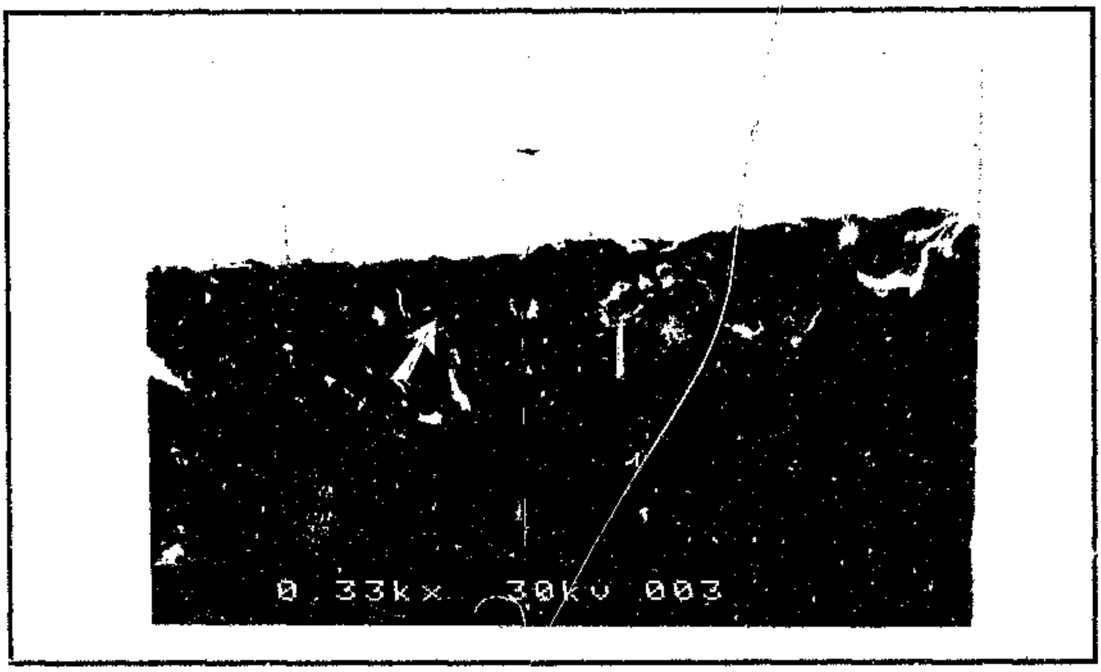

Fig. 5.5 - Initiation site of a fatigue crack in a plain I-beam. (x 330)

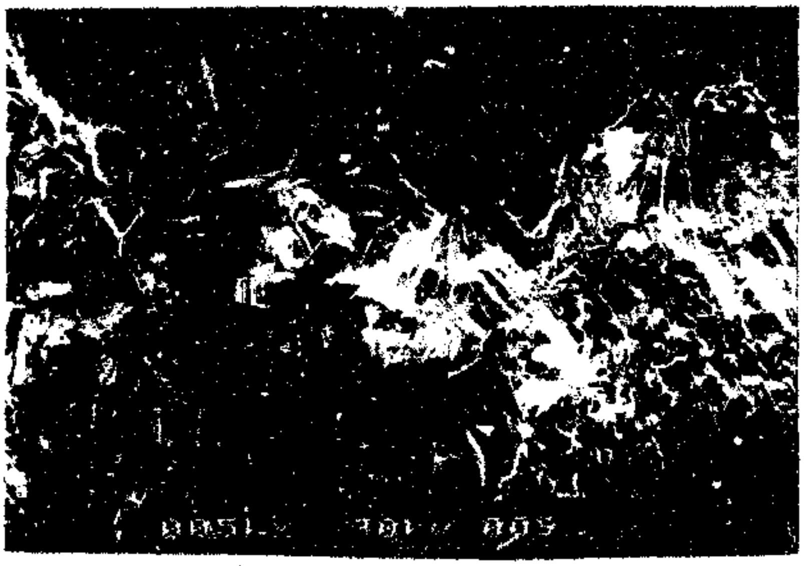

Fig. 5.6 - Initiation site in an I-beam with a weld run (x 5)

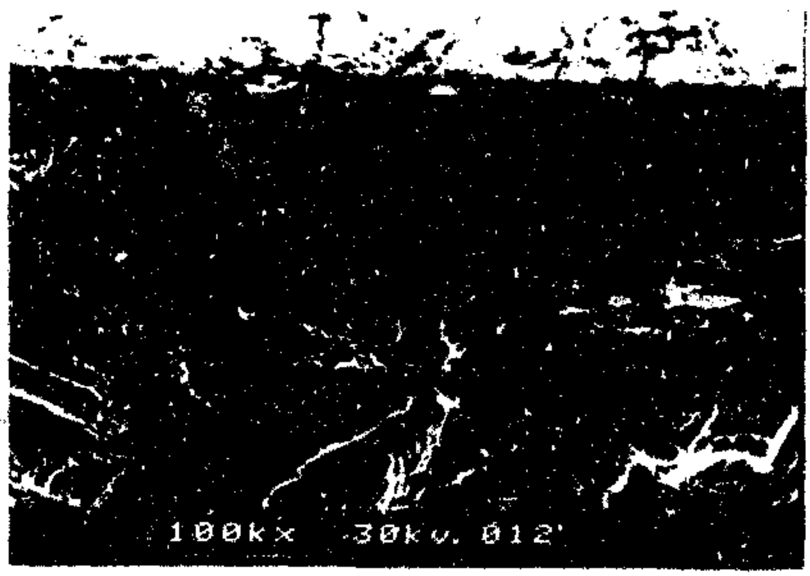

Fig. 5.7 - Magnification of Fig. 5.6 showing the initiation site of an I-beam with a weld run. (x100)

Fig. 5.8 - Shrinkage cracks at the corner of an end weld (x 10)

The first step taken to find initial defects was to inspect the surface of the welded I-beams, in order to see whether any defects could be found in the vicinity of the weld toes of the end welds. As can be seen in Fig. 5.8, shrinkage cracks were found at the weld toes of some of the I-beams with square and rounded end welded cover plate geometries. Cross sections of weld toe areas were cut, polished and etched. These are shown in Fig. 5.9, Fig. 5.10 and Fig. 5.11. Fig. 5.9 and Fig. 5.10 show shrinkage cracks running in the HAZ. When these are present at the weld toe, they lie almost perpendicular to the direction of the applied stress. As they follow the contour of the weld cross-section, however, they change direction

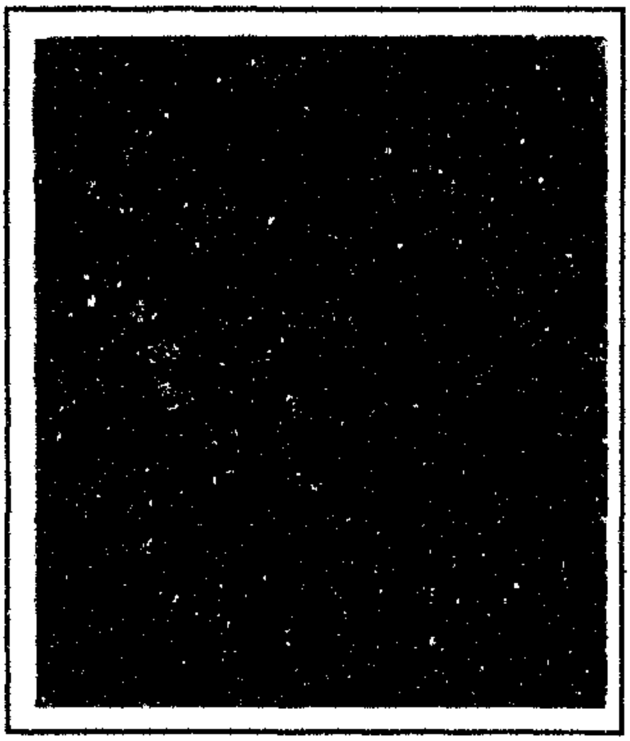

Fig. 5.9 - Cross section of an end weld with shrinkage cracks and porosity (x 40).

and eventually lie parallel to the direction of the stress. Thus, at a certain crack depth, these cracks will have little affect on the growth of the fatigue cracks.

A fatigue crack will always grow perpendicular to the direction of the applied stresses. Since the stresses that were applied to the I-beams were parallel to the flange surface, a crack would tend to grow into the flange. At the weld toe surface of the I-beams, there were already shrinkage cracks present which ran perpendicular to the applied stress. These cracks follow grain boundaries, and hence, at depth of approximately one grain below the surface of the I-beam they tended to become parallel to the stress axis. It was therefore the size of the surface grains which appeared to determine the size of the initial defect of the I-beams which were welded with cover plates. This initial defect size, a_0, seemed to vary between 0.3 mm and 0.8 mm. For the purpose of integrating the 'Paris Law', and to keep the predictions generally conservative, the initial defect size for I-beams welded with cover plates was estimated to be 0.7 mm. The fact that these shrinkage cracks did change direction at a depth of one grain is indicated in Fig. 5.12 and Fig. 5.13.

Fig. 5.10 - Etched cross section of a weld with subsurface intergranular shrinkage cracks and grain boundaries. (x 50)

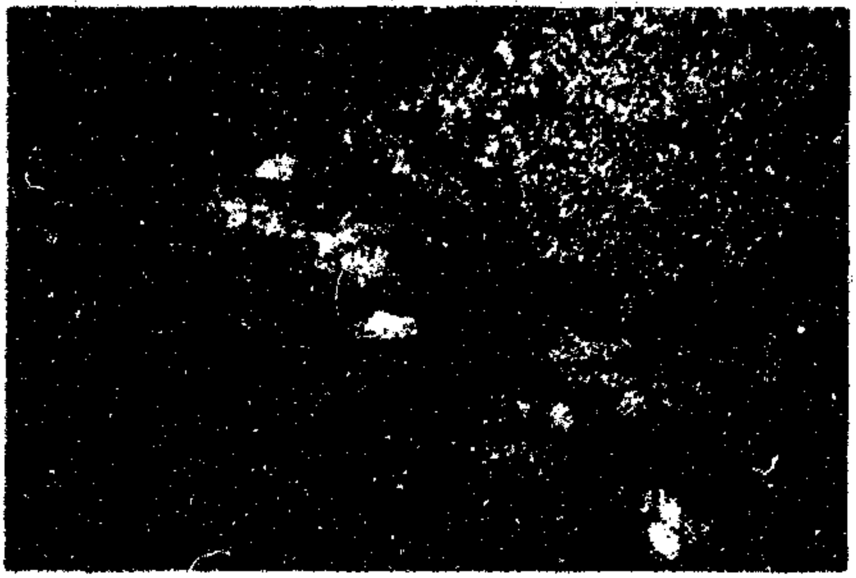

Fig. 5.11 - Cross section of an end weld showing shrinkage cracks (x 10).

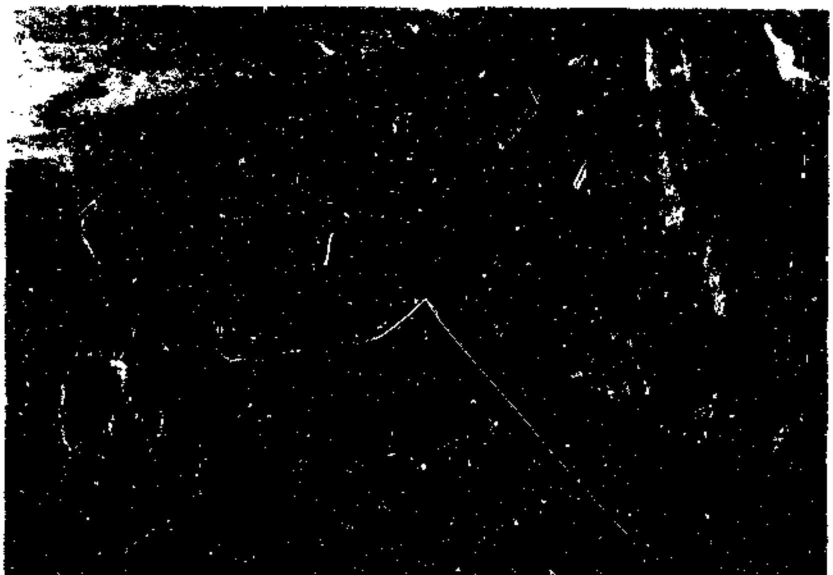

Fig. 5.12 - Fracture surface at the weld toe of an I-beam with a square, end welded cover plate. (x 95)

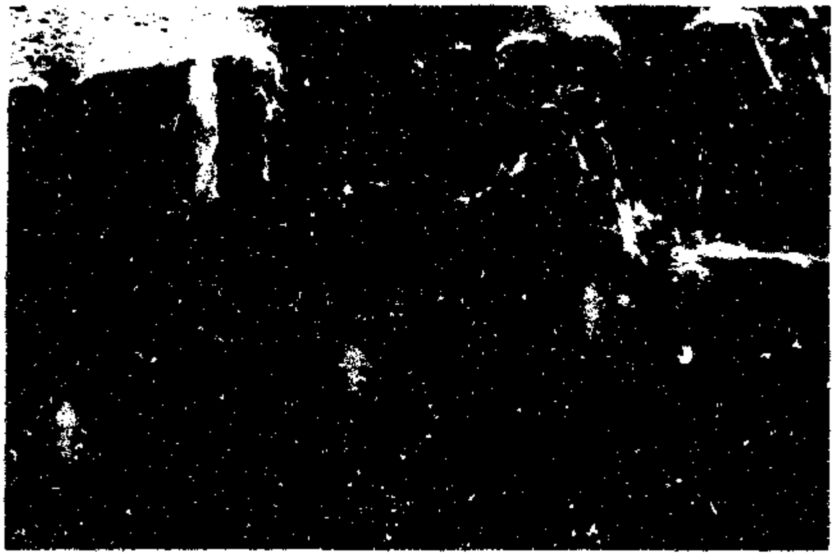

Fig. 5.13 - Fracture surface at the weld toe of an I-beam with a diamond, end welded cover plate. (x 50)

Fig. 5.14 gives an example where, on a few occasions, the fatigue crack followed the shrinkage crack to become roughly parallel to the stress axis for a short distance. Here, the fatigue crack initiated from the shrinkage crack at the weld toe of a square end welded cover plate. The fatigue crack followed the shrinkage crack and 'caved in' below the weld metal over a growth increment of about 0.6 mm. This type of 'caving in' did not occur very often. When it did occur, however, it was only a local occurrence over a small area of the weld.

Some fracture surfaces showed cracks, which appeared to be shrinkage cracks, which were at times present at great depths. Fig. 5.15 shows such shrinkage cracks at a depth of about 2 mm. When one glances at Fig. 5.11, the line A-A would approximately be the path that a fatigue crack would take. The welded I-beams contain a population of grain boundary cracks. If the fatigue crack approaches such a crack that is more or less perpendicular to the direction of the flange surface, it will follow the shrinkage crack as long as the direction does not change radically. If the shrinkage crack lies parallel to the direction of the flange surface, the fatigue crack will simply tend to ignore it and continue its growth through the next grain. This leads to the formation of intergranular regions on the fracture surface.

It is interesting to note that the presence of initial defects was not only limited to the 100 x 75 sized I-beam. Fig. 5.16 and Fig. 5.17 show that the same type of initial defects occur in the 150 x 101 mm and the 48 x 27 mm sized I-beams. The initial defect shown in Fig. 5.16 was measured to be about 0.6 mm. The size of initial defect ranged between 0.45 and 0.7 mm in all the 150 x 101 mm I-beams. An initial defect size of 0.6 mm was therefore used in the prediction procedure for the 150 x 101 mm I-beams. The initial defect size in the 48 x 27 mm I-beams lay in the range between 0.14 to 0.2 mm. An initial defect of 0.18 mm was therefore used in the prediction procedure for the 48 x 27 mm I-beams.

Since shrinkage cracks are present throughout the welds, the initial defects can be taken to be essentially as wide as the end weld. Thus, in the 100 x 75 mm I-beams, the square end weld and rounded cover plate geometry had a crack width, 2c, of approximately 40 mm and 30 mm respectively. The diamond end weld cover plate geometry had a crack width, 2c, of approximately 12 mm. The cover plate geometries with no end weld had a crack width, 2c, of about 7 mm. From this, one can determine the initial aspect ratio of crack depth to crack width, *i.e.* $2c / a_i$. This initial aspect ratio varied, when considering the extreme cases, between 133 and 9.

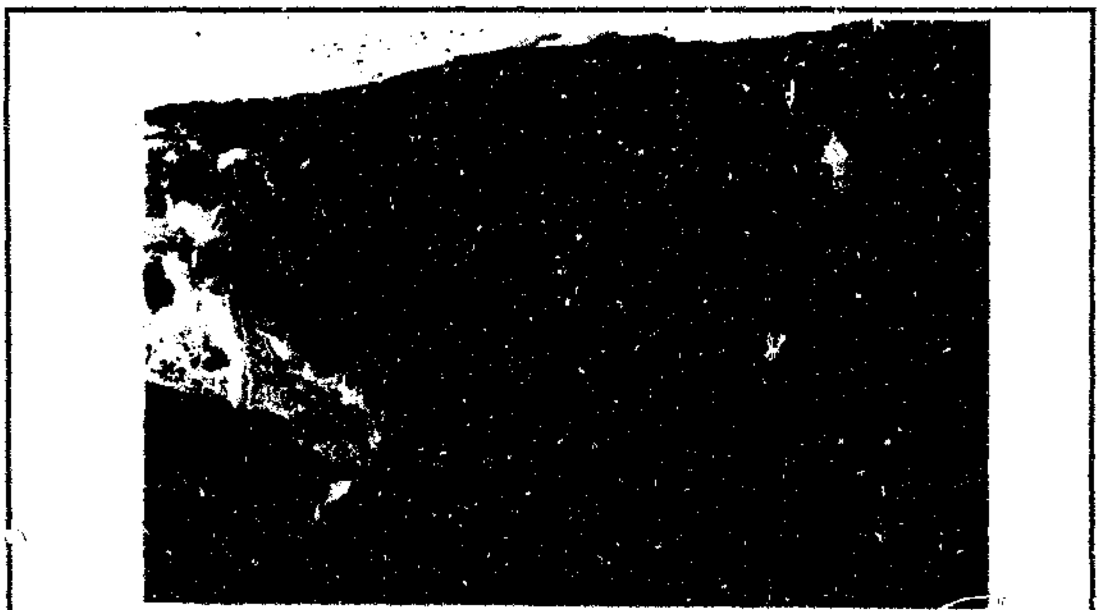

Fig. 5.14 - Fatigue fracture surface at the weld toe of an I-beam with a square end welded cover plate. (x 12)

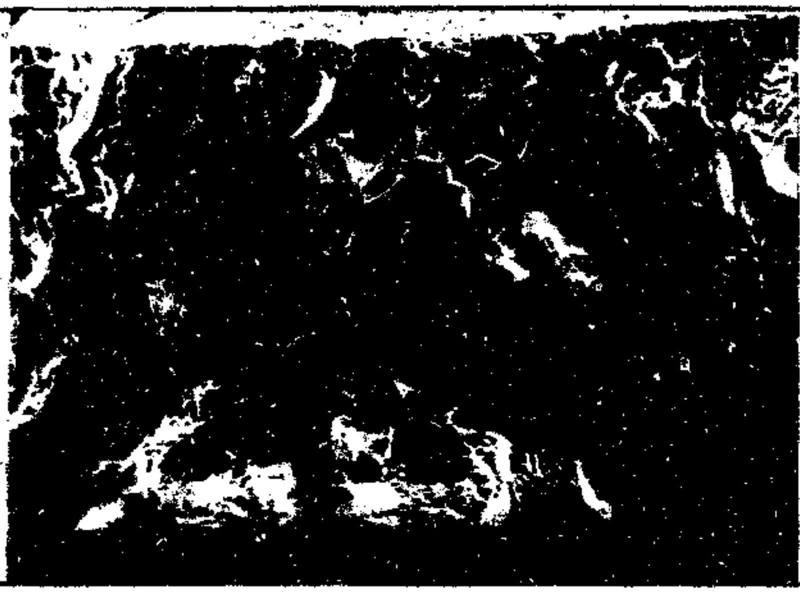

Fig. 5.15 - Fatigue fracture surface of an I-beam with a square end welded cover plate. (x20)

Fig. 5.16 - Typical initiation site of a 150 x 101 mm sized I-beam with a square end welded cover plate. (x 30)

Fig. 5.17 - Typical initiation site of a 48 x 27 mm sized I-beam with a square end welded cover plate. (x 240)

5.1.3. Mode of Fracture

The mode of fracture of the beams that were welded was significantly different to those that were not welded. The beams that were not welded showed a transgranular fracture mode. The welded beams, however, showed that both the transgranular and the intergranular fracture mode were at some stage the dominant mode of fracture.

Fig. 5.18 shows the typical fracture surface of an I-beam that was not welded. The crack initiated at a small defect, close to the surface of the beam, and then grew in a transgranular mode, transverse to the direction of the applied stress. The arrows indicate the regions, where the crack crossed grain boundaries.

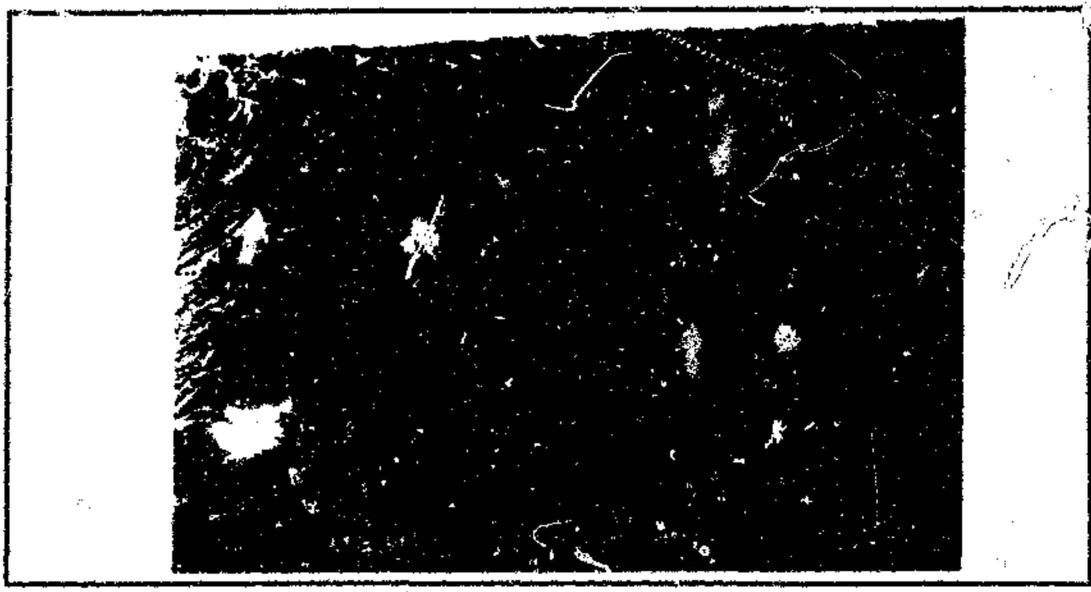

Fig. 5.18 - Typical fatigue fracture surface of a plain I-beam. (x 80)

Fig. 5.19 - Fracture surface at the weld toe of an I-beam with a square, end welded cover plate, showing intergranular and a transgranular fracture modes. (x 39)

The fracture surfaces of the welded beams show a different fracture mode to that of the plain I-beams. As can be seen in Fig. 5.19 they contain both transgranular and intergranular regimes. The reason for this has already been discussed in section 5.1.2, i.e. to the presence of shrinkage cracks. Edwards and Martin [37] have, however, shown that for peak aged Al-Mg-Si alloys, the degree of intergranular failure increases with stress intensity range and decreases as the volume fraction of dispersoids increases. It is thus important to view the fracture surfaces of the welded beams in this light.

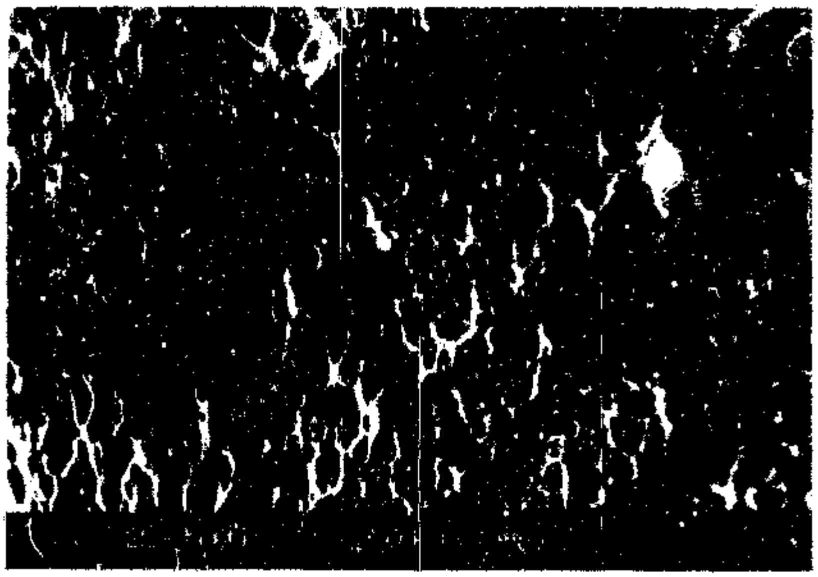

Fig. 5.20 - Fine dimples found on an intergranular surface of an I-beam welded with a square cover plate. (x 2500)

Due to the stress concentration at the weld toe, the stress intensity range there is up to 2.2 times higher than when there is no weld. As the crack grows below the weld toe, the crack tip stress intensity range decreases. This is due to the fact that the effect of the reduction of stress concentration with distance from the weld toe, far outweighs the effect of an increase in crack size. Thus, considering only argument given by Edwards and Martin[37], one would initially expect an intergranular fracture mode to occur, followed later, when the crack is larger, by a transgranular fracture mode.

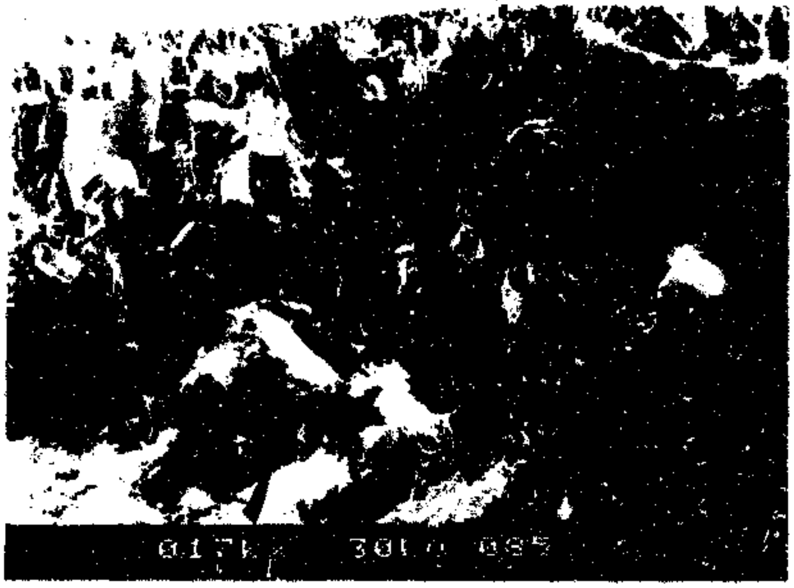

Fig. 5.21 - The areas where fine dimples, characteristic of microvoid coalescence, could be found. (x 17)

The I-beams were given a T6 temper during production. This involves solution treatment and then ageing to a peak hardness. The ageing process allows Mg_2Si dispersoids to precipitate out of solution. Further ageing would increase the volume fraction of dispersoids and lead to softening of the metal. When the beam is welded, the region surrounding the weld will have been subjected to further ageing because of the high temperatures associated with welding. This would introduce a higher volume fraction of Mg_2Si dispersoids into the base metal surrounding the weld. The amount of dispersoids that are added depends on the amount of heat introduced into the beam. It can thus be expected that the volume fraction of dispersoids is highest below the weld and decreases with distance from the weld, until the dispersoid volume fraction of the base metal has been reached. On the basis of the Edwards and Martin argument, this could lead to reduced intergranular fracture in the weld region.

These two effects, i.e. stress intensity range and volume fraction of dispersoids, oppose each other in determining which fracture mode will take place at the crack front. It is thus the most dominant effect which will dictate whether transgranular or intergranular fracture will occur.

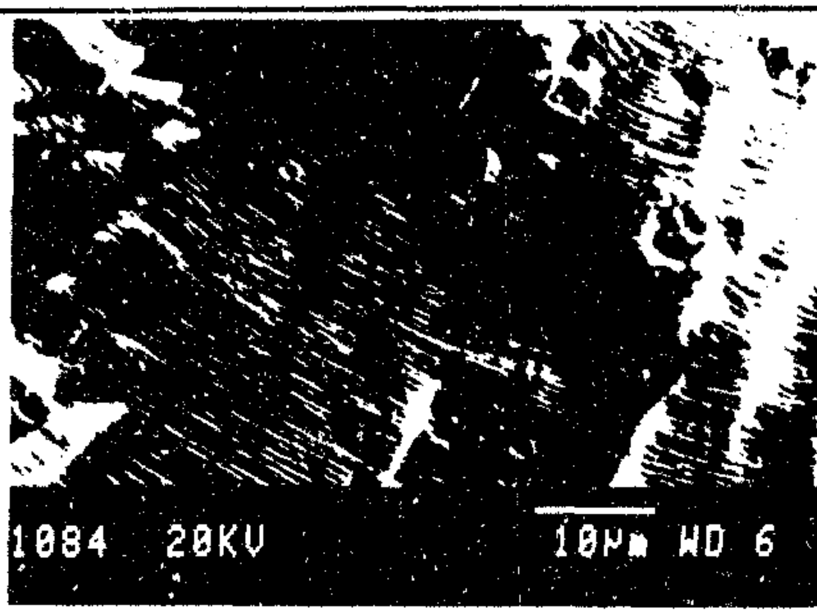

Fig. 5.22 - Striations visible at a distance of 20 mm from the initiation site of an I-beam welded with a square cover plate. (x 6500)

Edwards and Martin[38] have shown that only a percentage of their various fracture surfaces was intergranular. On closer examination by Edwards and Martin, the intergranular fracture surfaces could be seen to be covered in fine dimples. This indicated that microvoid coalescence took place along the grain boundary precipitate free zone. They suggested that grain boundaries, orientated favourably ahead of a crack tip, will fracture by microvoid coalescence along the precipitate free zone. Grains, whose grain boundaries are not favourably orientated to the crack, would fracture in a transgranular fashion, leaving striations behind.

As is shown in Fig. 5.20, this type of intergranular failure was sometimes observed on the fracture surfaces of the welded I-beams. The arrows in Fig. 5.21 show the few intergranular facets where the fine dimples characteristic of microvoid coalescence could be found. Other fracture surfaces such as that depicted in Fig. 5.22, showed markings characteristic of fatigue crack growth.

As the crack size increased, less and less intergranular fracture was observed, until the mode of fracture was transgranular only. This is a result of the effects of the reducing stress concentration and residual stresses as the crack grows away from the weld toe and the localisation of shrinkage cracks to the HAZ. Only once the crack had grown more than 15 mm from the initiation site, could striations be found. Fig. 5.22 shows striations on the fracture surface of a beam with a square cover plate.

Some I-beams were given a weld run, which was then ground flush with the flange surface. Fatigue cracks in these I-beams initiated at the surface of the weld metal and grew in a transgranular fashion into the parent plate. At no time did the crack initiate at the interface between the weld metal and base metal. A typical fracture surface of an I-beam with a ground weld run can be seen in Fig. 5.23.

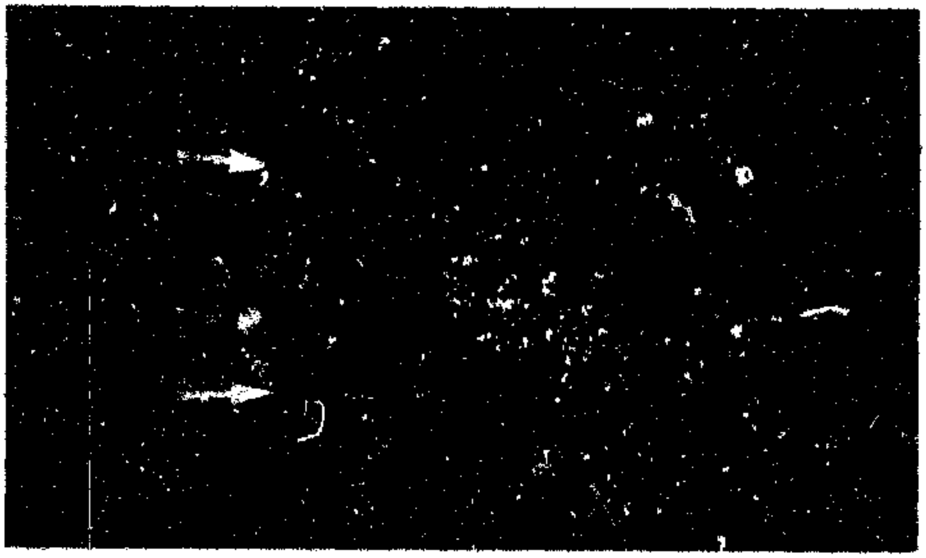

Fig. 5.23a - Macro section of an I-beam with a ground weld run showing that the fatigue crack grew through the weld. The arrow indicates the position of the fatigue fracture surface.

5.2. Fatigue Crack Growth Rate Data

The fatigue crack growth rate tests were done such that the fatigue crack growth rate was known for specific stress intensity ranges, ΔK. This in turn was used for the prediction of the fatigue lives of the I-beams.

from the initiation site, could striations be found. Fig. 5.22 shows striations on the fracture surface of a beam with a square cover plate.

Some I-beams were given a weld run, which was then ground flush with the flange surface. Fatigue cracks in these I-beams initiated at the surface of the weld metal and grew in a transgranular fashion into the parent plate. At no time did the crack initiate at the interface between the weld metal and base metal. A typical fracture surface of an I-beam with a ground weld run can be seen in Fig. 5.23.

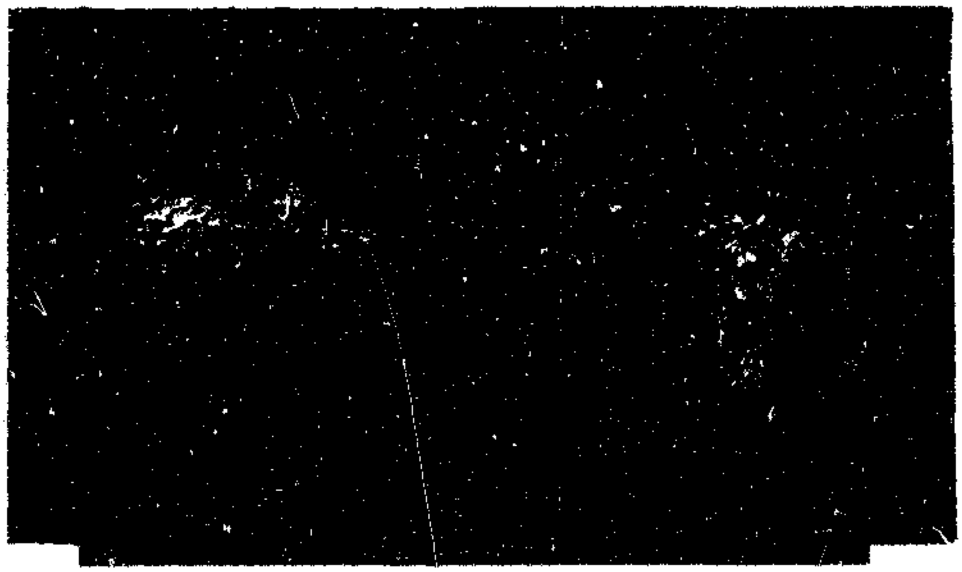

Fig. 5.23 - Fracture surface of an I-beam with a ground weld run. (x 10)

5.2. Fatigue Crack Growth Rate Data

The fatigue crack growth rate tests were done such that the fatigue crack growth rate was known for specific stress intensity ranges, ΔK. This in turn was used for the prediction of the fatigue lives of the I-beams.

fro
sur

So
Fa
tra
bet
we

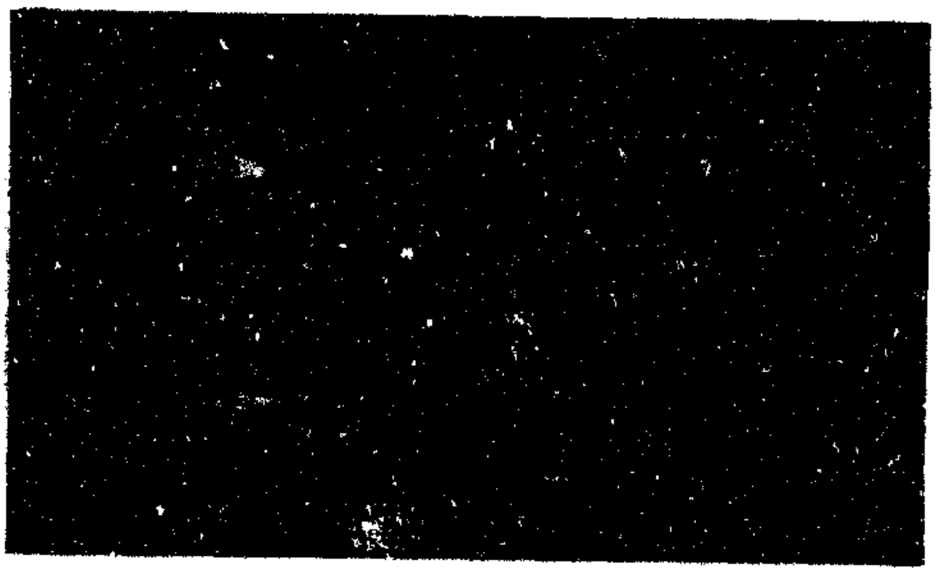

Fig. 5.23a - Macro section of an I-beam with a ground weld run showing that the fatigue crack grew through the weld. The arrow indicates the position of the fatigue fracture surface.

5

T
k
fi

The fatigue crack growth rate data, for the 6261-T6 aluminium alloy which was generated at stress ratios, R, of 0.1, 0.2, 0.5 and 0.7 are shown in Fig. 5.24, Fig. 5.25, Fig. 5.26 and Fig. 5.27 respectively. Fatigue cracks in the specimens that were tested at R = 0.1 and R = 0.2 would on occasion change their direction and / or branch. Fatigue cracks in the specimens tested at stress ratios of R = 0.5 and R = 0.7 behaved in a far more regular manner.

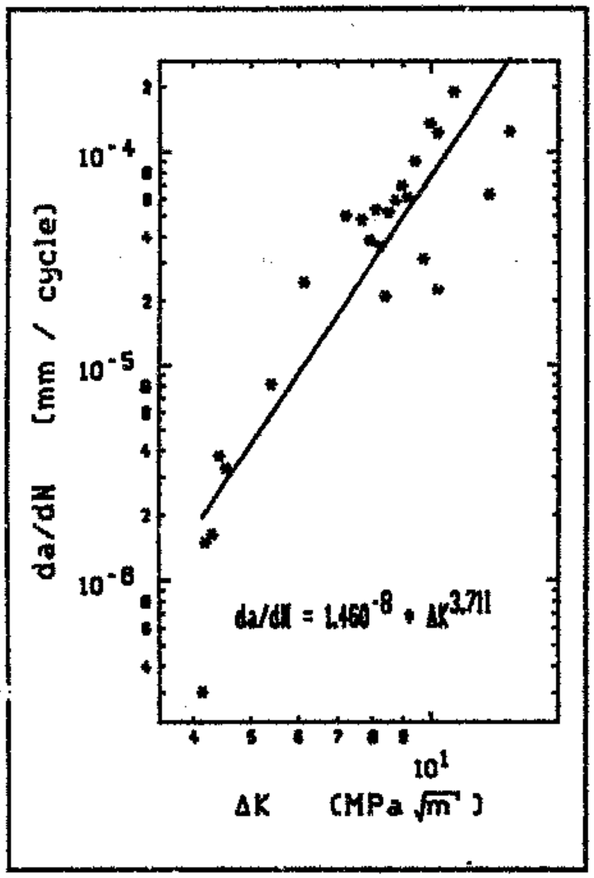

Fig. 5.24 - Fatigue crack growth rate curve of aluminium 6261-T6 at R = 0.1.

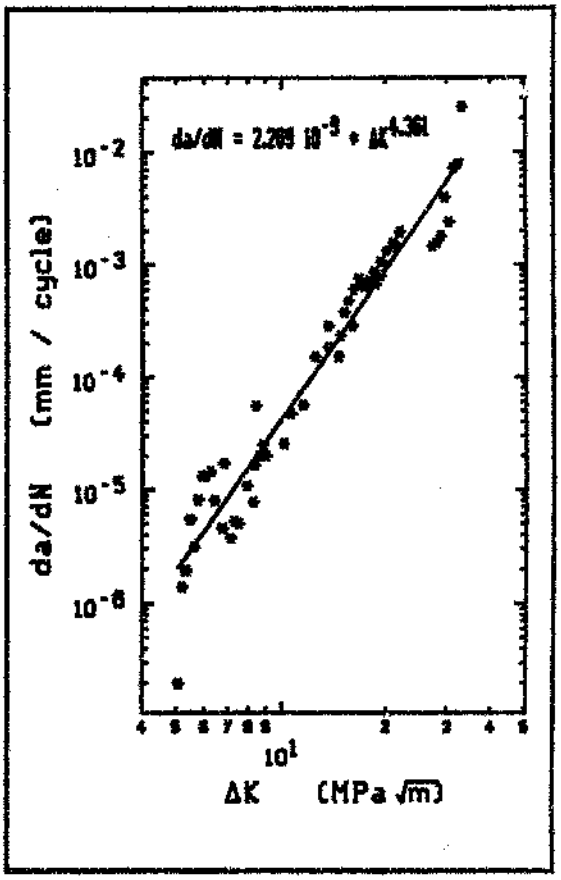

Fig. 5.25 - Fatigue crack growth rate curve of aluminium 6261-T6 at R = 0.2.

According to Ewalds[5], the threshold stress intensity range, ΔK_{th}, should decrease as the stress ratio is increased. This is because the amount of crack closure is reduced as the stress ratio is increased. Fig. 5.28 shows ΔK_{th} for the four stress ratios. One can see that the trend according to Ewalds is maintained, except for the threshold value at R = 0.1. Here the threshold value is less than that at R = 0.2. This behaviour could be attributed to material scatter in the data or to problems associated with crack branching.

Load-offset displacement plots were obtained, using back face strain gauges, corresponding to all of the data points of the various curves, except for the tests run at constant K_{max}. From these traces an attempt was made to find the stress intensity, K_{op}, at which the crack opened when the load was increased from the minimum load.

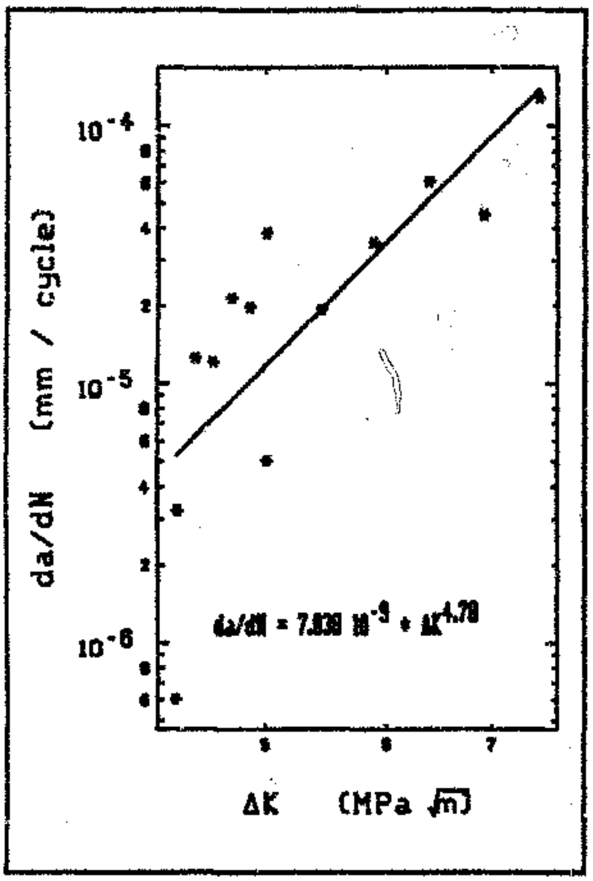

Fig. 5.26 - Fatigue crack growth rate curve of aluminium 6261-T6 at R = 0.5.

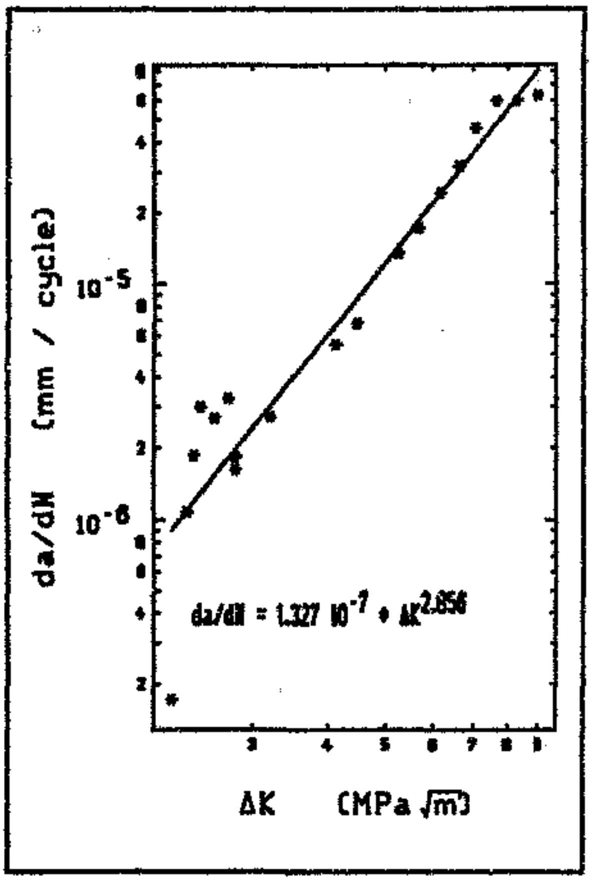

Fig. 5.27 - Fatigue crack growth rate curve of aluminium 6261-T6 at R = 0.7.

The K_{op} values were taken to be at the points of inflection. These points were, however, not always very clear since some traces appeared to have more than one point of inflection. Thus many of the K_{op} values were found by trial and error, where different possibilities were examined to see which gave the best fit, within the likely range of K_{op} on the trace. It is therefore not surprising that a large amount of scatter was found within the results.

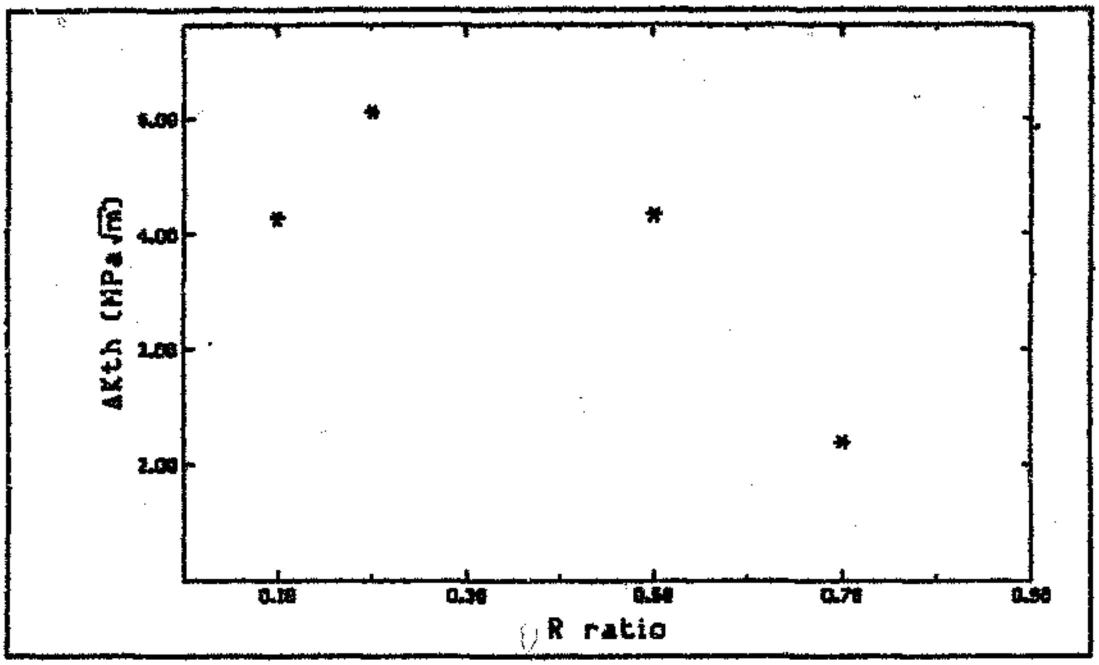

Fig. 5.28 - Threshold stress intensity range, ΔK_{Th}, for various stress ratios, R.

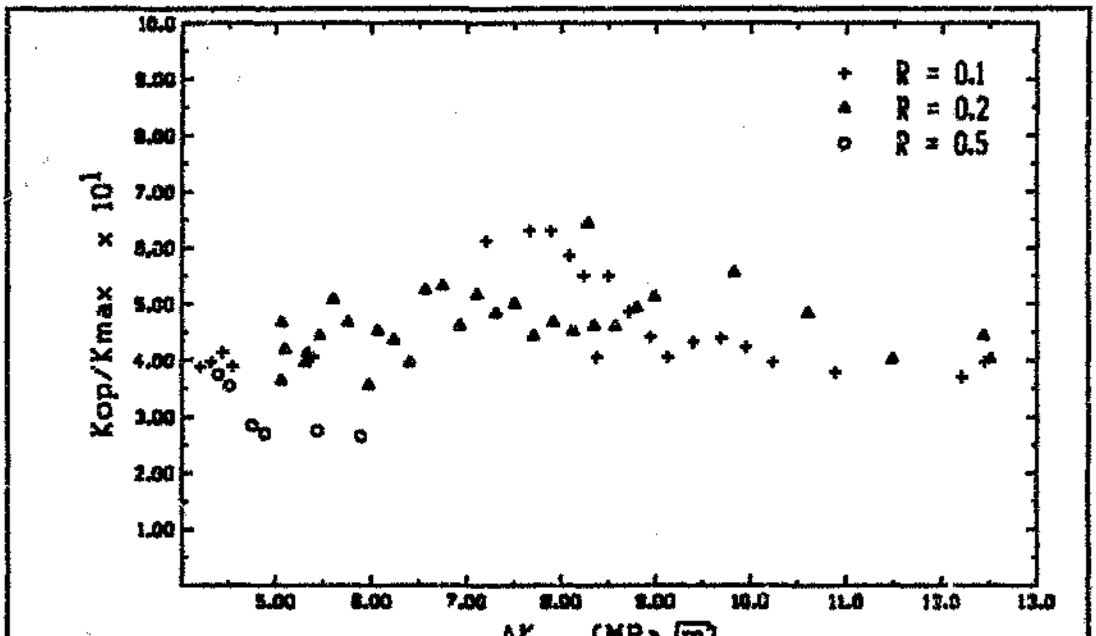

Fig. 5.29 - K_{op}/K_{max} against ΔK at various R ratios.

As was expected, crack closure was not found in specimen tested at R = 0.7. Fatigue crack closure was found to take place in the tests done at R = 0.1, R = 0.2 and R = 0.5. A plot of K_{op}/K_{max} versus ΔK is shown in Fig. 5.29.

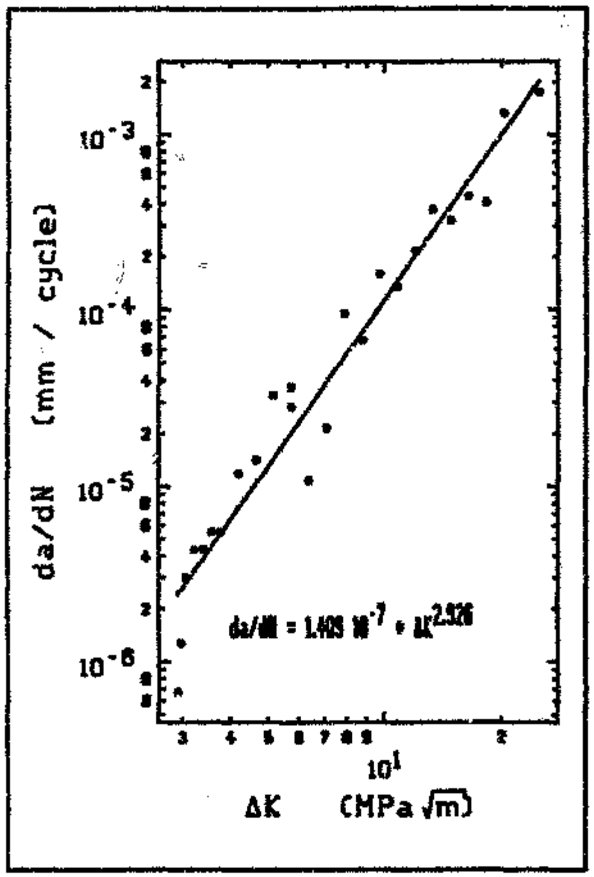

Fig. 5.30 - Fatigue crack growth rate curve of aluminium 6261-T6 at K_{max} = 30 MPa√m.

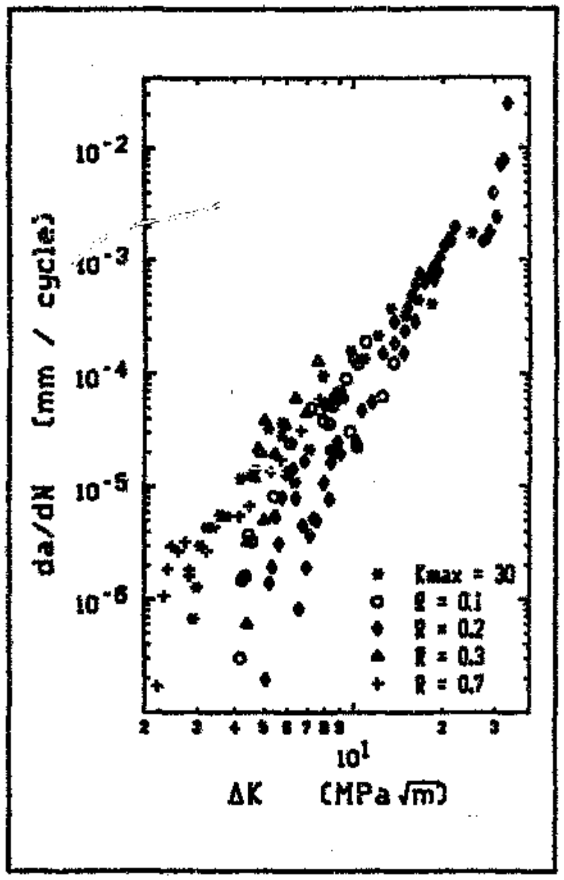

Fig. 5.31 - Comparison of fatigue crack growth rate curves of aluminium 6261-T6.

It is apparent from Fig. 5.29 that for ΔK values in the range 8 - 13 MPa√m the amount of crack closure increases with decreasing ΔK, in the tests performed at a stress ratio of 0.1, 0.2 and 0.5. This increase in closure can be attributed to the increased plasticity induced closure, caused by the load shedding routine[58,59]. This mechanism seems to be obvious for the specimen tested at R = 0.2. For the initial six data points, the loads were decreased by 10%. This left a large plastic zone behind the crack tip, causing the closure loads to increase. Once a load reduction of 5% was used, i.e for ΔK values less than 9 MPa√m, the closure loads were reduced. This resulted from the reduction of the plasticity induced closure.

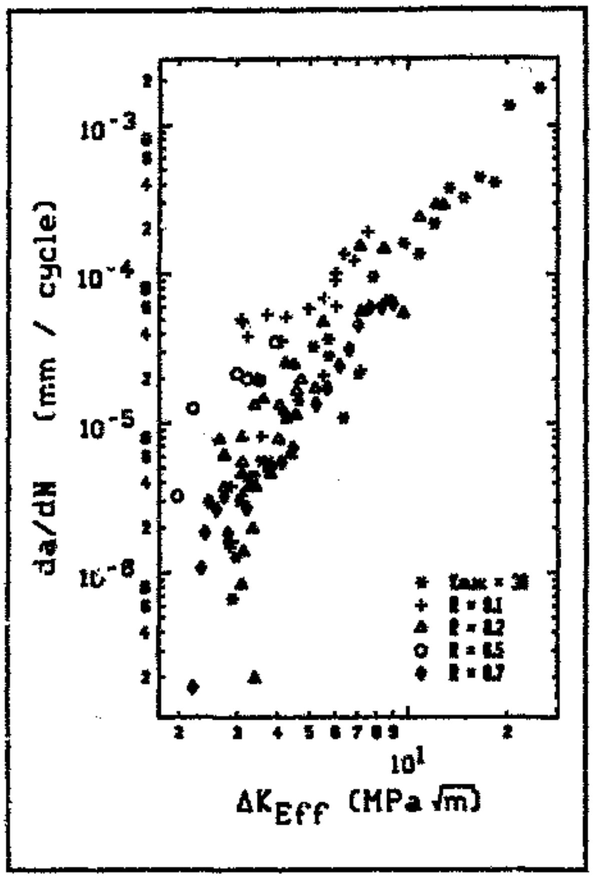

Fig. 5.32 - A comparison of fatigue crack growth rate curves of aluminium 6261-T6 after factoring out the effect of crack closure.

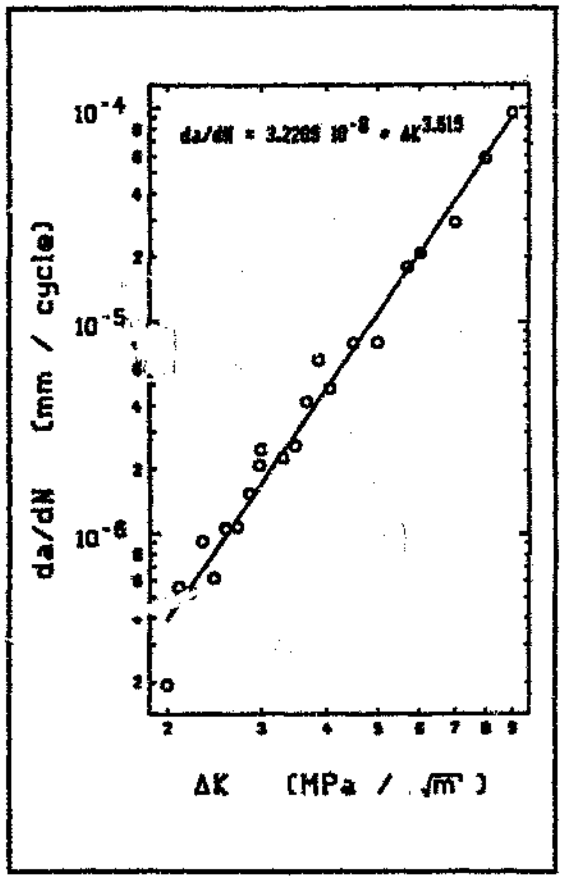

Fig. 5.33 - Fatigue crack growth rate data for the HAZ region at a constant K_{max} = 15 Mpa√m.

As the stress ratio, R, is increased, the effect of closure in the fatigue cycle is supposed to decrease[38]. This is because the load at which closure occurs remains more or less the same, whereas the minimum load is increased. Thus, the amount of closure that the specimen experiences over the load range is reduced. This is more or less the case for the lower ΔK values, i.e. less than 8 MPa√m, in Fig. 5.29, but the trends at the higher ΔK values are obscured by plasticity induced closure and scatter in the results.

Fatigue crack growth rate data was produced at a constant K_{max} = 30 Mpa√m and decreasing ΔK in order to get a curve that was free from the effect of crack closure and to compare it with curves generated at high stress ratios, which should also be closure free. This curve is shown in Fig. 5.30.

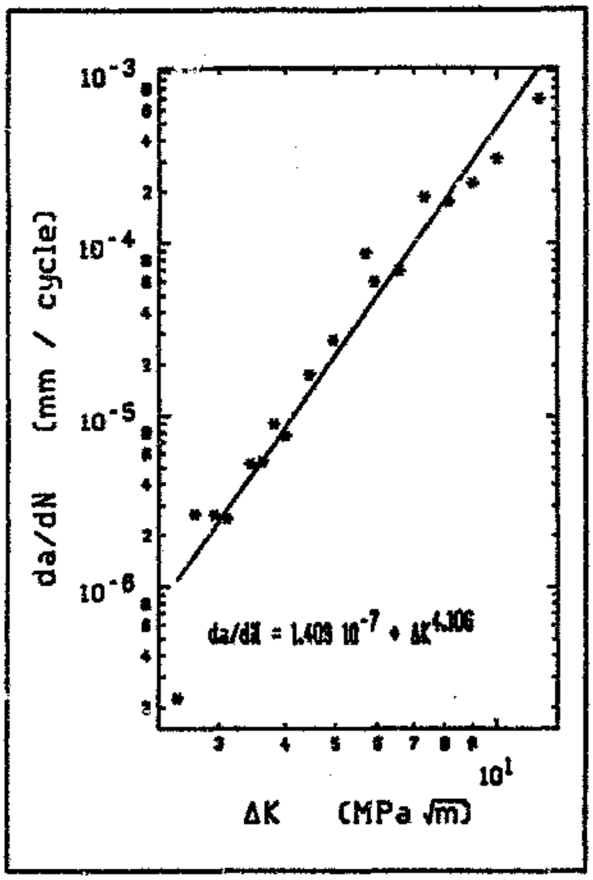

Fig. 5.34 - Fatigue crack growth rate data for the weld metal at a constant K_{max} = 20 MPa√m.

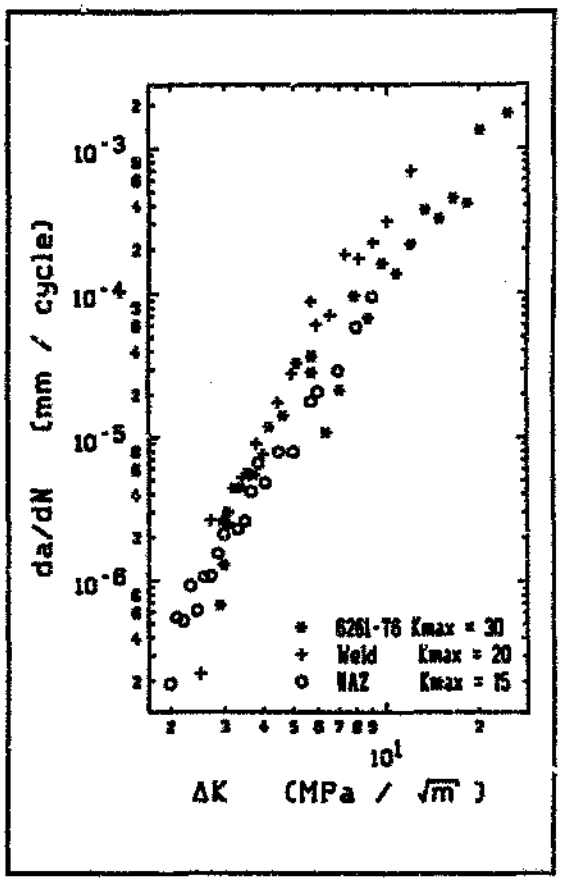

Fig. 5.35 - A comparison of fatigue crack growth rate curves for the parent plate HAZ and weld metal.

Fig. 5.31 shows a comparison of all of the fatigue crack growth curves already mentioned. It is interesting to observe that the curves generated at R = 0.7 and K_{max} = 30 MPa√m are almost the same. This leads to the conclusion that the fatigue crack growth curve at R = 0.7 is free from the effect of crack closure. One should also note the different slopes of the linear region of all curves. The difference in slopes between the various curves can be attributed to crack closure becoming more important in the threshold regime, particularly at the lower stress ratios.

Fig. 5.32 compares the effective stress intensity range, ΔK_{eff}, of the fatigue crack growth rate curves obtained at R = 0.1, R = 0.2 and R = 0.5 with the crack closure free curves obtained at R = 0.7 and at a constant K_{max} of 30 MPa√m (while ΔK was decreased). Data for the lower K values compare reasonably well with the closure free curve, with the K_{max} = 30 MPa$\sqrt{m}$ curve appearing to be the upper limit to the growth rate data. There is, however, a fair amount of scatter present in the data. The curves at R = 0.1 and R = 0.2 compare especially well with the threshold stress intensity range found in the K_{max} = 30 MPa$\sqrt{m}$ test. The threshold stress intensity range is however higher than that found at R = 0.7, which could be due the effect of mean stress on the threshold value.

Only the plain I-beams, which were not welded, experienced cracking in the unwelded parent plate. The rest of the I-beams failed either in the heat affected zone (HAZ) or the weld metal. It was for this reason that fatigue growth rate curves had to be produced for the HAZ and the weld metal. These are shown in Fig. 5.33 and Fig. 5.34 respectively.

Since the I-beams were tested at R of 0.1, an attempt was made to obtain a curve for the HAZ region at R = 0.1. This however became an impossible task, since the fatigue crack would consistently branch off, giving erroneous results. Once the tests were carried out at a constant K_{max} of 15 MPa$\sqrt{m}$ with decreasing ΔK, no fatigue crack branching occurred. This curve will also correspond to a closure free crack growth. The presence of a weld introduces high tensile residual stresses in the region of the weld toe. Since the fatigue cracks initiated at the weld toe, the residual stresses would reduce crack closure in I-beam specimens during testing. The crack growth rate curve using K_{max} = 15 MPa$\sqrt{m}$ is thus likely to represent the fatigue conditions actually experienced in the I-beam specimens.

A comparison of the fatigue crack growth rate curves for the 6261 parent plate, the HAZ and the weld metal are shown in Fig. 5.35. From this one can see that the slopes of the linear regions of the parent plate curve and HAZ curve are almost the same. The change in microstructure due to welding, did not therefore seem to affect the fatigue crack growth rate too much. The slope of the linear region of weld metal curve is slightly steeper than that of the other curves. This may be due to scatter or differences in material properties.

5.3. S-N Data

I-beam Geometry	$\Delta\sigma$ at 10^5 cyc (MPa)	$\Delta\sigma$ at 10^7 cyc (MPa)	Mean Linear Regression Equation
Plain	220	60	$\ln(N) = 36.40 - 4.613 \ln(\Delta\sigma)$
Square end weld	95	34	$\ln(N) = 31.88 - 4.471 \ln(\Delta\sigma)$
Square no end weld	120	24	$\ln(N) = 25.37 - 2.892 \ln(\Delta\sigma)$
Diamond end weld	112	34	$\ln(N) = 29.11 - 3.672 \ln(\Delta\sigma)$
Diamond no end weld	114	29	$\ln(N) = 27.49 - 3.373 \ln(\Delta\sigma)$
Rounded end weld	100	34	$\ln(N) = 31.00 - 4.222 \ln(\Delta\sigma)$
Weld Run	142	70	$\ln(N) = 43.84 - 6.520 \ln(\Delta\sigma)$
All of 100 x 75 mm	110	30	$\ln(N) = 28.53 - 3.618 \ln(\Delta\sigma)$
150 x 101 mm	66	25	$\ln(N) = 31.74 - 4.821 \ln(\Delta\sigma)$
48 x 27 mm	79	32	$\ln(N) = 34.13 - 5.169 \ln(\Delta\sigma)$

Table 5.1 - Fatigue strengths at 10^5 and 10^7 cycles and the mean linear regression equations of all the various cover plate geometries.

All the S-N data for the various I-beam geometries are shown in Fig. 5.36 to Fig. 5.43. The fatigue life curve for the plain I-beam is inserted in every figure as a reference line, so that meaningful comparisons can be made between figures. 80% and 95% confidence limit lines, which were statistically obtained using the t-distribution of the fatigue life data, were added to the curves. These limits show that S-N data lies, with a certainty of 80% or 95%, between the limit lines. The mean linear regression equations for the various cover plate geometries are given in Table 5.1.

From Fig. 5.44 one can see that the S-N curves have different slopes and that they intersect at about 6 x 10^5 cycles. Due to the difference in these slopes there are significant differences in the fatigue data at high and low fatigue lives. Fatigue data at 10^5 and 10^7 cycles was compiled in Table 5.1 in order to make comparisons between the different S-N curves. At 10^5 cycles the difference in the fatigue life stress range for the different 100 x 75 mm I-beam geometries welded with cover plates was about 26%. At 10^7 cycles the difference in fatigue life stress range was about 29%. These differences are significant and thus cover plate geometry should be taken into consideration when designing against fatigue.

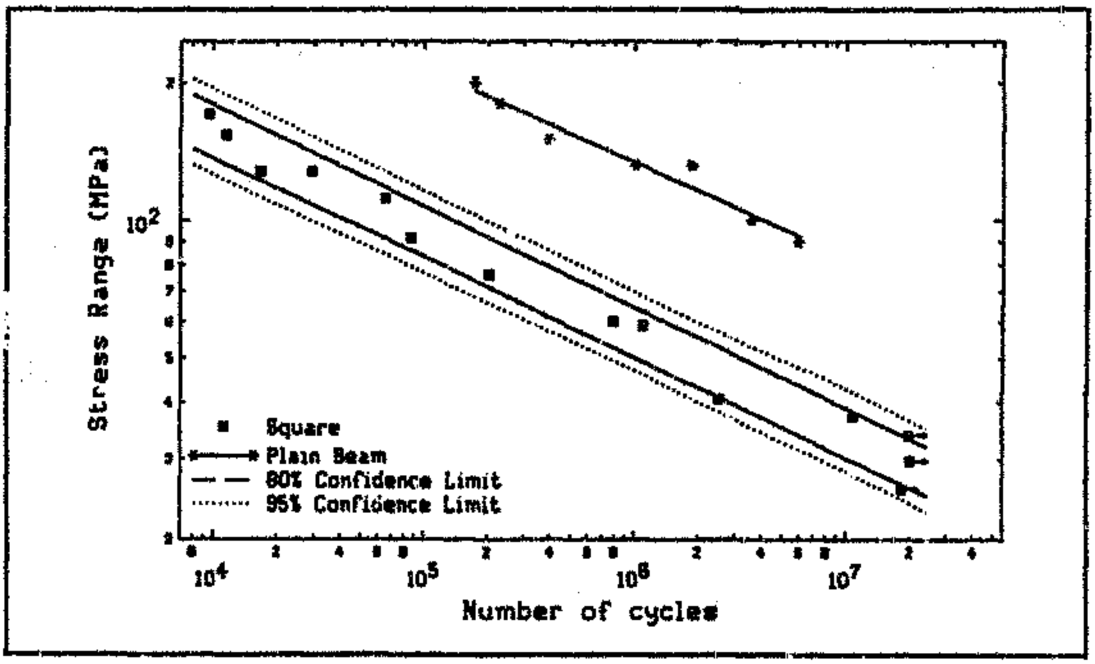

Fig. 5.36 - Fatigue life data for I-beams with square, end welded cover plates.

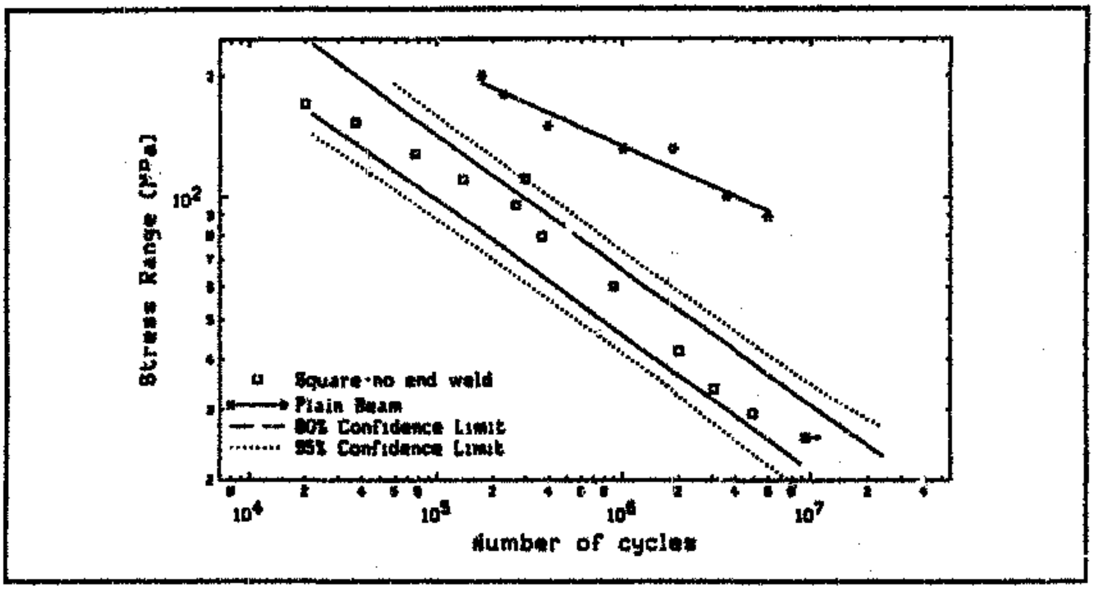

Fig. 5.37 - Fatigue life data for I-beams with square cover plates which had no end weld.

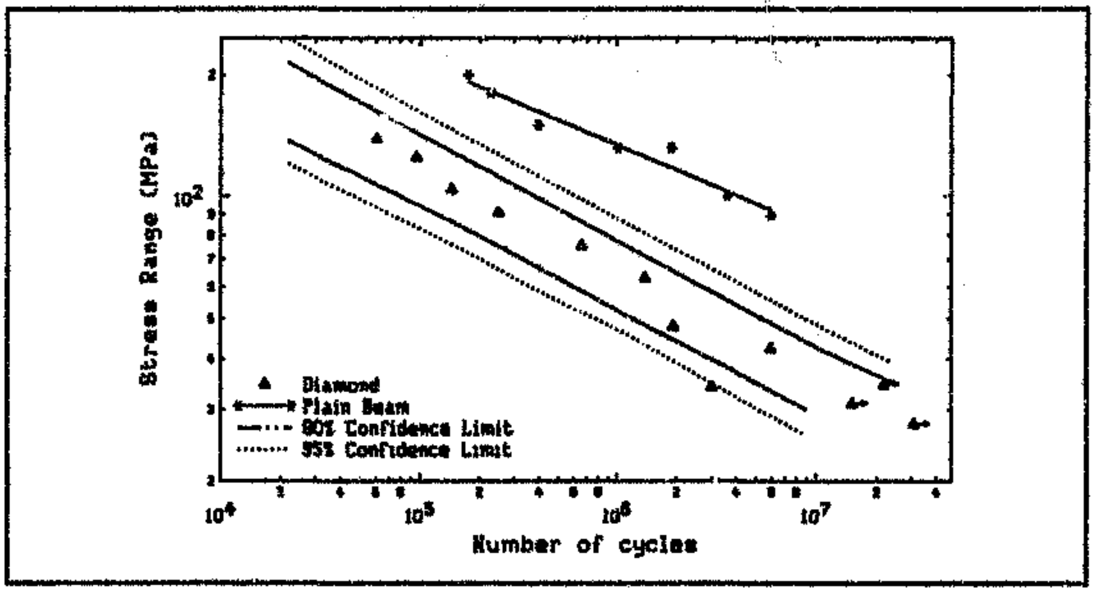

Fig. 5.38 - Fatigue life data for I-beams welded with diamond shaped cover plates.

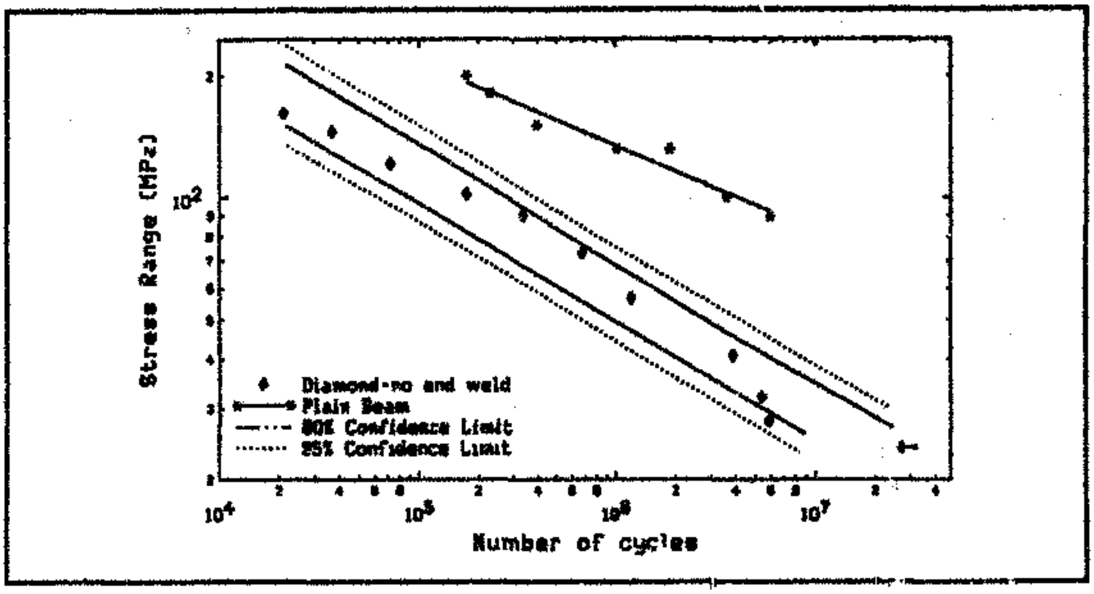

Fig. 5.39 - Fatigue life data for I-beams with diamond shaped cover plates which had no end weld.

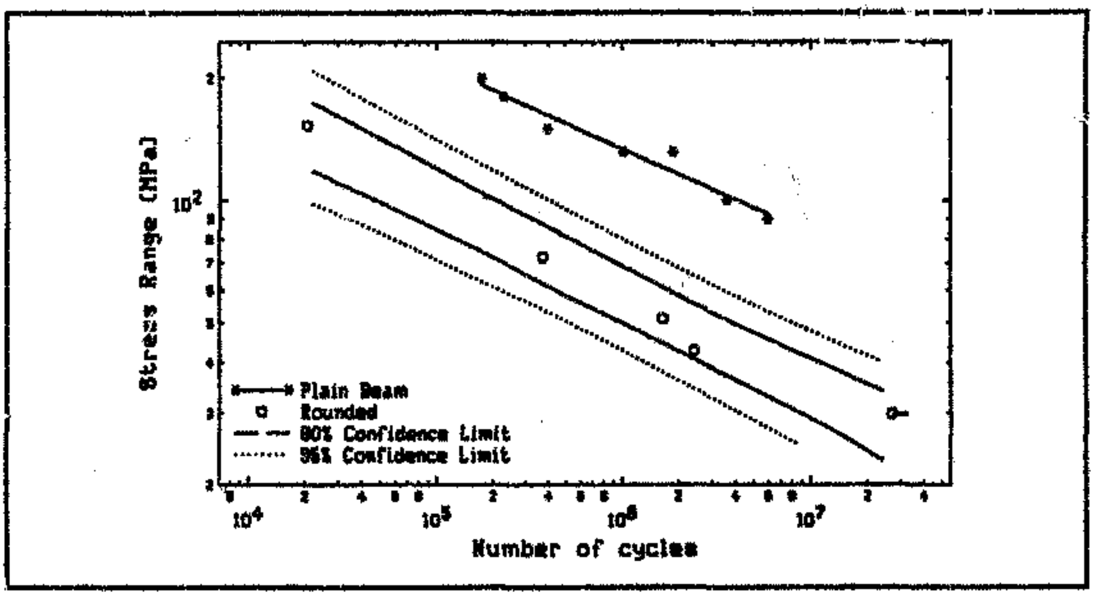

Fig. 5.40 - Fatigue life data for I-beams with rounded cover plates.

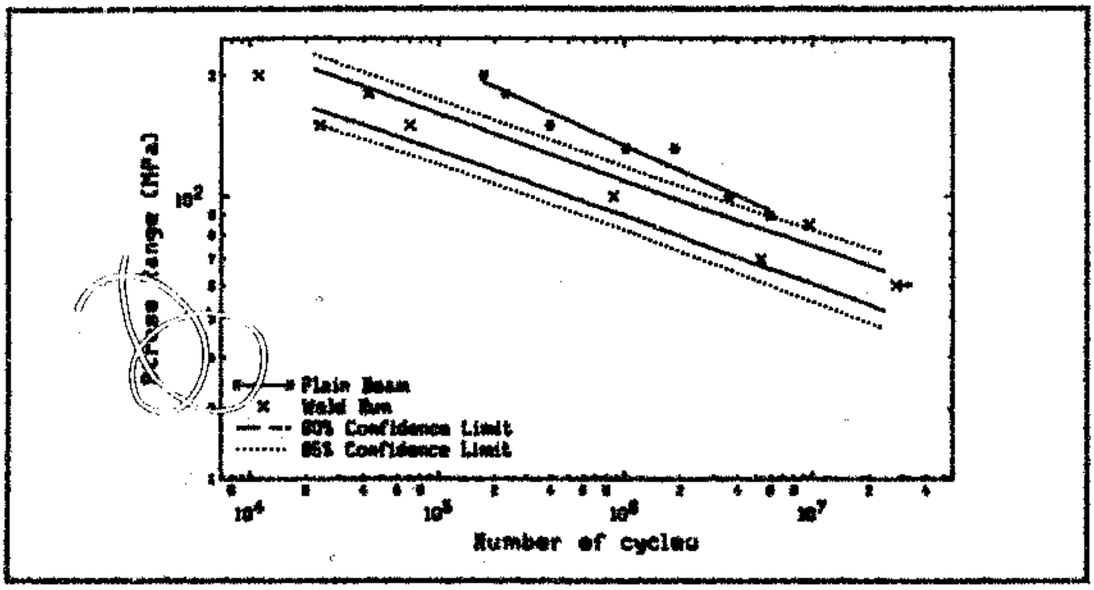

Fig. 5.41 - Fatigue life data for I-beams which were given a weld run.

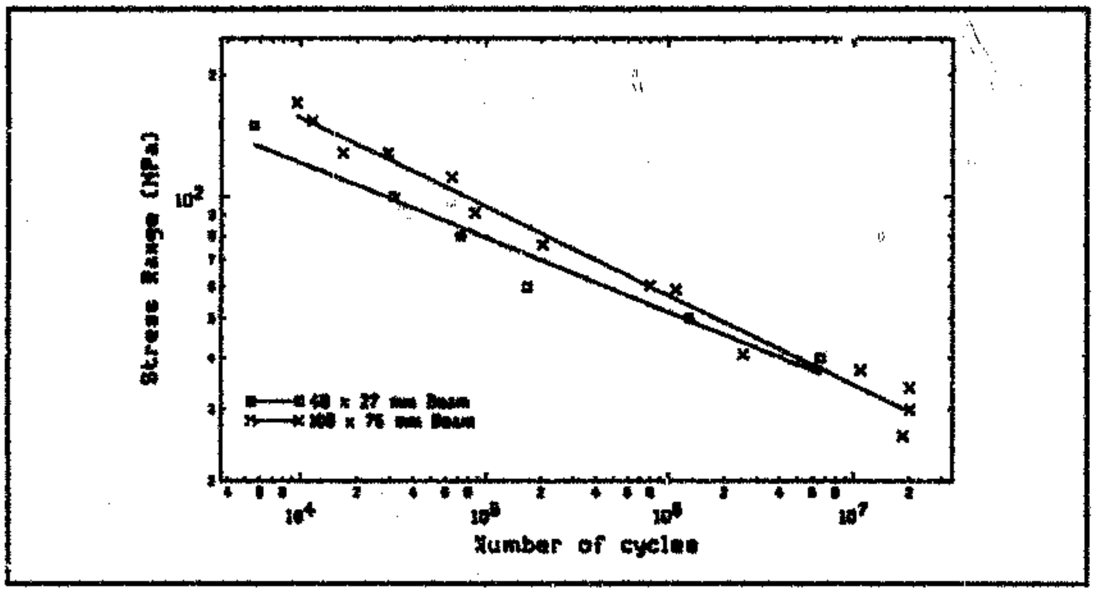

Fig. 5.42 - Fatigue life data for the 48 x 27 mm I-beams with square end welded cover plates.

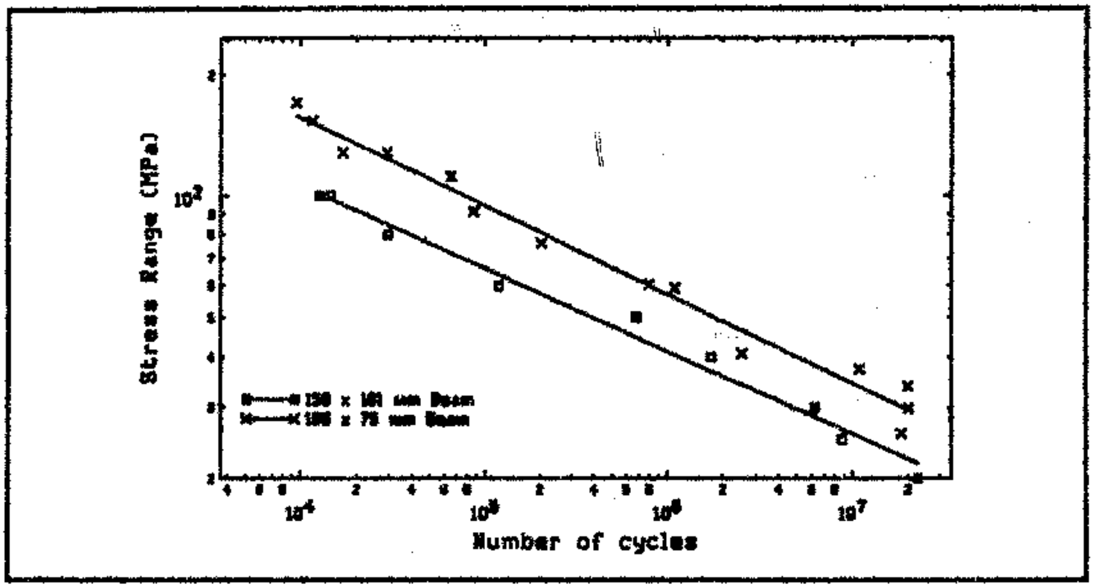

Fig. 5.43 - Fatigue life data for the 150 x 101 mm I-beams with square end welded cover plates.

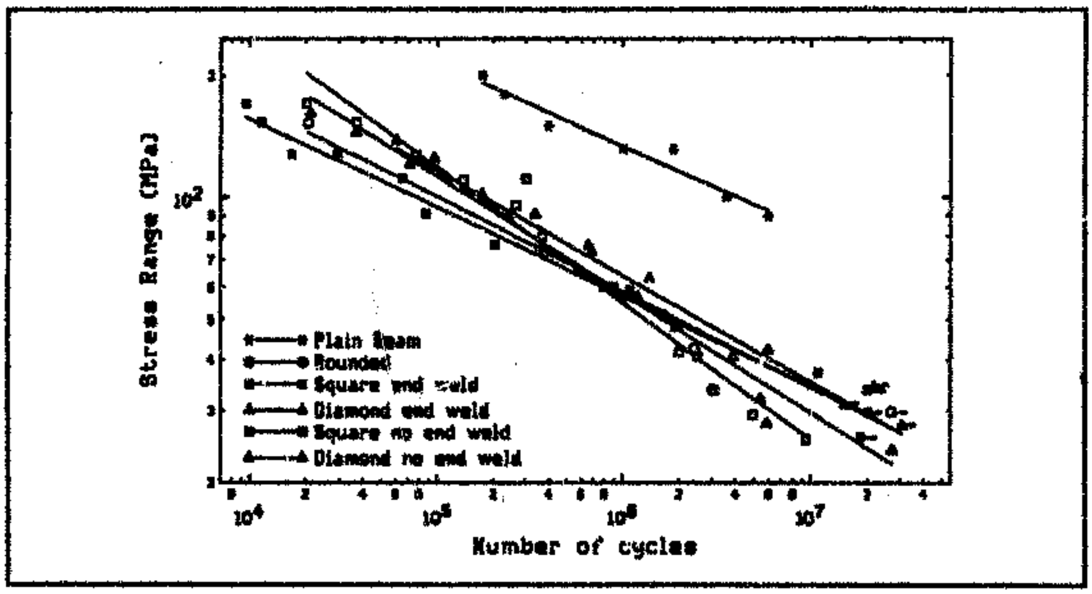

Fig. 5.44 - A comparison of the fatigue life data for the 100 x 75 mm I-beams which were welded with different cover plate geometries.

Fig. 5.44 compares the fatigue lives of the 100 x 75 mm I-beams with welded cover plates. It seems that the slopes of the S-N curves are inversely proportional to the width of the initiation sites. This seems to correlate with the work done by Fisher et al[10] and Yonji[20]. The square end welded cover plate geometry had the widest end weld of about 40 mm and thus the least slope. The respective widths of the rounded and diamond end welded geometries are about 30 mm and 12 mm. Fig. 5.45 shows differences in the S-N curves for the weld geometries with end welds.

The width of the weld ends are approximately the same for all the cover plate geometries without an end weld. The diamond geometry, however, initiated fatigue cracks at both of the longitudinal weld ends, whereas the square geometry initiated a fatigue crack at only one of the longitudinal weld ends. The diamond geometry therefore has a larger initiation area than that of the square geometry and hence the slope of its S-N curve is less steep than that of square geometry. It therefore seems that the square no end weld geometry yields the best fatigue

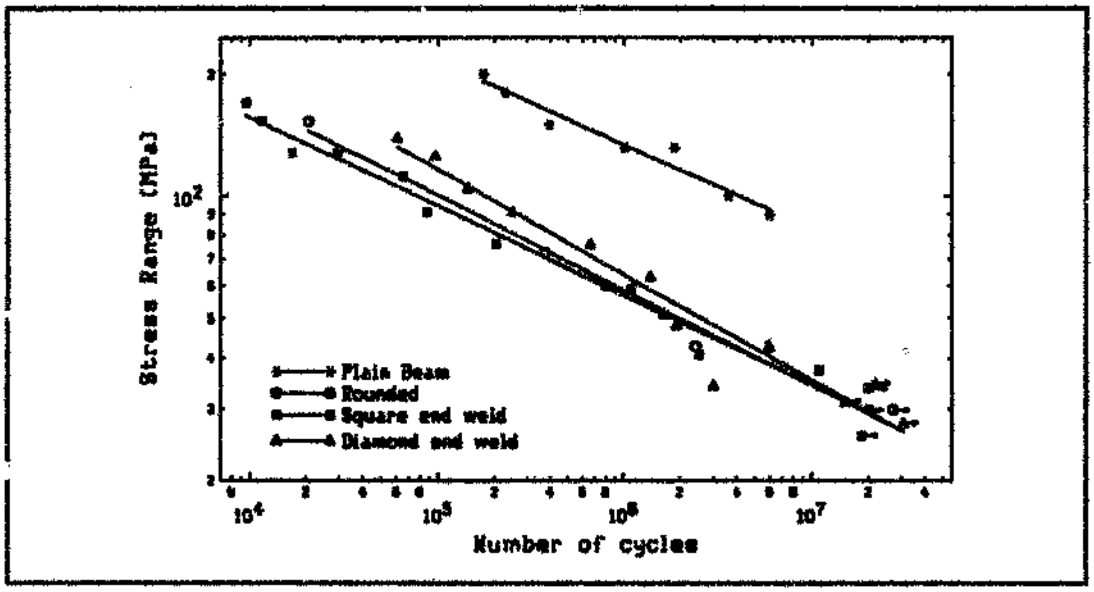

Fig. 5.45 - Comparison of fatigue life curves for the 100 x 75 mm I-beams with end welded cover plates.

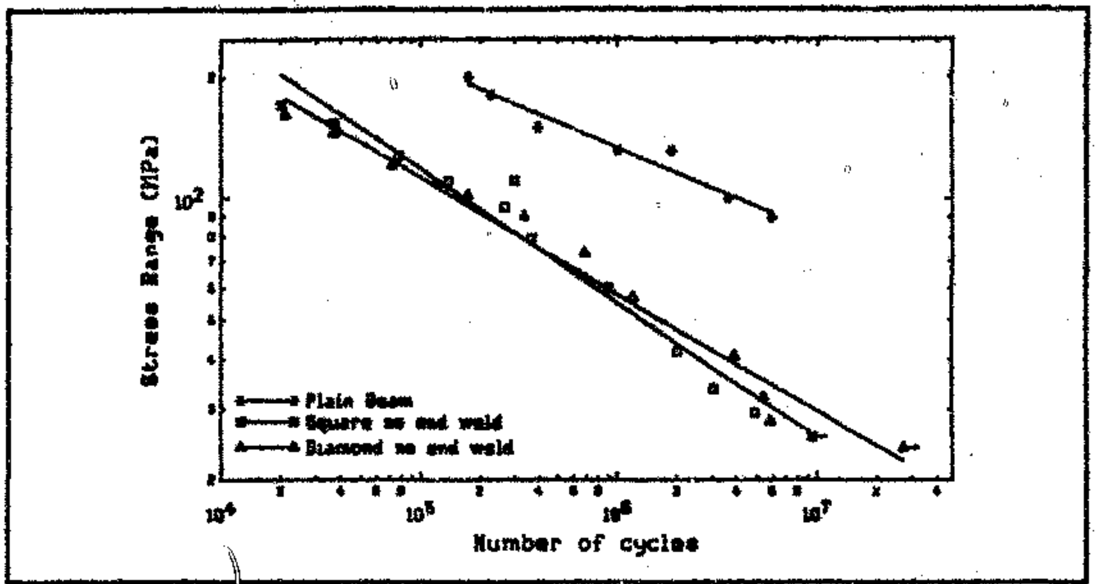

Fig. 5.46 - Comparison of fatigue life curve for 100 x 75 mm I-beams with cover plates with no end weld.

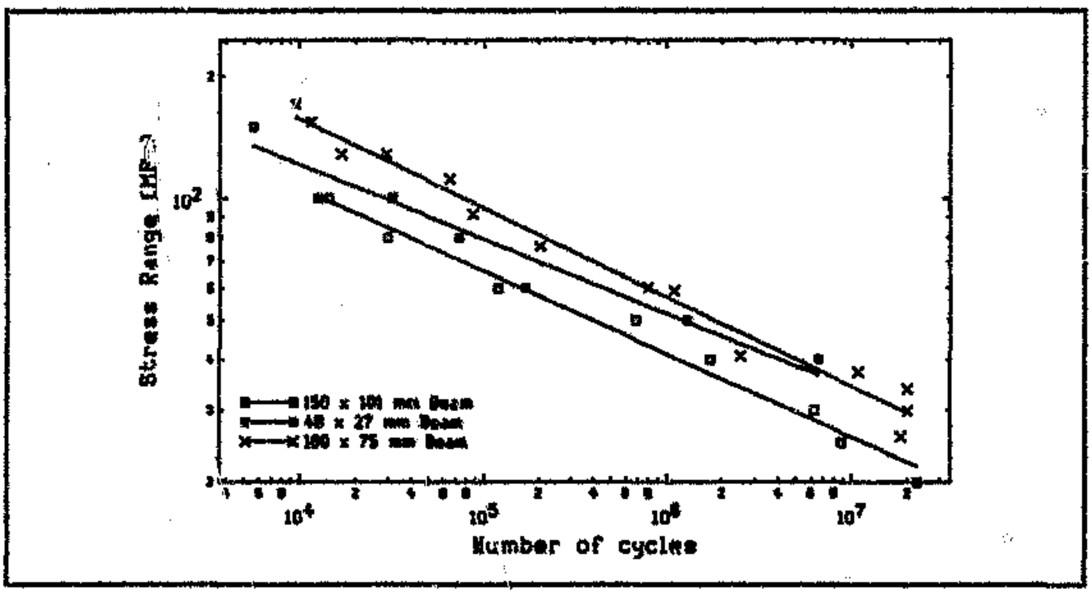

Fig. 5.47 - Comparison of the fatigue lives of different sized I-beams with square end welded cover plates.

strengths at low fatigue lives. Since the slopes of the S-N curves of the specimens with wider end welds are lower, their fatigue strength is higher at high fatigue lives. A comparison between the fatigue life curves of the I-beam for the weld cover plate geometries with unwelded ends is shown in Fig. 5.46.

The S-N curves of the 150 x 100 mm I-beams and the 48 x 27 I-beams show lower fatigue strengths than that for the 100 x 75 I-beams. The fatigue lives of the three sizes of I-beams with square end welded cover plates is shown in Fig. 5.47. A true comparison between the different sizes of I-beams cannot really be made. This is because various parameters which affect the fatigue life of the I-beams, i.e. initial defect, stress concentration, residual stresses and the amount of crack growth required to grow through the tension flange, changed as the I-beam size was changed. The weld profile was different for each size of I-beam which in turn changed the stress concentration. According to Fig. 3.6, the stress concentration effect of the 100 x 75 mm sized I-beam was the lowest of the three sizes of I-beams. Thus one would expect these I-beams to have the highest fatigue lives. The stress concentration effects of the 150 x 101 mm I-beams and the 48 x 27 mm I-beams are very similar. However, initial and final defect sizes are different and there is bound to be a difference in the residual stress distribution which, in turn would affect the fatigue lives of the I-beams. No adequate conclusions can be made as to why there was a difference in fatigue strengths for the various I-beam sizes, since some parameters, which could have affected the fatigue life of the specimen, could have changed with the change in I-beam size. It is however interesting to note that the slopes of the S-N curves of the three different sizes of I-beams are very similar.

5.4. Fatigue Life Prediction

Fatigue life predictions were performed for the plain 100 x 75 mm I-beam, the three different sizes I-beams welded with cover plates and those given a weld run. The stress concentration factor, M_k, was obtained for every size of I-beam welded with cover plates by modelling the cross section of a typical weld with the aid of a finite element analysis package. It is important to note that the cross section corresponded to a square cover plate geometry was chosen. Welding inconsistencies meant that some of the I-beams that were tested had different weld shapes to the one that was modelled. This would theoretically give them different fatigue lives since there would be a difference in stress concentration, and the fatigue life data did show some scatter.

The fatigue life data did, however, show a clearly defined trend. Thus, it is assumed that the fatigue life of the I-beams can be adequately predicted by a single, generalised geometry.

In predicting S-N curves for the plain 100 x 75 mm I-beams, the initial defect was chosen to be 0.1 mm (see section 5.1.2). No stress concentration effects were included since these I-beams had no cover plate welded onto them. Prediction curves for various R ratios were produced so that the differences in fatigue life of the parent plate, taking account of crack closure and thus also residual stresses, could be compared. The prediction curves, using the linear regime of the crack growth rate curves of R = 0.1, 0.2 and 0.7, are shown in Fig. 5.48. The prediction curve of R = 0.2 fits the fatigue life data of the plain I-beams very well. Since the plain I-beams were not welded, hardly any residual stresses are expected to be present in these I-beams. Thus some degree of crack closure can be expected to occur during fatigue testing. The prediction curve of R = 0.1 is lower than that of the S-N data . The prediction curve of R = 0.7 is much lower than that of the fatigue data of the plain I-beams. This is because this curve represents crack closure free crack growth, which is not expected to occur in the plain I-beams. It seems that the amount of crack closure that the plain I-beams experienced was similar to that of the

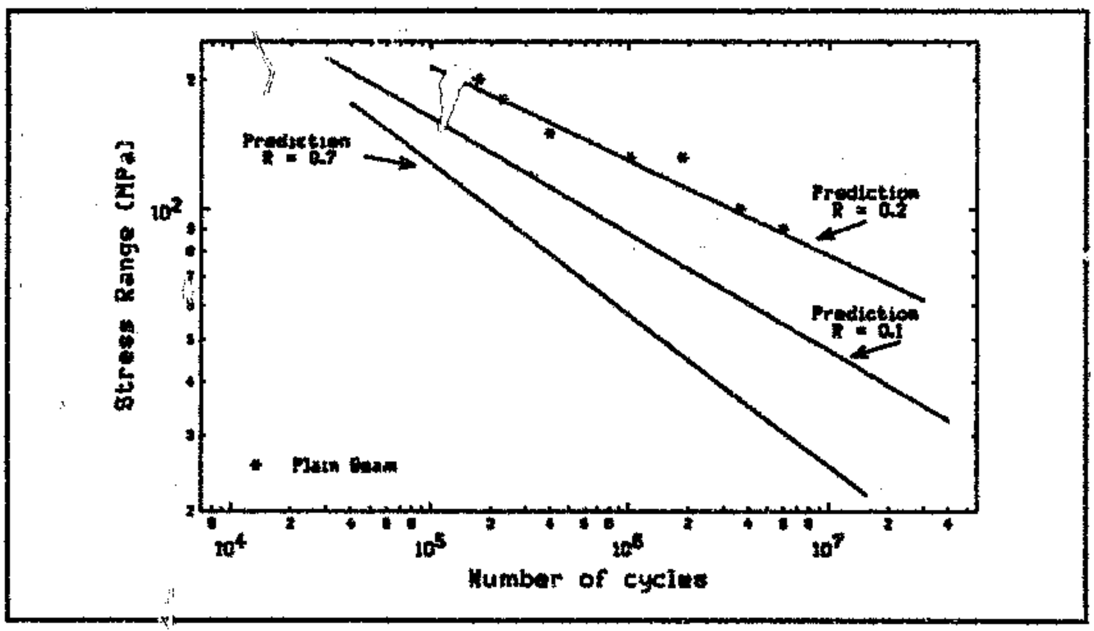

Fig. 5.48 - Prediction trends for the plain 100 x 75 mm I-beams.

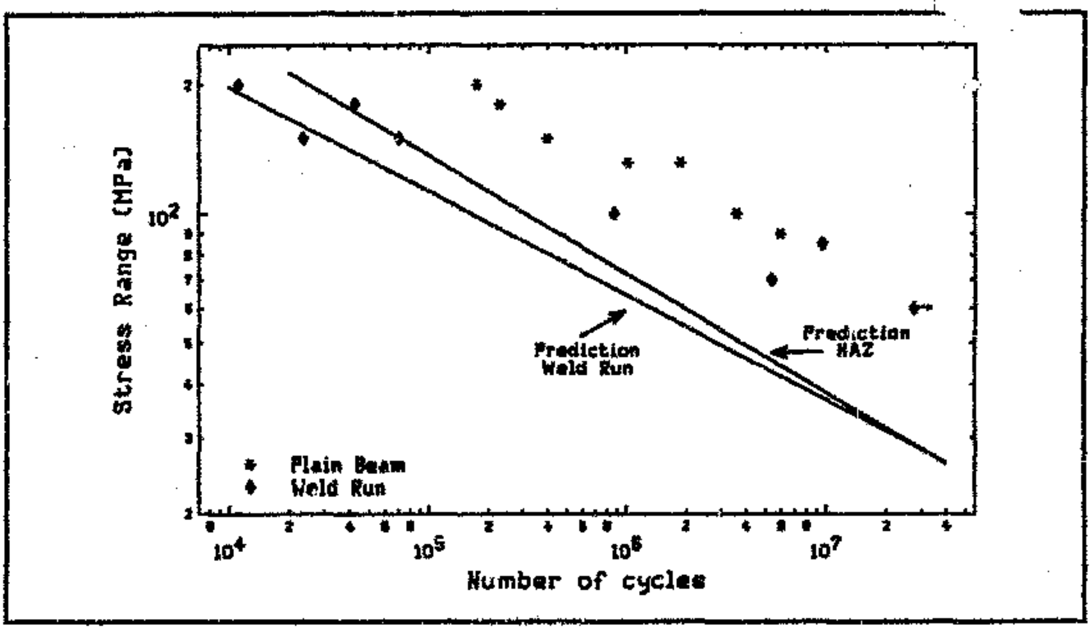

Fig. 5.49 - Prediction trends for 100 x 75 mm I-beams which were given a weld run.

fatigue crack growth rate specimens tested at R = 0.2. When the fatigue crack growth rate tests were performed, the fatigue crack took the form of a through-thickness crack. The fatigue cracks of the plain I-beams were semi-elliptical. It is thus likely the amount of crack closure in the plain I-beams which were tested at R = 0.1, was lower than that in the fatigue crack growth rate specimens tested at R = 0.1. Thus, a fatigue crack growth rate curve with less crack closure, i.e. the R = 0.2 curve, would give a better fit to the fatigue life data of the plain I-beams. The difference in the prediction curves could, however, also be attributed to scatter in the experimentally determined fatigue crack growth rate curves.

For the 100 x 75 mm I-beams which were welded with cover plates, the parent plate experienced a change in microstructure and residual stresses were introduced. To see how the fatigue strengths of the I-beams were affected by the welding rather than the presence of a cover plate, a weld bead was run across the width of the tension flange. This bead was subsequently ground flush with the flange surface to remove any stress concentrations. With the presence of high tensile residual stresses, little or no crack closure was expected to occur during fatigue crack growth in the I-beams. The fatigue crack growth rate curves for the HAZ and the weld metal, which were produced by keeping K_{max} constant, are essentially closure-free and were used in the prediction procedure. The initial defect in this case was taken as 0.12 mm (Section 5.1.2). The prediction curves based on growth in the heat affected zone and the weld metal are shown in Fig. 5.49. The slopes of the prediction curves are far steeper than that of the S-N curve for the weld run, although the predictions appear to fit the data at lives of around 10^5 cycles. Since the fatigue cracks initiated in the weld metal and there was a parent plate / weld metal interface with an unknown extent of residual stresses, there is no clarity as to which fatigue crack growth rate curve would be most appropriate for these I-beam specimens.

For the 100 x 75 mm I-beams welded with cove... ...s, various prediction curves were used in an endeavour to estimate the effects of crack closure and residual stresses on fatigue life. These are shown in Fig. 5.50. Thus parent plate fatigue life prediction curves for R = 0.1 and 0.2 and the closure free curve of constant K_{max}, were produced. To investigate the effect of a changes in fatigue strength due to microstructure, a fatigue life prediction curve for the HAZ was also produced.

The initial defect was chosen to be 0.7 mm which was close to the upper bound of observed initial defect size. Thus one would anticipate the prediction curves to more or less on the lower bound of the S-N data. The welded I-beams are expected to have high tensile residual stresses at the weld toe which would prevent crack closure from occurring. Thus the prediction curves of R = 0.1 and R = 0.2, which do include the effect of crack closure, would be expected to lie above the S-N data of the welded I-beams.

The prediction curves, which would represent the conditions under which the welded I-beams were tested, i.e. the curves of constant K_{max} and of the HAZ, do fit the S-N data of the welded I-beams well. The two lines are very similar since there is hardly any difference between these two fatigue crack growth rate curves. However, the slope of the HAZ prediction line fits the S-N data better than that of the K_{max} curve. The HAZ prediction curve gives thus the best fit to the S-N data. Fig. 5.51 shows S-N data with the HAZ prediction curve.

Since the prediction curves of the 150 x 101 mm and the 48 x 27 mm I-beams gave the same trends for both sets of I-beam data, they will both be discussed simultaneously. These curves are shown in Fig. 5.52 and Fig. 5.53 respectively. The initial defects of the 150 x 101 mm I-beams was assumed to be 0.6 mm and that of the 48 x 27 mm I-beams, 1.8 mm.

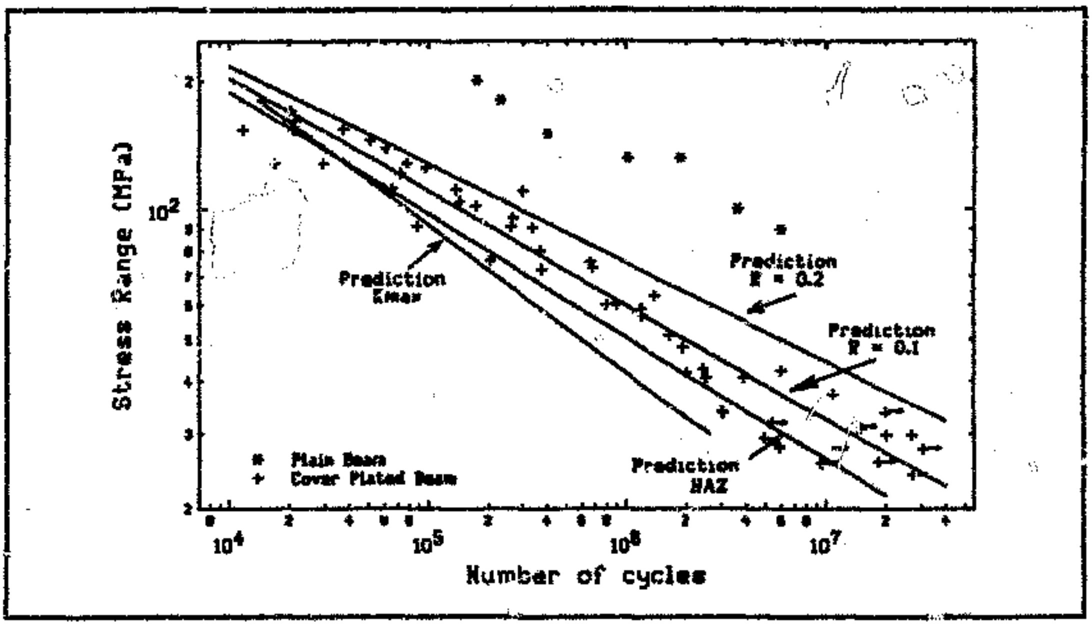

Fig. 5.50 - Prediction trends for 100 x 75 mm I-beams which were welded with cover plates.

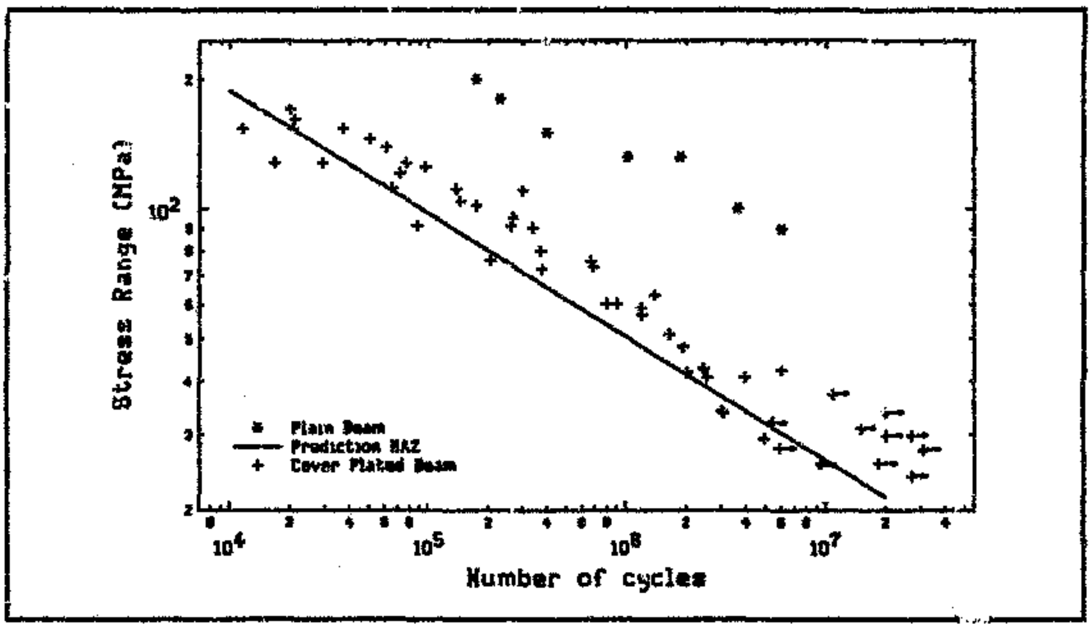

Fig. 5.51 - HAZ prediction trend for 100 x 75 mm I-beams which were welded with cover plates.

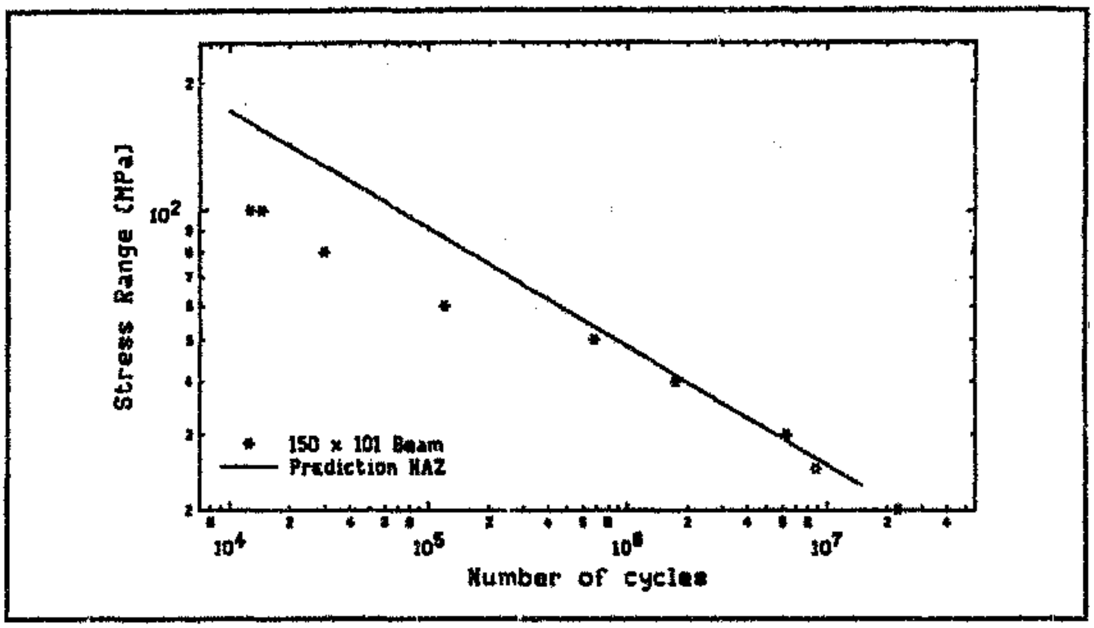

Fig. 5.52 - Prediction trends for 150 x 101 mm I-beams which were welded with cover plates.

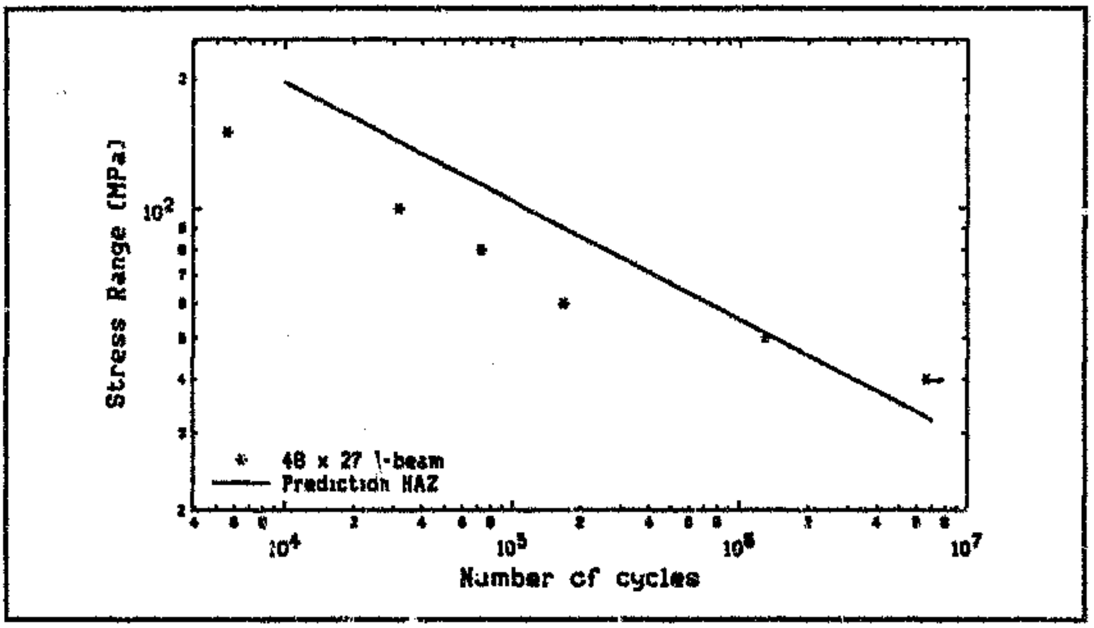

Fig. 5.53 - Prediction trends fc 48 x 27 mm I-beams which were welded with cover plates.

The 150 x 101 mm and the 48 x 27 mm I-beams were welded with cover plates. Thus the prediction behaviour was very similar to that of the 100 x 75 mm I-beams. The prediction curves of the HAZ do not fit the S-N data as well as for the case of the 100 x 75 mm prediction curves. This scatter can be ascribed to the undefined effects of the size and residual stresses.

5.5. Comparison with Design Curves

The fatigue life data for the I-beams that were welded with cover plates and for the plain I-beams was compared with the British Standards Institution Codes of Practice, CP118[31] for aluminium and BS5400 Part 10[30] for Steel. These comparisons are shown in Fig. 5.54 to Fig. 5.57 respectively.

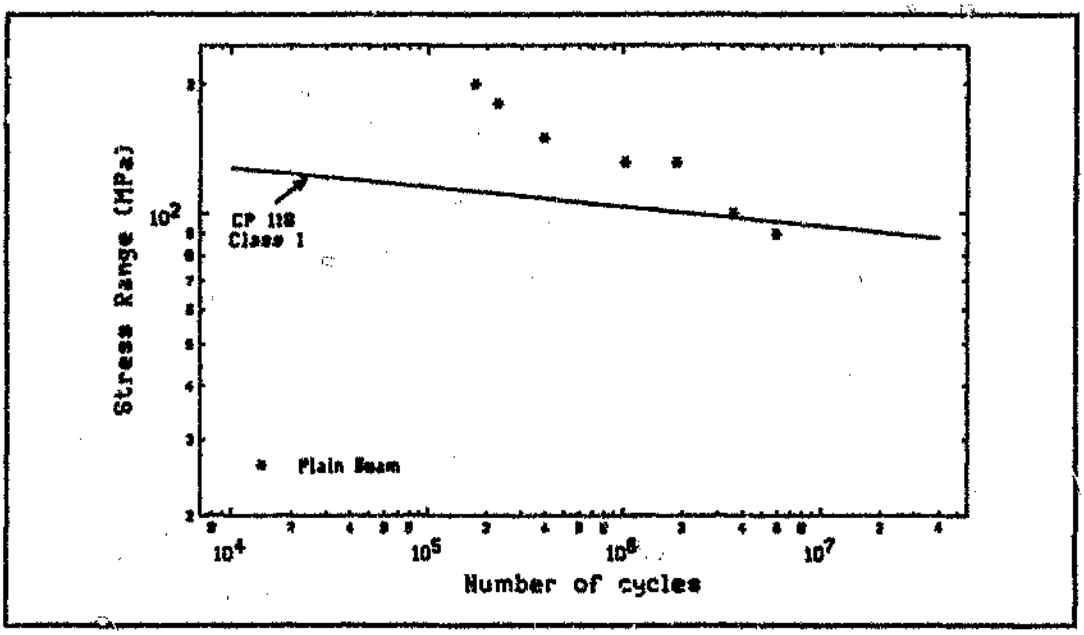

Fig. 5.54 - A comparison between fatigue life data for the 100 x 75 mm plain I-beams and CP 118 Class 1 design curve.

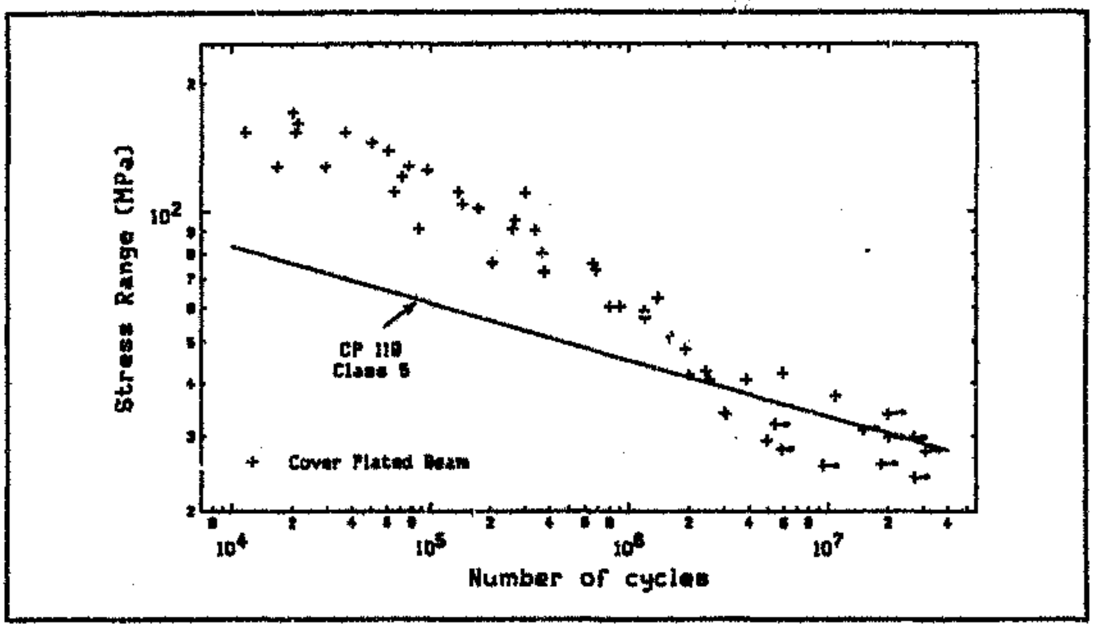

Fig. 5.55 - A comparison between fatigue life data for 100 x 75 mm I-beams welded with cover plates, and CP118 Class 5 design curve.

It is clear from Fig. 5.54 and Fig. 5.55, that the fatigue life data for both the plain I-beams and those with cover plates do not correlate at all with CP118. Class 1 would represent the plain extruded aluminium alloy I-beams and Class 5 would represent the aluminium alloy I-beams welded with cover plates. The slopes of the CP118 design curves are considerably less than the respective fatigue life curves. This would mean that the fatigue life of an I-beam could be greatly increased, from say 10^4 to 10^6, by just reducing the applied stress by 20 MPa. This is not the case for the I-beams that were tested during this project. Thus it would appear that the provisions of CP 118 for fatigue have to be treated with circumspection.

The fatigue design curves of BS 5400 Part 10[3] for welded joints is based on the presence of initial defects, high tensile residual stresses and stress concentrations. Thus the fatigue initiation stage of fatigue growth does not contribute towards the fatigue lives of the members. The fatigue design curves are presented on a conservative basis, i.e. the mean minus two standard deviations curves are used for design purposes.

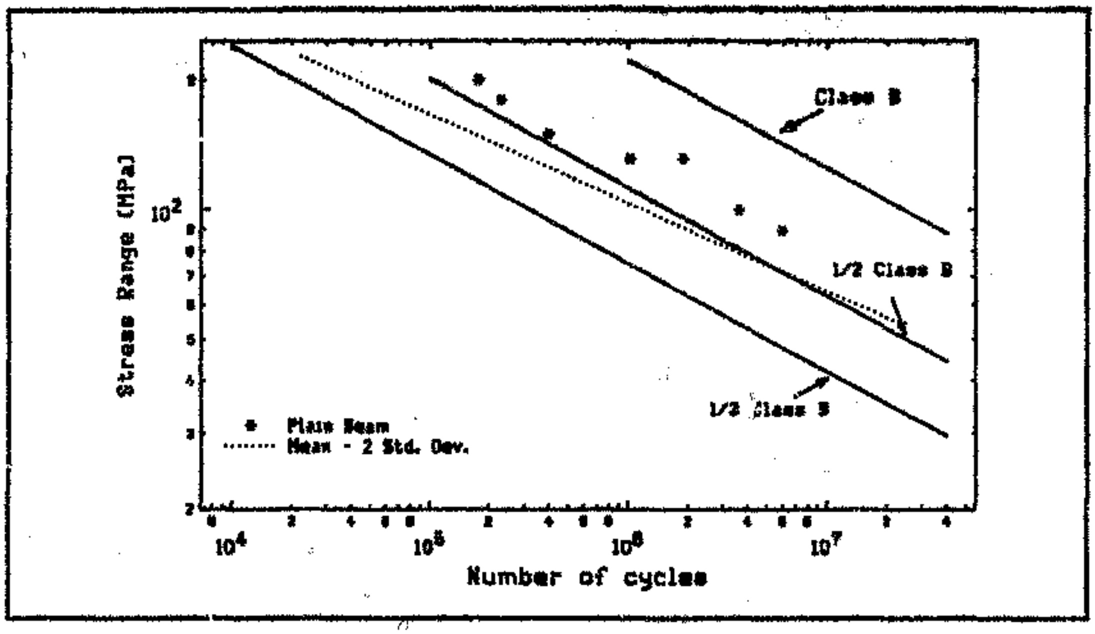

Fig. 5.56 - A comparison between fatigue life data for 100 x 75 mm I-beams welded with cover plates, and BS 5400 Class B design curves.

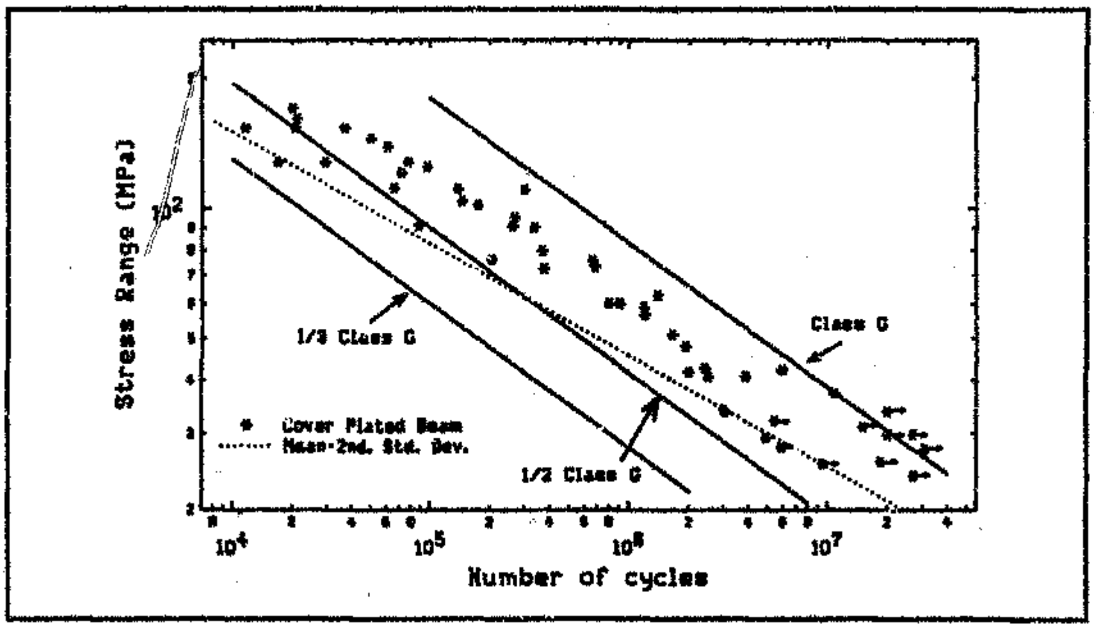

Fig. 5.56 - A comparison between fatigue life data for the 100 x 75 mm plain I-beams and BS 5400 Class B design curves.

Maddox[7] pointed out that the factors which affect the life of welded steel structures, i.e. an initial defect, residual stresses and a stress concentration, are also present in aluminium. Thus, the aluminium alloys should behave in a similar fashion to that of the steel alloys. Because BS 5400 Part 10 for welded joints is based on the presence of initial defects, residual stresses and stress concentrations, the fatigue life of aluminium alloys should relate in some way to design curves of BS 5400 Part 10. If a relationship could be found between the two types of metals, then the design code for steel, i.e. BS 5400 Part 10, can be modified to suit aluminium alloys.

Maddox suggested that the fatigue strengths of the alloys correlated on the basis of $\Delta K/E$, where E is Young's modulus. This would simply mean that the fatigue strength of steel would have to be divided by 3 to determine the fatigue strength of aluminium.

The fatigue design curves for the plain extruded I-beam represent Class B in BS 5400 Part 10[30]. The fatigue life design curves for the I-beams welded with cover plates represent Class G in BS 5400 Part 10. The design curves, i.e. Class B and Class G, proposed by Maddox for the aluminium alloys are compared in Fig. 5.56 and Fig. 5.57 with the S-N data, which was obtained experimentally. One can see that the design curves are conservative with respect to the mean minus two standard deviation lines of the S-N data if the design curves are divided by 3.

When the design curves of Class B and Class G are divided by 2, as is shown in Fig. 5.56, they seem to fit the mean minus two standard deviations curve of the S-N data better. At low fatigue lives for the I-beams with cover plates, this limit becomes less conservative. However, a division of the design curves of Class B and Class G by 2 would be sufficient to describe the fatigue lives of the plain I-beams and those welded with cover plates. For Class G, this curve is not recommended at low fatigue lives, i.e.5 x 10^4 cycles, since some of the S-N data fell below this curve. A division by 3 would make the design curves for aluminium more conservative and add a factor of safety to them.

6. Summary of Conclusions

The primary objectives of this projects were to be able to produce fatigue life prediction curves of aluminium 6261-T6 I-beams welded with cover plates and to compare the S-N data of these I-beams with the fatigue design codes BS 5400 Part 10[3] and CP 118[6].

These objectives were achieved by :

1 - producing S-N curves for three sizes of aluminium 6261-T6 I-beams welded with various cover plate geometries.

2 - producing fatigue crack growth rate curves for the aluminium 6261-T6 alloy at various stress ratios and at constant K_{max}, with decreasing ΔK. Fatigue crack growth rate curves were also produced for the 6261-T6 HAZ condition and the aluminium 5356 weld metal alloy.

3 - determining the effect of stress concentration with respect to crack size with the aid of finite element analysis.

4 - determining the sizes of the initial defects of the I-beams welded with cover plates.

5 - producing fatigue life prediction curves for the various I-beams welded with cover plates.

6 - comparing the S-N data of the I-beams with fatigue design codes.

From the work performed in this project the following conclusions can be made :

1 - In all the I-beams welded with cover plates the fatigue crack initiated at the weld toe of the end weld of the cover plates and penetrated the parent plate of the I-beams. There were significant differences between the slopes of the fatigue curves of the various cover plate geometries. The slope of the S-N curves of the different cover plate geometries seemed to be inversely proportional to the width of the end weld.

2 - The initial defects were attributed to the presence of shrinkage crack in the parent plate at the weld toe. The initial defect size in the 150 x 101 mm I-beams was estimated to be about 0.6 mm, that in the 100 x 75 mm I-beams, 0.7 mm and that in the 48 x 27 mm I-beams, 0.18 mm.

3 - The fracture surfaces of the welded I-beams was partially intergranular and partially transgranular near the origin of the fatigue crack. As the crack grew the fracture mode became more and more transgranular. This was partly attributed to the presence of the shrinkage cracks and partly to the fact that the degree of intergranular failure increases with stress intensity factor range.

4 - Fatigue life prediction curves for I-beams welded with cover plates fitted the S-N data the best when the growth rate data for HAZ was used. From this it was concluded that the residual stresses at the weld toes are high enough to prevent crack closure from occurring. The life predictions of the HAZ material related fairly well to the different sizes of I-beams, even though the effects of size on residual stresses were unknown.

5 - The fatigue life data of the I-beams welded with cover plates did not compare well the design curve for of CP 118 for that particular geometry. The fatigue design curves of BS 5400 Part 10 compare better with the mean minus 2 standard deviations curve of the S-N data, which was obtained experimentally, if the stresses of the BS 5400 Part 10 curves are divided by 2. At low fatigue lives, i.e. at 5×10^4 cycles, the BS 5400 Part 10 curve, which is divided by two is not recommended for design purposes, since some of the fatigue data fell below this line.

Recommendations for Future Work

On the basis that the prediction procedure, used in this project, has worked reasonably well, recommendations for possible future work have been made :

1 - In order to determine whether the prediction procedure employed in this project is generally feasible, the project could be extended to different geometries and different materials.

2 - A three dimensional finite element model of the weld toe region could be produced, in order to improve the accuracy in determining the stress concentration.

3 - Tests could be performed on I-beams with welded cover plates, which were heat treated to a T6 temper after welding, in order to exclude the effects of residual stresses and the HAZ material on the fatigue life.

4 - Fatigue crack growth rate equations, other than the Paris Law, e.g. the Forman[8] equation or the Hartman[30] equation could be used in the mathematical prediction procedure, to determine how well these prediction procedures compare to that of the Paris Law.

References

(1) - British Standards Institution, *Concrete and Composite Bridges*, London, 1980, BS 5400 Part 10.

(2) - BS code of Practice CP 118, 1969, *The structural use of aluminium*, British Standards Institution.

(3) - Fisher, J.W, Frank, K.H., Hirt, M.A. and McNamee, B.M. Effect of weldments on the fatigue strength of steel beams, *NCHRP Report 102*, Highway Research Board, National Academy of Science, National Research Council, Washington, 1970.

(4) - Gurney, T.R. *Fatigue of Welded Structures*, Cambridge University Press, Cambridge, 1979.

(5) - Ewalds, H.L. *Fracture Mechanics*, 2nd ed., London, Edward Arnold (Publ.), 1985.

(6) - Irwin, G.R. Crack extension force for a part through crack in a plate, *Journal of Applied Mechanics and Transition ASME*, Vol. 84, 1962, pp. 651-654.

(7) - James, N. Some aspects of fatigue crack growth (Part 1), *The South African Mechanical Engineer*, Vol.35, Oct. 1985, pp.444-449.

(8) - Lieurade, H.P. Effect of residual stress and stress ratio on the fatigue strength of welded components, *Welding in the world*, Vol.26, No.7/8, pp. 158-187,1988.

(9) - Smith, I.F.C and Smith, R.A. Defects and crack shape development in fillet welded joints, *Fatigue of Engineering Materials Structure*, Vol.5, No.2, pp.151-162, 1982.

(10) - Maddox,S.J. Analysis of fatigue cracks in fillet welded joints, *International Journal of Fracture*, Vol.11,No.2, April 1975, pp.221-24

(11) - Yamada, K. and Albrecht, P. Fatigue Behaviour of Two Flange Detail, *Journal of Structural Division*, ST4, April 1977, pp.781-791.

(12) - Verreman, Y., Bailon, J. and Masounave,J. Fatigue life prediction of welded joints-a re-assessment, *Fatigue Fracture of Engineering Materials and Structures*, Vol.10, No.1, 1987, pp.17-36

(13) - Scott, P.M. and Thorpe, T.W. A critical review of crack tip stress intensity factors for semi-elliptical cracks, *Fatigue Fracture of Engineering Materials and Structures*, Vol 4, No.4, 1981, pp. 291-309.

(14) - Pierce, W.S. and Shannon, J.L., Jr. Surface crack shape change in bending fatigue using an inexpensive fatigue apparatus, *Journal of Testing and Evaluation*, Vol.6, No.3, May 1978, pp.183-188.

(15) - Mahmoud.M.A. and Hosseini, A. Assessment of stress intensity factor and aspect ratio variability of surface cracks in bending plates, *Engineering Fracture Mechanics*, Vol.24, No.2, pp.207-221, 1986.

(16) - Mahmoud, M.A. Growth patterns of surface fatigue cracks under cyclic bending - A quantitative analysis, *Engineering Fracture Mechanics*, Vol.31, No.2, pp.357-369, 1988.

(17) - Marrs, G.R. and Smith, C.W. A study of local stresses near surface flaws in bending fields, *Stress Analysis and Growth of Cracks, Proceedings of the 1971 National Symposium of Fracture Mechanics, Part I, ASTM STP 513*, American Society for Testing and Materials, 1972, pp 22-36.

(18) - Gross, B. Stress Intensity factors for a single edge notch tension specimen by boundary collocation of a stress function, *NASA Technology*, Note D-2395.

(19) - Paris, P.C. and Erdogan, F. A critical analysis of crack propagation laws, *Journal of Basic Engineering Transition. ASME*, Vol. 85, 1963, pp. 528-534.

(20) - Terada, H. and Nakajima,T. Analysis of stress intensity factor of a crack approaching welding bead, *International Journal of Fracture*, Vol.27, 1985, pp.83-90.

(21) - Gurney, T.R. and Johnston, G.O. A revised analysis of the influence of toe defects on the on the strength of transverse non-load carrying fillet welds, *Welding Resear... International Report*, 62/1978/E.

(22) - Maddox, S.J. A fracture mechanics analysis of the fatigue behaviour of a fillet welded joint, *Welding Research International*, Vol.6, No.5, 1976.

(23) - Maddox, S.J, Assessing the significance of flaws in weld subject to fatigue, *Welding Research Supplement.*, September 1974, pp 401s-410s.

(24) - Smith, I.F. and Gurney, T.R. Changes in the fatigue life of plates with attachments due to geometrical effects, *Welding Research Supplement*, September 1986, pp.244s-250s.

(25) - Glinka, G. Fatigue life calculation and testing of full-scale welded I-beams, *Fatigue of Engineering Materials and Structures* , Vol.4, No.1, pp.35-48, 1981.

(26) - Leis, B.N. and Forte, T.P. Fatigue growth of initially physically short cracks in notched aluminium and steel plates, *Fracture Mechanics: Thirteenth Conference, ASTM 743*, Roberts,R.,(Ed.), American Society for Testing and Materials, 1981, pp.100-124.

(27) - Smith, I.F.C and Smith, R.A. Fatigue crack growth in a fillet welded joint, *Fatigue of Engineering Materials and Structures*, Vol.18, No.4, pp.861-869, 1983.

(28) - Bowman, M.D. and Yao, J.T.P Fatigue damage assessment of welded steel structures, *Metal Structures*, Vol.10, No.3, 1984, pp.45-69.

(29) - Hartman, A. and Schijve, J. The effects of environment and load frequency on the crack propagation law for macro fatigue crack growth in aluminium alloys, *Engineering Fracture Mechanics*, Vol.1, 1970, pp. 615-631.

(30) - Gurney, T.R. Finite element analysis of some joints with the welds transverse to the direction of stress, *Welding Research International*, Vol.6, No.4, 1976, pp. 40-72.

(31) - Garz, R.E., Fatigue crack closure and closure development in a high strength aluminium alloy, *MSc dissertation at the University of the Witwatersrand*, 1988.

(32) - Sabo, S. and Thuestad, J.G. The effect of weld profile on the fatigue life of aluminium butt- and fillet welds. *Proceedings of the Third International Conference on Aluminium Weldments*, Munich, F.R.G., April, 1985.

(33) - Maddox, S.J. An introduction to the fatigue of welded joints, *Improving the fatigue performance of welded joints*, Welding Institute.

(34) - Pirsarski, H.G. Fatigue crack propagation in an aluminium alloy weldment, *Metal Construction*, Vol.9, No.3, pp. 123, March 1977.

(35) - Nui, X. and Glinka, G. The weld profile effect on stress intensity factors in weldments', *International Journal of Fracture*, Vol.35, 1987, pp.3-20

(36) - Metals Handbook (1948), *The American Society for Metals*, T.Lyman (ed.), American Society for Metals (Publ.)

(37) - Edwards, L. and Martin, J.W., Effect of dispersoids on fatigue crack propagation in aluminium alloys, *Metal Science*, Vol.17, November 1983, pp. 511-518.

(38) - Raymond, P.V. and Martin, J.W., The influence of dispersoids on the fatigue crack propagation in Al-Mg-Si alloys, *Zur Metallkunde*, Vol. 70, 1979, pp. 80-84.

(39) - Robertson, I. and Dwight, J.B. HAZ softening in welded aluminium, *Proceedings of the Third International Conference on Aluminium Weldments*, Munich, F.R.G., April, 1985.

(40) - Enjo, T. Kuroda, T. Quantitative evaluation of microstructure in weld heat affected zone of commercial Al-Mg-Si Alloy by means of electrical resistivity measurement,

Light Metals Abstracts, 1983-1984.

(41) - Booth, G.S. A review of fatigue strength improvement techniques, *Improving the fatigue performance of welded joints*, Welding Institute.

(42) - Homes, G.A. Relation between endurance limit and porosity of arc welds in mild steel, *Arcos*, Vol.15, No.89, 1938, pp. 1951-1957.

(43) - Gurney, T.R. The influence of artificially induced residual stresses on the fatigue strength of welded light alloy specimens, *British Welding Journal*, Vol.9, No.2, 1962, pp.90-95.

(44) - Warren, W.G. Fatigue tests on defective butt welds, *Welding Research International*, Vol.6, No.6, 1952.

(45) - Woodley, C.C Practical application of weld toe grinding, *Improving the fatigue performance of welded joints*, Welding Institute.

(46) - Webber, D. Evaluation of possible life improvement methods for Aluminium-Zinc-Magnesium alloy fillet welded details, *Fatigue Testing of Weldments*, ASTM STP 648, Hoeppner, D. W., Ed., American Society for Testing and Materials, 1978, pp.7?-88

(47) - Polmear, I.J. and Wilkinson, D.R. Effects of GTA dressing on the fatigue properties of aluminium alloy welded, butt jointed and fillet welded plates, *Welding Journal*, Research Supplement, March 1983, pp.78s-81s.

(48) - Hausammann, H., Fisher, J.W. and Yen, B.T. Effect of peening on fatigue life of welded details, *Metal Structures*, Vol.5, No.2, 1981, pp.71-83.

(49) - Maddox, S.J. Fatigue design of welded aluminium alloy structures, *Proceedings of the Second International Conference on Aluminium Weldments*, Munich, F.R.G., 24 to 26 May, 1982.

(50) - Niem, E., Knuuttila, E. and Nurkkala, P. Fatigue testing of welded aluminium ship detail, *Proceedings of the Third International Conference on Aluminium Weldments*, Munich, F.R.G., April, 1985.

(51) - Aabo, S. and Paauw, B. The effect of the R-ratio on fatigue life *Proceedings of the Third International Conference on Aluminium Weldments*, Munich, F.R.G., April, 1985.

(52) - Yongi,S., Yanman, Y., Xingduo, Zhiqiang, S., Fatigue behaviour of cover plated beams, *Proceedings of the Pacific Structural Steel Conference*, Auckland, New Zealand, August 4-8, 1986.

(53) - Basler, K. ,Mueller, J.A., Ozen, A.M., Zuurbier, G.W. and Fisher, J.W. Commentary on welded cover plated beams, *Proceedings of ASCE Journal of Structural Division*, Vol.93, ST4, Aug.1967, pp.95-122.

(54) - American Association of State Highway and Transportation Officials, Washington, D.C., 1974.

(55) - Simon, S. and Albrecht, P. ,Adding fatigue life to cover plate ends, *Proceedings of ASCE Journal of Structural Division*, Vol.7, No.5, pp.923-935, May 1981.

(56) - Albrecht, P., Wattar, F.and Sahli, A. Towards fatigue-proofing cover plate ends, *Proceedings of the W.H. Munse Symposium: Behaviour of Metal Structures, Research to Practice*, Philadelphia, USA, May 17, 1983.

(57) - Hobbacher, A. Establishing fatigue design recommendations for welded aluminium joints in IIW, *Proceedings of the Third International Conference on Aluminium Weldments*, Munich, F.R.G., April, 1985.

(58) - Armstrong, R.A. Design and fatigue prediction techniques for welded aluminium joints, *Proceedings of the Third International Conference on Aluminium Weldments*, Munich, F.R.G., April, 1985.

(59) - Wilson, W.M.,Munse,W.H. and Snyder, I.S. Fatigue strength of various types of butt welds connecting steel plates, *University of Illinois EES. Bulletin No.384*, 1950.

(60) - Munse, W.H. and Stallmeyer, J.E. Fatigue in welded beams and girders, *University of Illinois*, CES SRS 259, 1962.

(61) - Orjaseater, O and Haagensen, P.J. Comparison of fatigue design codes for aluminium weldments, *Proceedings of the Third International Conference on Aluminium Weldments*, Munich, F.R.G., April, 1985.

(62) - ASTM Standard E 647-86a "Measurement of fatigue crack growth rates Fatigue", *1986 Annual Book of ASTM Standards*, Vol. 03.01.

(63) - Murakami, Y.(ed.), *Stress Intensity Handbook*, Vol.1, Pergamon Press, 1974, Oxford

(64) - Booth, G.S. and Maddox, S.J., Influence of various factors on the fatigue strength of steel plates with fillet welded attachments, *The Welding Institute*, 93/1979, June 1979.

Appendix A

<u>Welding Parameters</u>

Welder:	G.Nell
Welding Process:	GTAW Manual
Joint Design:	Fillet
Base Metal:	Aluminium 6261-T6
Filler Metal:	Aluminium 5356
Preheat:	40°C
GAS:	99.95% pure Argon
Current:	AC
Polarity:	Straight
Amps:	100-120
Volts:	12-14
Tungsten Tip Size:	3.2 mm
Number of Passes:	One
Trav l Speed:	80-100 mm / min

Appendix B

```
Program Integrete_crack_growth_equation (INPUT,OUTPUT);

{ This programme integrates the equation, da = C*dK^m, defined in the 'Equation '
procedure through an iterative loop, cyc'e by cycle. This is repeated at various stress levels
in order to obtain a S-N curve. The data is then stored on disk }

{---------------------------------------------------}

{ stress_range = stress range  stress_change = the stress range which was varied due to the
crack penetrating the beam
  a  = instant crack length
  ai = initial crack length
  af = final crack length
  N  = number of cycles
  da = change in cra' length
  Mk = stress concen ation correction factor
  Y  = geometry correction factor
  dK = stress intensity range
  C  = equation constant
  m  = equation constant
  filing = the variable used to file the parameter onto disk
  filename  name of the file onto which data is saved onto disk
  count = counter variable
  i = counter variable
  thickness = thickness of flange
  height = height of I- beam
  depth = ratio of a / thickness }

{-----------------------------------------------------------}

VAR

  stress_range, a, ai, af, N, Mk, da, z, x, dK, C, m,
  stress_change, height, thickness, depth          : REAL;
  count, i                                         : INTEGER;
  filing                                           : TEXT;
  filename                                         : STRING;

CONST

  pi = 3.141592654;

{-----------------------------------------------------------}

{ This function generates the power function of z to the power of x }
```

```
Function Power (z,x : REAL) :REAL;          { z to the power of x }
  BEGIN
       power := exp (x * ln(z));
  END;

{------------------------------------------------------------------}



{ This procedure obtains all the input required to run the programme }

Procedure Input (VAR  filename :STRING;
            VAR  stress_range, af : REAL );

  BEGIN
    Write ('Enter the File Name onto which you want to Save your Data : ');
    ReadLn (filename);
    Write ('Enter the value for "C" : ');       { da = C * dK^m }
    ReadLn (C);
    Write ('Enter the value for "m" : ');
    ReadLn (m);
    Write ('Enter the Initial Crack Size : ');
    ReadLn (ai);                        { if the final crack size is smaller than the initial crack size}
     REPEAT                             { then repeat}
       Write ('Enter the Final Crack Size : ');
       ReadLn (af);
     UNTIL (af > ai);
    Write ('Enter the height of the I-beam : ');
    ReadLn (height);
     stress_range := 180;
     Assign (filing, filename);    { opens the 'filename' file }
    Rewrite (filing);              { resets the 'filename' file }
    WriteLn (filing, 1);          { '1' for One Curve for the
                                     "PLOT" programme }
    WriteLn (filing,6);     { '6' for six data points for"PLOT"
      programme }
   thickness := af;


  END;

{------------------------------------------------------------------}

{ This procedure generates the equation da = C * dK^m }

Procedure Equation (VAR da, dK, Mk : REAL);

  BEGIN
   depth := a /thickness;

   Y = 1.122 - 0.231 * (depth) + 10.55 * power(depth,2)
```

```
      - 21.7 * power(depth,3) + 33.19 * power(depth,4);
    Mk := 1.125 - 0.376 * ln(a) - 0.037 * ln (a) * ln (a);
                         { equation obtained from finite element analysis }
    dK := Y * Mk * stress_range * SQRT(pi * a / 1000); { divide by 1000 to get MPaSQRT(m)
}
    da := C * power(dK,m);

  END;

{------------------------------------------------------------}

Procedure Iterate ( VAR N, a:REAL);

{ This procedure iterates the equation da = C * dK^m from the initial    crack length to the
final crack length, cycle by cycle.  It will     write out onto the screen the various parameters
after every 100     cycles. }


  BEGIN

      N := 0;
      a := ai;              { start at initial crack length }
      count := 0;
       REPEAT
         Equation (da, dK, Mk);
         a := a + da;        { increase the crack length by da }
         stress_change := stress_range * (1 - a/50);
                  { the stress range is decreased due to the crack penetrating the beam }
         N := N +1;             { count the number of cycles }
         count := count +1;
           If count >= 100 THEN
               { writes out the status after every 100 cycles }
             BEGIN
               Write ('dS = ',stress_change:3:0,'  Mk = ',Mk:4:2);
               WriteLn ('   dK = ',dK:5:3,'   da = ',da:10,
                       '   a = ', a:6:4,'   N = ',N:8:0);
               count := 0;
             END;
       UNTIL (a >= af);          { end at final crack length }
  END;

{------------------------------------------------------------}

{ This procedure writes out the number of cycles requires for the     crack to grow from the
initial crack length to the final crack      length at a certain stress range.  It then saves the
number of     cycles and stress range onto disk. }

Procedure Output (VAR stress_range,N : REAL);

 BEGIN
    WriteLn;
```

```
    WriteLn;
    WriteLn ('It took ',N:8:0,' cycles to grow the crack from '             ,ai:4:3,' mm');
    WriteLn ('to ',af:6:3,' mm with a stress range of ',
          stress_range:4:0,' MPa.');
    WriteLn;
    WriteLn;
    Write (filing, N:8:0);
    WriteLn (filing,stress_range:4:0);
  END;

{-----------------------------------------------------------}

 { Main Programme
  The main programme call the input procedure and iterates the
  da = C * dk^m equation for various stress ranges. It then closes the file on disk }

  BEGIN
    Input (filename, stress_range, af);
    REPEAT
      Iterate (N,a);
      Output (stress_range, N);
      stress_range := stress_range - 30;
    UNTIL (stress_range < 30);
    Close (filing);
  END.  {end programme}

{-----------------------------------------------------------}
```

Appendix C

Plain Beam	
N (Cyc)	Sr (MPa)
17470	200
223150	180
396440	150
1875900	132
1017500	132
3609500	100
5919200	90

Square - end	
N (cyc)	Sr (MPa)
9550	171
11600	154
16840	128
29300	128
65200	112
87100	91
204300	76
796900	60
1188600	59
2533800	41
10900800	37
20000000 ?	34
20116000 ?	30
18452900 ?	26

Square - no end	
N (cyc)	Sr crack (MPa)
20100	171
36960	154
77090	128
300000	110
136200	111
266000	95
366300	90
898000	60
2006000	42
3075800	34
4922600	29
9441900 ?	26

Diamond end	
N (cyc)	Sr (MPa)
60630	139
96320	125
144190	104
249600	91
659200	76
1391900	63
1928600	48
5952400	42
21713200 ?	34
3014300	34
15113200 ?	31
30729900 ?	28

Diamond - no end	
N (cyc)	Sr crack (MPa)
21190	1[illegible]1
50130	145
71710	121
173500	102
335900	90
630600	73
1202600	57
3892500	41
5415100	32
5859200	28
27170000 ?	24

Rounded	
N (cyc)	Sr crack (MPa)
20649	154
375700	72
1648800	51
2430900	43
27017800 ?	30

Weld Run	
N (cyc)	Sr (MPa)
1174	200
42436	180
70256	150
873200	100
5371600	70
27700000	60

Big Beam	
N (cyc)	Sr (MPa)
12640	100
14437	100
29642	80
118875	60
679800	50
1763500	40
6248800	30
8784200	25

Small Beam	
N (cyc)	Sr (MPa)
5568	150
31370	100
72760	80
168410	60
1295320	50
9617310	40